EXTERNAL CAVITY LASER WITH COHERENT AMPLIFIER ARRAY AND MULTIPLE SLIT SPATIAL FILTER

by

ROBERT PERRY SCHLOSS

S.B., Elec. Eng., Massachusetts Institute of Technology (1978)

S.B. Physics, Massachusetts Institute of Technology (1978)

S.M., Elec. Eng., Massachusetts Institute of Technology (1981)

SUBMITTED IN PARTIAL FULFILLMENT
OF THE REQUIREMENTS FOR THE DEGREE OF

DOCTOR OF PHILOSOPHY

at the

MASSACHUSETTS INSTITUTE OF TECHNOLOGY

DECEMBER, 1985

Signature of Author.....
Department of Electrical Engineering and Computer Science
October 11, 1985

Certified by.....
Robert H. Rediker
Thesis Supervisor

Accepted by.....
Arthur C. Smith
Chairman, Department Committee on Gaduate Students

EXTERNAL CAVITY LASER WITH COHERENT AMPLIFIER ARRAY
AND MULTIPLE SLIT SPATIAL FILTER

by

ROBERT PERRY SCHLOSS

Submitted to the Department of Electrical Engineering
and Computer Science on October 11, 1985
in partial fulfillment of the requirements
for the Degree of Doctor of Philosophy

ABSTRACT

A novel technique is described for obtaining coherent output from an ensemble of discrete semiconductor-diode lasers. A multiple slit spatial filter incorporated into an external cavity provides the interaction necessary to obtain coherent operation of the array of antireflection-coated diode lasers. An apparatus has been designed and fabricated in order to show feasibility of the technique. Design details are presented.

Initial experiments with the external cavity laser show that coherent operation is obtained. Different spatial filters, varying in period and duty cycle, are used in the laser. The data point to the conclusion that the spatial filters used lack influence of the kind or degree necessary to ensure that the coherent output spectrum is consistently monochromatic and tunable. In addition, operation of the laser with larger duty cycle spatial filters is more prone to multimode output spectra than with smaller duty cycle spatial filters. Various processes are indicated which explain the observed behavior.

A monochromatic theory of the external cavity laser is developed. The interaction provided by the spatial filter is analyzed for both non-detuned and detuned modes of operation. The mechanism of gain is approximated as resulting from a two-level system with negligible lower level population. Connections with measureable quantities are described in order to facilitate the determination of realistic values for parameters of the theory.

A computer model based on the theory is presented. Simulation studies investigate the effect of spatial filter duty cycle on coherent threshold, detuning on power output, and gain dependent phase on stability. Interpretations are offered.

Thesis Supervisor: Dr. Robert H. Rediker

Title: Senior Research Scientist, Department of
Electrical Engineering and Computer Science

ACKNOWLEDGEMENTS

The submission of this thesis signifies an end to my formal education, a task which has taken most of my life to complete, and as such merits serious introspection. Those who are close to me know that there is much in the recent past that I would undo if I could, yet there have also been changes which are cause for celebration. For the latter I am grateful.

I acknowledge Dr. Robert Rediker for the large part he has played in the course of the research culminating in this thesis. I also appreciate and thank the many faculty and staff members, too numerous to mention, that I have had the privilege of knowing both at MIT and at MIT Lincoln Laboratory. What I have learned from them in informal meetings rivals what was taught in classrooms and lecture halls.

Two persons affiliated with the research program should be mentioned. Farhad Hakimi was my fellow graduate student during an earlier period. I benefitted greatly from the stimulating discussions we had. Kristen Anderson has started where I left off and is attaining further goals of the program. She has proven to be an eminently capable researcher. I have enjoyed imparting to her whatever knowledge I have gleaned concerning the external cavity laser. And while learning from mistakes may be a necessary part of research, I wish that Kristen may avoid those abysses typical of some into which I fell.

This work was supported in part by the United States Office of Naval Research, MIT Lincoln Laboratory, and the MIT Department of Electrical Engineering and Computer Science. The work itself was conducted at MIT Lincoln Laboratory and in the MIT Research Laboratory of Electronics.

I thank my family and the members of my "other" family, the Tang Gang, with whom I lived for many years. Thanks guys, you made it bearable. I specially mention Isaac Cohen and Mark Bressler, dear friends both. I especially thank Barry Wyshogrod, who put up with me while putting me up at his apartment during my last months of work at MIT.

Above all, with words that fail miserably, I thank my wife René, and not only for the typing of the manuscript. Through it all she has been a source of strength, inspiration, common sense, and love. I couldn't have done it without her.

To my parents, of blessed memory.

TABLE OF CONTENTS

LIST OF FIGURES AND TABLES

Chapter 1. Introduction

This thesis documents a technique for obtaining coherent optical power from what would otherwise be an ensemble of mutually incoherent lasers. By involving a multiplicity of lasers, the technique poses the promise of a high-power coherent optical source. The potential uses of such a source are manifold. In the following pages historical background will be presented on the problem of synchronizing and obtaining coherent power from an ensemble of oscillators of various kinds (Chapter 2) of which the laser is but one. A model is described which incorporates the specific technique under investigation for obtaining coherent output from an ensemble of lasers (Chapter 3). Analogies are drawn suggesting connections to the familiar process of forced modelocking in lasers. Also, some details, present even in the conceptual model, are explored which greatly influence the operation of the technique. The experimental apparatus is detailed (Chapter 4). The author's contribution to the design process and in debugging the delivered apparatus are mentioned, in addition to details of the design itself. Initial experiments are documented and discussed (Chapter 5). Coherent operation is demonstrated repeatedly and the nature of the spectral output of the coherent ensemble is analyzed. A theoretical model is developed (Chapter 6). The model incorporates many realistic features, such as numerical aperture limitations, gain nonlinearities, and frequency detuning. Significantly, the development of the model extends to determination of realistic values for the theoretical parameters from convenient laboratory measurements. Computer simulation of the model is presented along with some simulation studies (Chapter 7). The computer model is viewed as a research goal in itself and provides a tool for

further investigations. Conclusions and comments are summarized and topics of possible future interest are presented (Chapter 8).

Chapter 2. Historical Background

In order to obtain more power at a given frequency than is available from a single oscillator, it has been proposed to combine the outputs from two or more oscillators. Part of the problem is the combining of outputs. The more interesting part of the problem is procuring two or more oscillators that are operating at the same frequency. In this section background is presented on the issue of oscillator synchronization and, when incorporated in addition to this, output combining schemes Power combining circuits and devices per se are not discussed, although an extensive body of literature on the topic does exist.

2.1 Master-Slave Synchronization

The classic paper on synchronization is Adler's 1946 article [1]. The core of the article is a differential equation describing the evolution of the phase of a radio-frequency vacuum tube oscillator in the presence of an impressed external signal. While several important effects are considered, the relevant conclusion from this work is that for a sufficiently strong and near-tuned impressed external signal,the frequency of the oscillator, although different initially, will in the steady state lock to the frequency of the external signal. More recently, Kurokawa has considered the injection locking of a class of solid state microwave oscillators [2]. The method of description reflects the three decade difference between this and Adler's paper, utilizing circuit model analogs and graphical constructions. The conclusion that a slave oscillator will lock to a sufficiently strong and near-tuned master oscillator remains basically unchanged. Two important additions are a consideration of the stability of

lock and noise in the locked signal.

It has also been suggested to use a single master oscillator to lock several slave oscillators, the outputs of the latter then being combined [3]. See Figure 2.1. The number of slave outputs that can be efficiently combined in such a scheme is limited by losses in the circulators.

2.2 Mutual Synchronization

It is an often observed result that when oscillators exchange energy, locking takes place. This can be deduced from two premises; that losses in the coupled system often are at a relative minimum when all oscillators are operating in coherence, and that a system with limited gain will evolve to a minimum loss condition. The latter statement expresses the "maximum emission principle". Rigorously, it is Hamilton's principle that should be used to determine system behavior, but the maximum emission principle is likewise fulfilled in most cases of interest [4].

When a system composed of interacting oscillators has attained coherence, the relative amplitudes and phases of the oscillators are fixed. This fixed relationship is a superposition of modes of the system. The coupling between oscillators plays a major role in determining the permissible modes of the system. In order to determine to which mode(s) the system will in fact evolve, the stability of each mode must be considered. The well known "moding" problem is a result of slight perturbations of coupling or other factors causing gross changes in operation due to near degenerate mode energies [5].

Many types of coupling schemes have been proposed for use with microwave and lower frequency oscillators, but the approach which is nearest to this thesis involves having the ensemble of oscillators interact

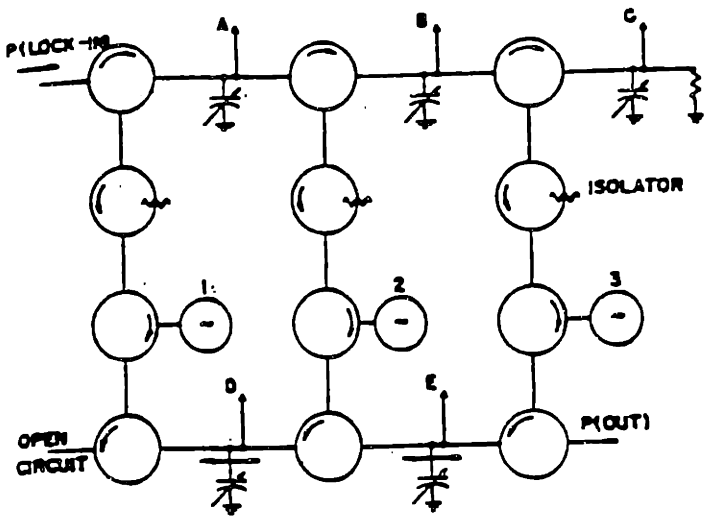

a) Schematic of 3-module power combiner.

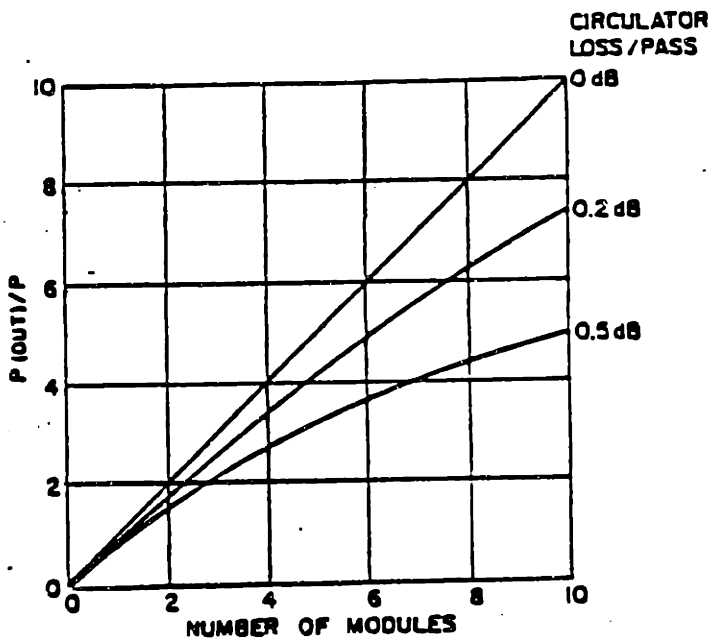

b) Power enhancement possible for n identical modules using circulators with identical loss/pass.

Figure 2.1. Master-multiple-slave technique of obtaining high power, per Reference 3. a) Circuit topology. Master oscillator is injected at upper left corner. Slave oscillators are labelled "1", "2", "3". Output is taken at lower right. b) Calculated output power.

by coupling each one to a common external resonator. Theoretical treatments of this approach have appeared in both the Russian and American literatures [6-8]. Figure 2.2 and 2.3 better indicate the coupling geometries being considered.

2.3 Coherent Semiconductor Lasers Arrays

Semiconductor-diode injection lasers are extremely attractive sources of radiation owing to their quantum efficiency, reliability, compactness, and such applications as fiber-optic telecommunications, laser printing and compact disc recording and playing. A major limitation, however is the power available from a single device. There is, therefore, interest in producing coherent arrays of diode lasers which would have an ensemble output exceeding that possible from a single laser, yet retaining monochromaticity and coherence.

One approach which is receiving considerable attention entails fabricating a monolithic array of semiconductor lasers with coupling between adjacent laser waveguides [9-21]. The behavior of the coupled array has been analyzed in terms of "supermodes" [22,23]. In contrast with the ensemble of synchronized oscillators discussed previously, the coupling between lasers is distributed over their length, as opposed to occurring between terminals or output ports.

Another approach to obtaining a coherent laser array, uses terminal rather than distributed coupling [24]. An antireflection coated monolithic laser-diode array (no waveguide coupling assumed) is placed between two spherical lenses and the Fourier transform property of lenses is used. Each lens is spaced one focal length away from the respective array facet. In the second focal plane of one lens is a plane mirror. In the second

a)

$$[Y(U, s)]\,[u] = \begin{bmatrix} Y_{00} & Y_{10} & Y_{10} & \dots & Y_{10} \\ Y_{10} & Y_{11} & Y_{12} & \dots & Y_{12} \\ Y_{10} & Y_{12} & Y_{22} & \dots & Y_{12} \\ \dots & \dots & \dots & \dots & \dots \\ Y_{10} & Y_{12} & Y_{12} & \dots & Y_{nn} \end{bmatrix} \begin{bmatrix} u_0 \\ u_1 \\ u_2 \\ \dots \\ u_n \end{bmatrix} = 0,$$

b)

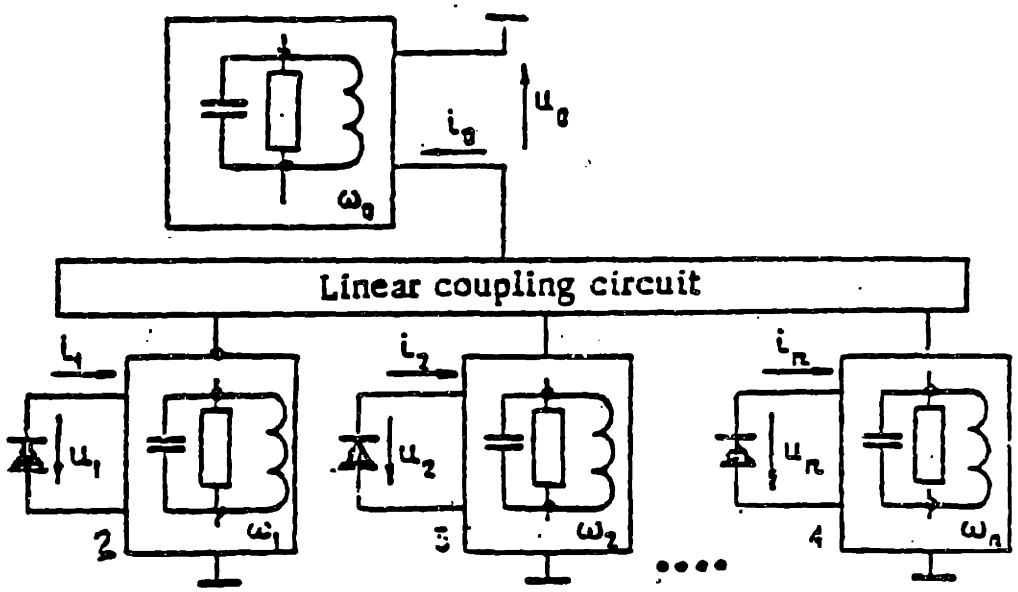

Figure 2.2. Ensemble of oscillators coupled to each other and to a common external resonator, per Reference 6. a) Network equations. b) Network topology.

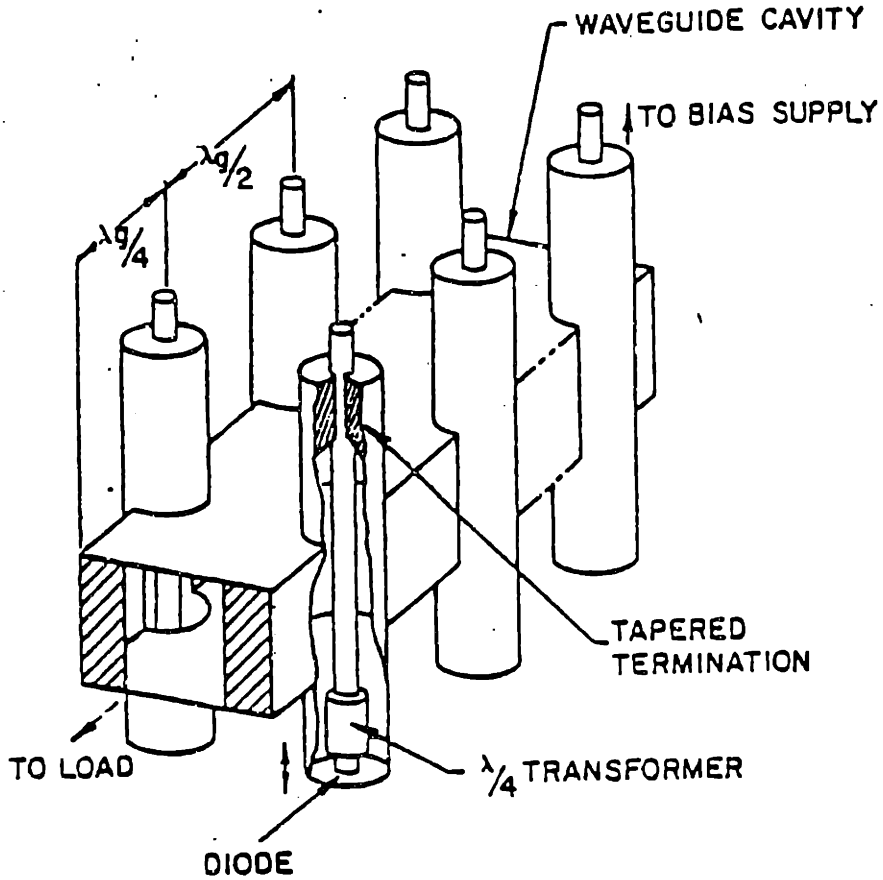

a) Single-cavity multiple-device oscillator.

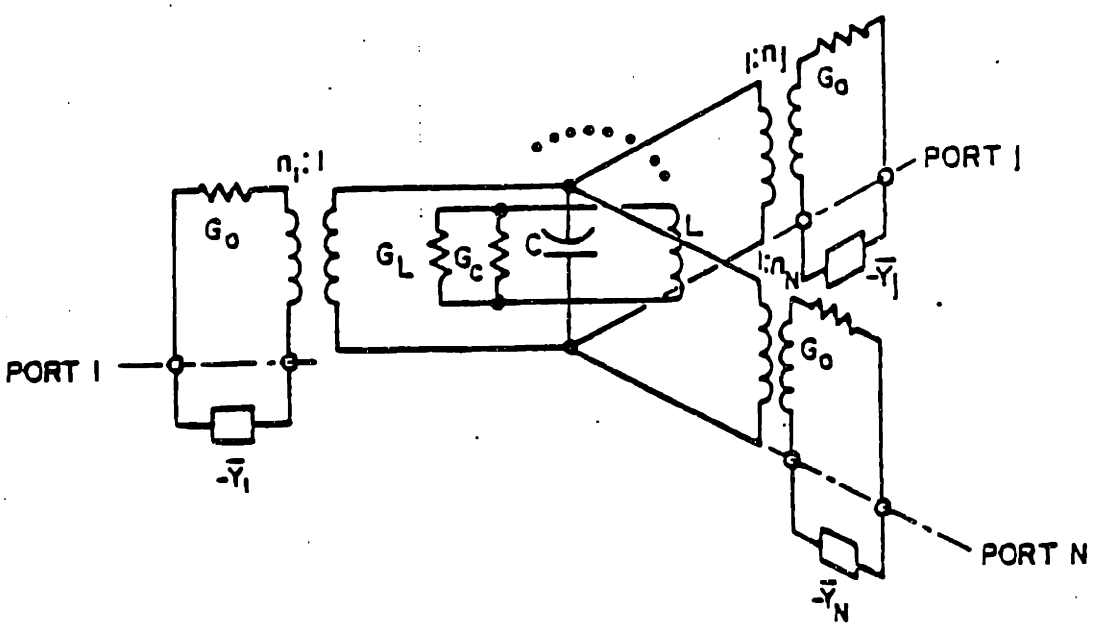

b) Equivalent circuit of the oscillator shown in (a) near each resonant frequency of the cavity. Dots signify the existence of N branches, although only three are shown.

Figure 2.3. Single-cavity multiple device oscillator of Reference 8.

focal plane of the other lens is a spatial filter. The spatial filter is formed by highly reflective strips and "matches" the interference pattern which results when the fields of the lasers in the array are in the lowest-order transverse mode and when the fields are all in phase. Phase-locked results are obtained.

Chapter 3. Model of External Cavity Laser with Coherent Amplifier Array and Multiple Slit Spatial Filter

In this section the particular method investigated in this thesis for obtaining coherent output from an ensemble of lasers is presented. An intuitive picture is given.

The External Cavity Laser with Coherent Amplifier Array and Multiple Slit Spatial Filter, hereafter referred to as the Laser, is illustrated in Figure 3.1. At the right end of the laser is an array consisting of five discrete (non-waveguide-coupled) semiconductor diode lasers which have been antireflection coated on their left facets. These coated lasers are referred to as gain elements. The right facet of each gain element is partially reflective. A lens situated to the left of each gain element collimates the divergent beam emitted from the gain element's left facet. The five collimated beams impinge on the large primary lens and converge onto (and through) the spatial filter. The purpose and details of the spatial filter will be given shortly. The light passing through the spatial filter is collimated by the secondary lens onto the output mirror. (It should be noted that the spatial filter and the five collimating lenses are positioned with respect to the primary lens such that the exact Fourier transform relation holds between the field exiting the collimating lenses and the field incident on the spatial filter. Similarly, the spatial filter and the output mirror are positioned with respect to the secondary lens such that the exact Fourier transform relation holds between the field exiting the spatial filter and the field incident on the output mirror.) The light incident on the output mirror reflects and passes back through the optical system into the array of gain elements. A reflection from the

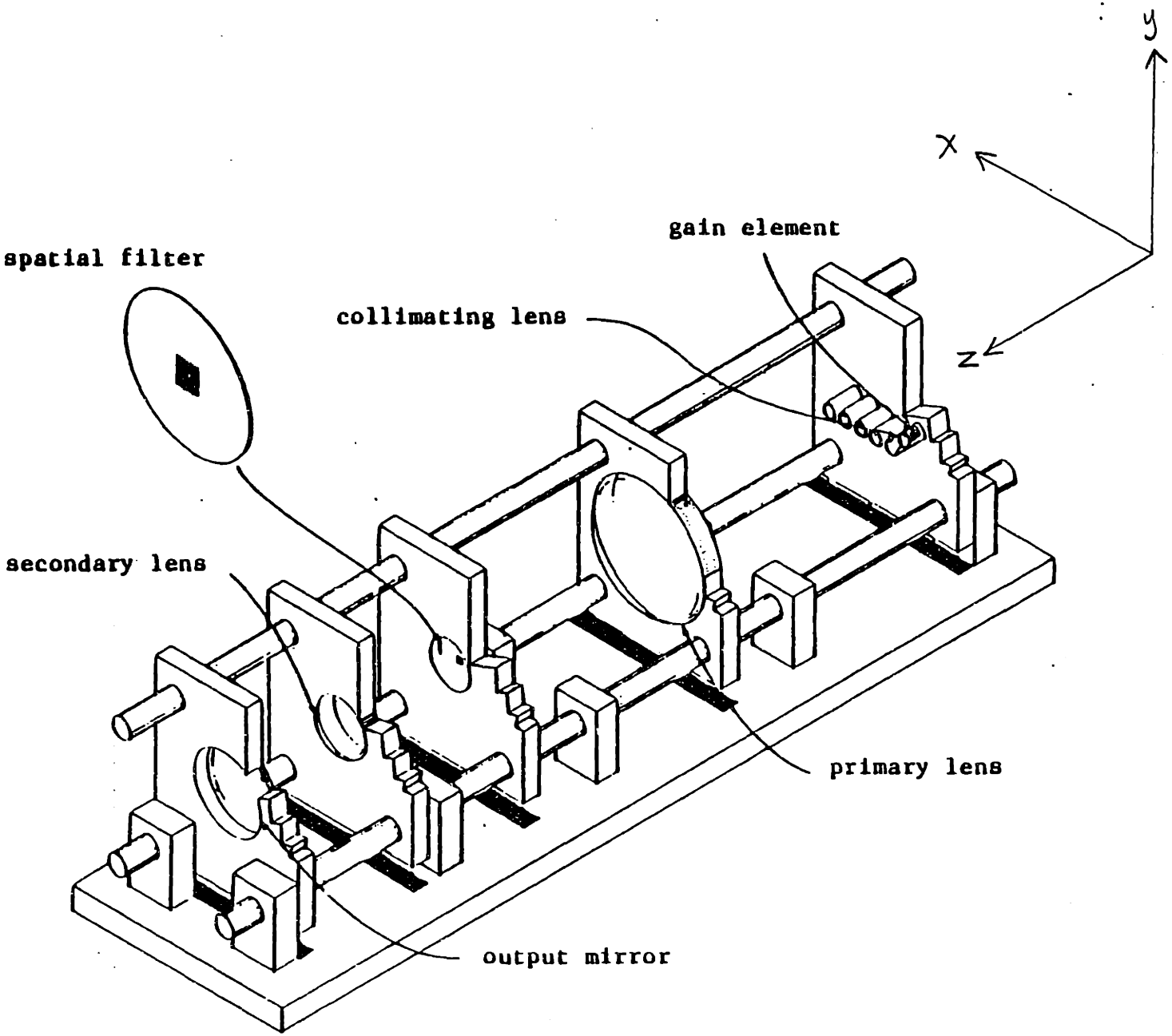

Figure 3.1. Artist's concept of External Cavity Laser with Coherent Amplifier Array and Multiple Slit Spatial Filter.

right facets of the gain elements completes one round trip around the Laser.

In any system of coupled oscillators there must be a mechanism through which the oscillators can exchange energy, or communicate. This is the role played by the spatial filter, Indeed, in the absence of a spatial filter the five beams that converge at the common focus of the primary and secondary lenses would pass through each other; each beam would be "unaware" of the presence of any other beam. The result would be an ensemble of five uncoupled external cavity lasers. Considering the broad gain curve of each gain element, the fine spacing of the external cavity resonances, and possible optical path length differences, it would be quite remarkable if the five lasers operated at the same frequency.

In the presence of the spatial filter the individual lasers are coupled as follows. In the plane where the five beams cross, an interference pattern occurs. When the output from the ensemble of five gain elements are coherent, the interference pattern is stationary. The general appearance is an elliptical envelope subdivided into narrow bright vertical fringes (constructive interference) alternating with broad dark ones (destructive interference). Figure 3.2 shows a cross-sectional plot through the interference pattern along the x-direction, the same direction as the baseline of the gain element array. The broad envelope is a function of the array element shape, while the fine structure is related to the array spacing and the number and weights of elements in the array. For Figure 3.2, five equally weighted elements are assumed. Mention of secondary maxima within the dark fringes is omitted at this point since it would not qualitatively change any conclusion.

The spatial filter is designed to favor a coherent mode of operation

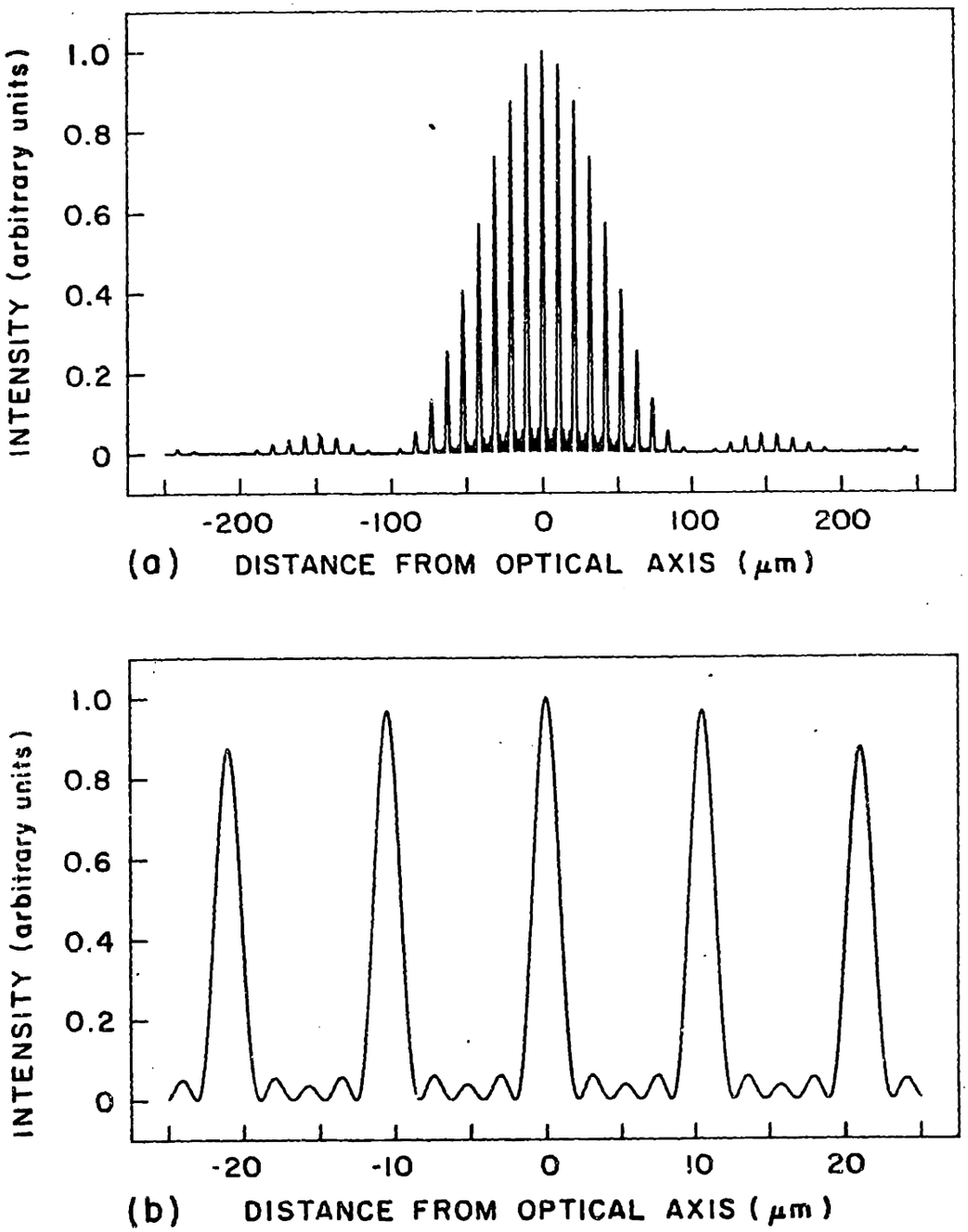

Figure 3.2. a) Magnitude-squared Fourier transform of output of five-element array. Equal excitation, 0.2 cm element width, flat-top element profile, 2.0 cm array spacing, and 0.84 um wavelength are assumed. Abscissa is transverse dimension in focal plane of 25 cm focal length lens. b) Expanded plot of central portion of pattern.

of the ensemble, and to discriminate against an incoherent mode of operation. To that end, the spatial filter is "matched" to the interference pattern just mentioned. That is, the spatial filter is transparent over the bright fringes of the interference pattern and opaque over the dark fringes. When the ensemble operates coherently, the radiation in focal plane is bunched so that it efficiently passes through the spatial filter. On the other hand, when the ensemble of gain elements is incoherent, any interference pattern washes out (when time-averaged). Specifically, there are no dark fringes aligned with the opaque areas of the spatial filter and the light that is instead illuminating these areas is subsequently lost. Application of the maximum emission principle would indicate that the system will adopt a coherent mode of operation, since in this case the radiation from the ensemble passes through the spatial filter more efficiently.

An alternative way of viewing the operation of the Laser is to note that the spatial filter, as described, is an amplitude transmission grating. Each output from a gain element, when focussed onto the spatial filter at the respective angle, gives rise to a multitude of grating orders. Some of these orders fall in the (zero-order) direction of the beams from the other gain elements. Other orders fall outside the acceptance angle of the system and are lost. The radiation is convolved and apertured a second time on the return from the output mirror to the gain elements. Therefore some of the radiation from each gain element is distributed and injected into the other gain elements to act as synchronizing signals. Results have already been cited that show that for near-tuned oscillators free from moding problems, stable locking will occur. It can also be shown that when the (time-averaged) superposition of

all grating orders due to a coherent ensemble of gain elements is considered, the power lost by the system in the form of high grating orders is minimized.

A useful analogy exists in connection with the theory of forced mode locking, a means commonly used to make lasers produce trains of very short pulses. The work of Haus [25] is cited in particular, since he unifies the dual views of mode locking. Consider a laser resonator at one end of which is a lossy element that is modulated by an external periodic signal. In the time domain picture this is the equivalent of a repetitively tripped shutter, open briefly and closed during the remainder of the cycle. In practice the shutter need only close slightly, and the duration of the "on" time is not critical. Given that the laser gain medium and the set of cavity resonances is such that a large number of longitudinal modes will be supported, the phases of the modes will adjust so that the superposition of modes will construct a wave packet bouncing around inside the resonator and timed such that it passes through the lossy element at precisely that moment when its loss is least. This is to be compared to the "bunching" view of the Laser, that the ensemble will adopt a mode of operation such that the radiation bounces in a stationary interference pattern and passes through the spatial filter precisely at the uniformly spaced transparent slits.

In the frequency domain picture of forced mode locking the lossy element is viewed as an AM modulator. The waveform during the modulator is periodic but need not be sinusoidal (simplest case). FM modulation can also be used to achieve modelocking. The action of the modulator on a mode of the cavity is to generate sidebands of definite phase relationship and amplitudes dependent on the harmonic content of the modulation signal.

Because the fundamental modulation frequency equals the longitudinal mode separation, the sidebands from one mode act as synchronizing signals for neighboring modes and phase locking can occur. These modes then have definite phase relationship to the first mode; their sidebands then communicate phase information to their neighbors, etcetera. In this way, all modes are able to co-phase with the first mode. This is to be compared to the "diffraction" view of the Laser, that the spatial filter generates grating orders from the beam from each gain element with definite phase relationship, and that some of these grating orders end up being injected into the other gain elements to lock them.

Although earlier in this chapter a specific output of the gain element array was assumed, à priori, in order to explain the selectivity of the spatial filter towards a coherent vs. incoherent mode of operation, this was in fact an oversimplification. It is not possible to divorce the output of the array from the (round-trip) transmission of the filter. Because the latter constitutes the feedback into the gain elements, the two are interdependent. A solution for the array output must be self-consistent. That is, the spatial filter operates on the transform of the array output and thus influences the feedback to the array. With amplifications dictated by the gain element drive currents and saturation parameters, the feedback, when amplified, must reproduce the assumed solution, both in magnitude and in phase.

Several very basic design considerations of a practical nature bear discussing with regard to the just-mentioned self-consistency requirement. They are mentioned briefly here, and will be discussed more fully in chapters to follow.

The primary and secondary lenses have a finite numerical aperture.

Because the spatial filter is a grating, the focussed output of an array element will give rise to many diffraction grating orders. The finite numerical aperture implies that only a relatively small number of these grating orders remain within the optical system. The others are lost. Moreover, which orders are saved depend on the transverse position of the array element relative to the optic axis. Assuming equal drive currents, which for no filter would lead to equal uncoupled powers, the positional discrimination implied by the system's numerical aperture can be shown, via the self-consistent analysis in Chapter 6, to lead to a tapering-off of power toward the ends of the array. This is not unlike the envelope of the supermode of a finite sized diode laser array [22,23].

Closely related to this, when viewed from another perspective, is the fact that the simple spatial filter discussed is not an exact match to the transform of the output of a coherent 5-element array. Appealing to Figure 3.2, but not ignoring the secondary maxima, it can be seen that some power invariably is lost illuminating the spatial filter. The transmitted light, in a complementary fashion, diffracts. Some of this light escapes the numerical aperture of the system.

If a spatial filter could be designed that completely transmits the transform of a coherent array, but still discriminates against incoherent operation, no diffraction would result. In the alternate view of the spatial filter, the orders arising from any particular element that would escape the system are instead cancelled by appropriately phased orders from the other elements. It should then be possible to obtain coherent operation without the suppressing effect on peripheral power dictated by the numerical aperture.

Some effort was expended in this direction in the course of this

thesis. Instead of designing a spatial filter which would block the secondary maxima in Figure 3.2 with broad opaque strips, an alternative filter was designed. This new design had slits for the secondary maxima as well as the principal ones, with only very thin opaque strips where the transform nulls occurred. Unfortunately, these filters did not survive fabrication. However the formalism developed in Chapter 6 is more than adequate to accommodate this type of filter.

Of practical future interest, the transform of a coherent array simplifies dramatically when the number of elements is increased. Figure 3.3 is a plot of an equally weighted 25-element array with a fill factor (ratio of element width to array spacing) identical to Figure 5.2 but with one-fifth the array spacing, so that the overall array size is maintained. It is clear that fabricating a filter matched to this transform is much easier than in the previous case, since no secondary maxima of significance occur in the intervals between principal maxima. It is not clear, however, nor is it addressed, what special criteria are involved in the design of spatial filters for the transforms of many-element arrays. For example, a certain amount of loss may act as a stabilizing influence, in analogy with coupled systems of oscillators.

Adding a final dimension to the analysis of the external cavity laser, for better or for worse, phase shifts must be considered. Most important are the gain-dependent phase shifts accrued by the circulating fields in the laser as they pass through the gain elements. In order to have self-consistency, the fields must reproduce in magnitude and in phase after each circuit. Although it is easy to satisfy the phase condition in a single gain-element laser, it is not obvious that a solution even exists when five gain elements are involved. In order to satisfy the phase condition it is

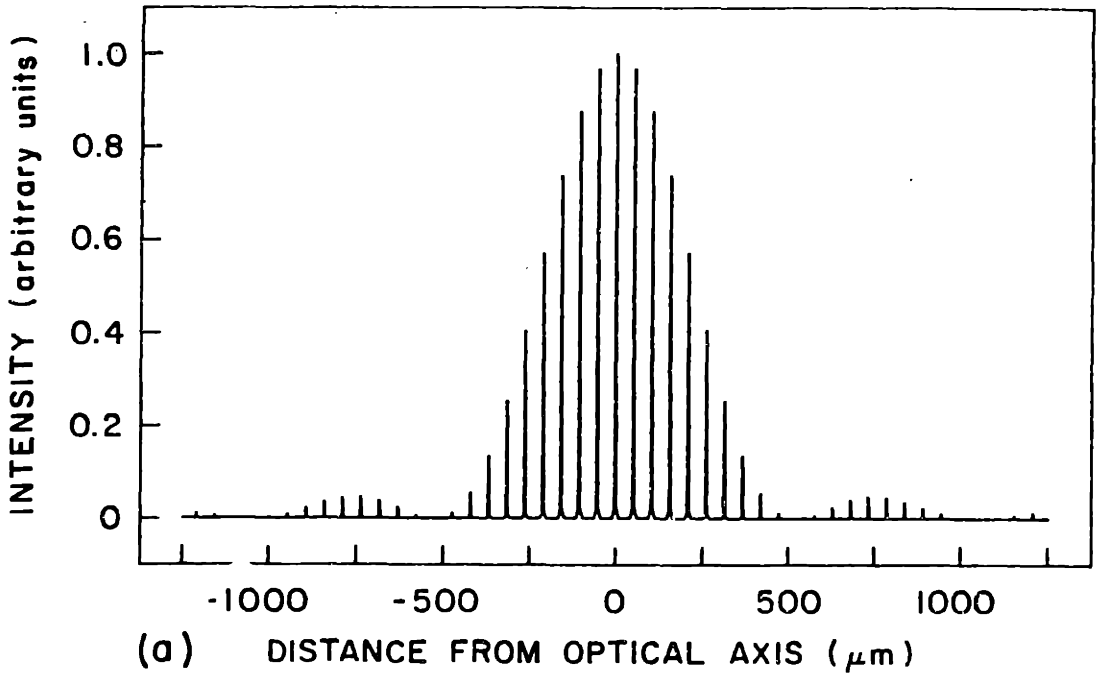

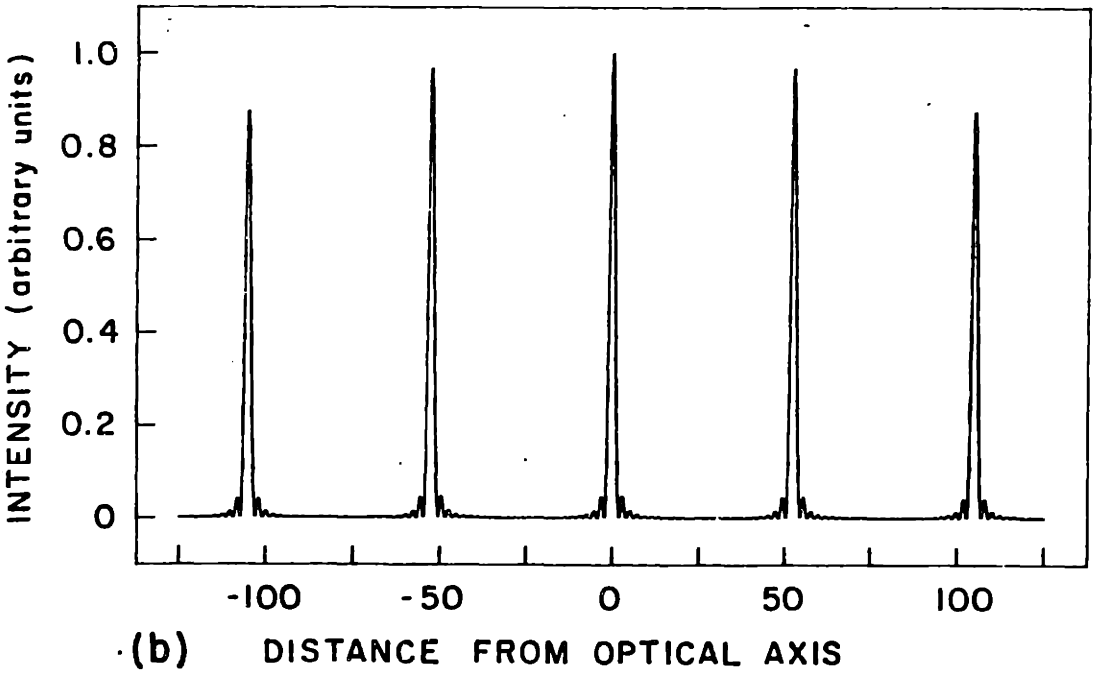

Figure 3.3. a) Magnitude-squared Fourier transform of output of twenty-five element array. Equal excitation, 0.04 cm element width, flat-top element profile, 0.4 cm array spacing, and 0.84 um wavelength are assumed. Abscissa is transverse dimension in focal plane of 25 cm focal length lens. b) Expanded plot of central portion of pattern.

probable that the fields in the laser must be modified.

These are some of the unavoidable factors affecting the operation of the external cavity laser, as opposed to parameters over which there is some control, such as diode current or alignment. Especially relevant is the effect that these factors have on the self-consistent fields and powers that evolve in the laser. Although no experiments are reported in Chapter 5 which investigate the distribution of powers in the laser (in analogy with the shape of a supermode of a diode laser array) the theory in Chapter 6 and the computer model in Chapter 7 are applicable. Incorporated in both are the effects of numerical aperture, the mismatch of filter to interference pattern, and gain-dependent phase.

Chapter 4. Realization of External Cavity Laser with Coherent Amplifier Array and Multiple Slit Spatial Filter

The external cavity laser was designed over a period of six months and included a series of technical meetings at MIT Lincoln Laboratory, at which were typically present the author, his supervisor, a laser expert, an optics expert, and a mechanical engineer. Consideration was given to which parameters were critical, the degree of mechanical control required (micromanipulator or piezoelectric), the incorporation of a temperature control system that would not compromize the mechanical degrees of freedom, etcetera. Concurrently, an alignment protocal was developed by the author. The mechanical drawings, fabrication and assembly were arranged by Lincoln Laboratory under subcontract to the MIT Research Laboratory of Electronics. This phase of the program took approximately six months. A final six month period was required before initial operation of the external cavity laser, with all components and support systems, could take place. During this period it was the responsibility of the author to debug the design and to specify corrective measures that were time and cost effective. One of the major goals of the design of the apparatus, and the experiments performed with it, was to facilitate the determination of which degrees of freedom were needed and where more careful control was required.

An artist's rendering, Figure 3.1, was described from a functional standpoint in the previous chapter. A photograph of the Laser in situ appears in Figure 4.1. A physical description of the Laser is given next.

Referring to Figure 4.1, the Laser consists of five plates supported and aligned by four super-invar rods. The plates are spaced such that exact Fourier transform relations hold between the various elements of the

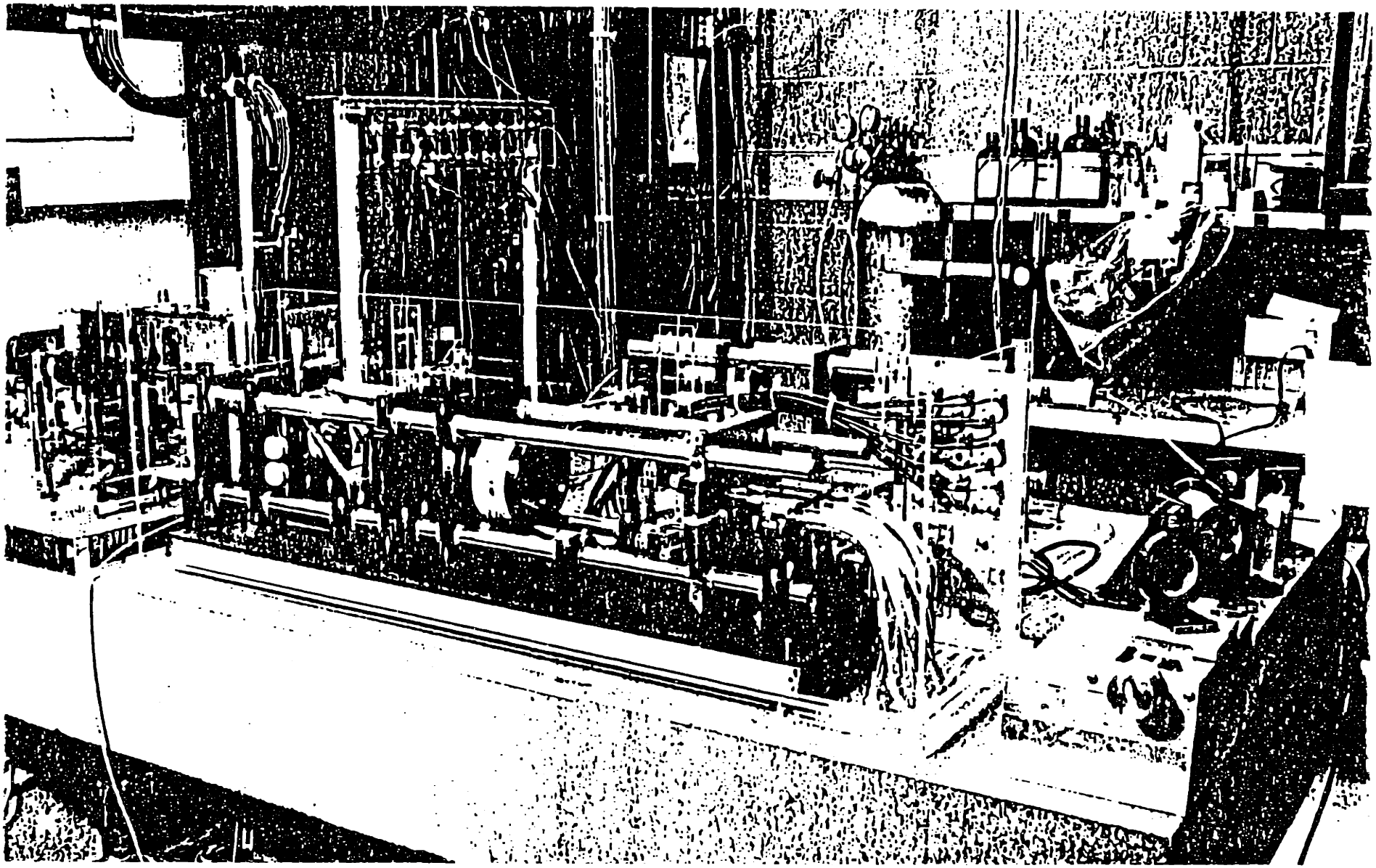

Figure 4.1. Photograph of External Cavity Laser with Coherent Amplifier Array and Multiple Slit Spatial Filter.

Laser, as discussed in Chapter 3. Starting at the right in Figure 4.1, the first plate holds micromanipulators and piezoelectric transducers (PZT's) used to properly orient the five collimator pen subassemblies. The nominal center to center spacing of the collimator pens is 1.98cm. Centering and coarse pitch-yaw adjustments are performed by mechanical micromanipulators. Because the collimator pen outputs must be accurately parallel in order to overlap in the focal plane of the primary lens, fine pitch-yaw adjustments are accomplished with PZT's. PZT's are also used to give slight axial displacements to each collimator pen, thereby controlling the relative phase of the outputs of the collimator pens if necessary. Each collimator pen consists of a gain element (a semiconductor diode laser which has been antireflection coated on one facet) and a collimating optic. The gain elements will be discussed separately. The collimating optic is a 20x microscope objective, its lenses having been transferred to a customized barrel in the interests of compactness and part count reduction. Centering of the diode relative to the collimating optic is performed in a special pre-alignment jig, and then locked, prior to insertion of the collimator pen into the Laser. Final focussing of the collimator optic is done after the pen is in the cavity. Errors in centering persisting past the pre-alignment stage may be corrected by inserting appropriate shims behind the collimator pens until pen parallelism can be attained using the pitch-yaw micromanipulaters. Electrical heaters and temperature sensors are also included in each collimator pen. Heat sinking is provided by a bank of thermoelectric coolers connected to the collimator pens by flexible copper straps so as not to impede the motion of the micromanipulators. The coolers and their associated water supply/return lines are behind (i.e., to the right of) the first plate.

The second plate of the Laser holds the primary lens which focuses the collimated radiation from the gain elements onto the spatial filter. That is, it produces the Fourier transform of the output of the collimator pen ensemble. The primary lens has a 10 cm diameter aperture and a 25 cm focal length, and is antireflection coated for the wavelength range of interest. The only adjustment to lens orientation is the position of the plate along the super-invar rods. Each plate of the Laser includes this degree of freedom, in addition to any explicitly stated motions.

The third plate of the cavity carries the spatial filter. The prototype spatial filter consisted of eleven 3.8 um slits on 10.47 um centers. The slit period, together with the lens focal length and collimator pen spacing, is consistent with an operating wavelength of 830 nm. The filter is produced from a silicon wafer that has been coated with a silicon nitride film on one side. Integrated circuit techniques are used to selectively remove strips from the silicon nitride film down to the silicon substrate and to form a window in the silicon substrate up to the silicon nitride film. The result is a silicon nitride film with slits supported by a frame of solid silicon. For the experiments reported in this thesis, one side of the film is blackened as a final step. Mechanical micromanipulators position the spatial filter at the focus of the primary lens at which point the output from the collimator pens converge. A rotation stage is used to align the slits of the spatial filter parallel to the interference fringes in the transform of the coherent ensemble. A PZT is used for fine adjustment of the spatial filter in a direction perpendicular to the fringes.

The fourth plate of the Laser supports the secondary lens which recollimates the light transmitted by the spatial filter. The secondary

lens has a 3.5 cm diameter aperture and an 8.75 cm focal length. Like the primary lens, it has been antireflection coated. Three translation (xyz) and two rotational (pitch-yaw) degrees of freedom allow the secondary lens to be optimally aligned with respect to the other optical elements in the Laser. The choice of a smaller focal length than the primary lens results in a reduction in the width (and height) of the output of the Laser, permitting the use of smaller, less expensive optics in the diagnostic system.

The leftmost plate of the Laser holds the end mirror assembly. Initial operation was with a 90 percent reflectivity dielectric mirror. The mirror is attached to a piezoelectric aligner/translater containing three PZT stacks that can be driven differentially or in common. It, in turn, is mounted in a gimballed mechanical micromanipulator for coarse pitch-yaw adjustment.

A sixth plate, not shown in Figure 4.1, was used only briefly. Positioned between the collimator pens and the primary lens, this plate carried five independantly tiltable etalons. The plate and its components were designed by the author to integrate with the given overall design of the external cavity laser with a minimum of inconvenience. It was at one time believed that the free-running wavelengths of the collimator pens (in the absence of the spatial filter) needed to be "near-tuned" in order that insertion of the spatial filter would cause locking. However, the lasing spectra of the uncoupled collimator pens were not all single-mode, thus complicating the concept of "near-tuning". The etalons were used to obtain tunable, single-mode spectra. The etalon thickness was .03 cm, although other thicknesses could also have been used. Each etalon was packed into a small aluminum cell and affixed to a tilting sub-plate. Normal incidence

was avoided. One mechanical motion controlled the pitch of each sub-plate. No yaw control was necessary. After the fact, it became evident that etalon tuning was not essential to the coherent operation of the Laser. The time spent on design, fabrication, procurement of components, and actual use of this sixth plate was limited to a five month span.

The gain elements are produced from AlGaAs semiconductor diode lasers supplied by Philips Research Laboratories, Eindhoven. They have a channeled-substrate-planar (CSP) structure [26] resulting in a mode that has negligible astigmatism. The active region is undoped because, à priori, a broad maximum of gain versus wavelength is advantageous when trying to obtain coherent action from a multiplicity of gain elements. (It is of interest to note that diode lasers were supplied by Philips only on the assurance that accurate individual temperature control would be available. Temperature control can be used to control the operating wavelength of a diode laser. As shown in the next chapter, this control was not in fact needed.) The actual devices were made from a channeled n+ substrate with a channel width of 5-7 um at the top and 4 um at the bottom, and a channel depth of 1.3 um. The n-type $Al_{.33}Ga_{.67}As$ cladding layer has a thickness of 1.62 $\pm$ 0.04 um inside the channel and 0.296 $\pm$ 0.06 um adjacent to the channel. The flat active layer has a thickness of 0.10 $\pm$ .02 um. The p-type $Al_{.33}Ga_{.67}As$ cladding layer has a thickness of 3.13 $\pm$ 0.68 um and a p-type GaAs to layer of 0.5 um provides good ohmic contact. The lasers are 250 um long. Each facet is coated with a half-wavelength thickness of Al_2O_3. The lasers are mounted p-side-down on a SOT-148 header. The threshold current and lasing wavelength of each gain element was checked upon receipt from Philips. The lasers were then shipped to a vendor who antireflection-coated one facet of each laser with a quarter-

wavelength thickness of HfO_2. Upon return, the effect of the coating was verified by attempting to measure the increased threshold current. No threshold was observed up to 140 mA, a conservative limit set for laser reliability. To make sure however, that the gain elements were not simply damaged as a result of the coating procedure, each one was inserted into a simple, non-temperature-stabilized external cavity consisting of the gain element, a microscope objective, and a partially reflecting mirror. Lasing was obtained. Typical values for the threshold currents were: 86 mA as received from Philips , >140mA after deposition of the antireflection coating, and 88mA in the simple external cavity.

Several equipment groups are needed as support systems for the operation of the laser. The electrical system consists of low-ripple power supplies to drive the gain elements. Each gain element is protected by a noise filter to guard against transients on the line. Also included in the electrical system are high-voltage power supplies to drive the pitch-yaw PZT's on the collimator pen mounts, the lateral motion PZT on the spatial filter mount, and the 3-element PZT aligner-translater in the end mirror mount. The temperature control system consists of a plexyglass cover for the Laser (which also afford some acoustic isolation), a closed-loop water system (pump up, gravity-feed down) to absorb heat that the thermoelectric coolers pull out of the collimator pens, a high-current power supply to run the thermoelectric coolers, and the temperature controller itself. The controller is actually five separate temperature controllers, one per gain element. (Collaborators at Lincoln Laboratory contributed the printed circuit boards, but development of the boards into a finished product took place under the day-to-day supervision of the author.) Each controller processes the signal from the temperature sensor incorporated into the

collimator pen, compares it to a reference, and generates a proportional/integral feedback signal which is applied to the heater inside the collimator pen. The circuit on which the controller is based has been known to stabilize the temperature of a diode laser to 3×10^{-4} ^{o}C. The range of each temperature controller in its present implementation is approximately $20^{o}C$. For a standard diode laser, this would amount to control of the operating wavelength over a 5 nm range.

Chapter 5. Experimental Studies

In this chapter are documented initial experimental studies on the external cavity laser. The emphasis in these studies was to define broad, global behavior of the device, rather than to analyze anomalous effects that may be due to causes beyond practical control (e.g. nonuniformities between diodes, or imperfect antireflection coatings). The distinction is admittedly a gray one, since the utility of the device may ultimately be limited by one's ability to eliminate these anomalies.

Initial measurements will be described that quantify the diode lasers that were used in the external cavity lasers, both before and after anti-reflection coating. A chronology culminating in the first successful operation of the external cavity laser follows with discussion. The various spatial filters which are used in the main body of experiments are described, both in construction and in organization. Experimental results are presented which investigate the interaction of spatial filter parameters with other operational parameters. The object of scrutiny in most cases is the output spectum of the external cavity laser. In particular, it is found that coherent operation is easily obtained, although a tunable monochromatic spectrum does not necessarily follow from this. In one case though, an instrument limited linewidth of less than 7.5 MHz is obtained. Finally, a comprehensive discussion of the observed behavior of the laser is presented, wherein many of the principles by which the external cavity laser operates are clarified and refined.

5.1 Preliminary Measurements

The gain elements for the external cavity laser were received as

semiconductor-diode lasers, and were quantified before being anti-reflection coated. Basic characteristics of the diode lasers are summarized in Table 5.1. A typical spectrum appears in Figure 5.1. After anti-reflection coating, the gain elements were operated in the external cavity, but with no spatial filter present. Results are summarized in Table 5.2. A comparison can establish upper bounds for coated facet reflectivity, coupling between gain element and external reflection, etc., but only after additional parameters are determined, such as the relationship between unsaturated gain and injection current.

The latter measurement (gain versus current) requires an anti-reflection coated gain element but no external reflection. The technique is described by Kaminow [27], and consists mainly of recording the fringe contrast of a series of superluminescent diode spectra taken at different injection currents. Typical raw data is shown in Figure 5.2, and the relevant measured values are given in Table 5.3. Analysis of this data is deferred until later.

Temperature control of the gain elements was exercised to a limited degree. In most cases the intent was to stabilize the temperature to within $1^{o}C$, a very easily achieved goal. It was not necessary to null the error signal to the temperature controller (i.e., close the loop), but merely to have the heaters and coolers operating in the presence of the ambient heat leaks. Without this control, the diode heat sink would undergo a temperature rise of several degrees over several hours. There are a number of reasons to want to avoid this temperature change: thermal misalignment of the gain element; refractive index shift which could alter the operating point of the locked system; gain shift in both magnitude and in spectrum.

DIODE LASER NUMBER	THRESHOLD CURRENT	ABOVE-THRESHOLD SLOPE	TYPICAL WAVELENGTH		CURRENT USED FOR SPECTRUM
1	82.5 mA	.143 mW/mA	831.3 nm	@	89.9 nm
2	81.5 mA	.139 mW/mA	833.3 nm	@	89.0 mA
3	94.0 mA	.109 mW/mA	834.5 nm	@	104.4 mA
4	93.0 mA	.109 mW/mA	836.4 nm	@	103.0 mA
5	79.0 mA	.147 mW/mA	832.9 nm	@	86.3 mA

Table 5.1. Operating characteristics of diode lasers. Values were obtained at ambient temperatures. The lasers were later antireflection-coated to be used as gain elements in the external cavity laser.

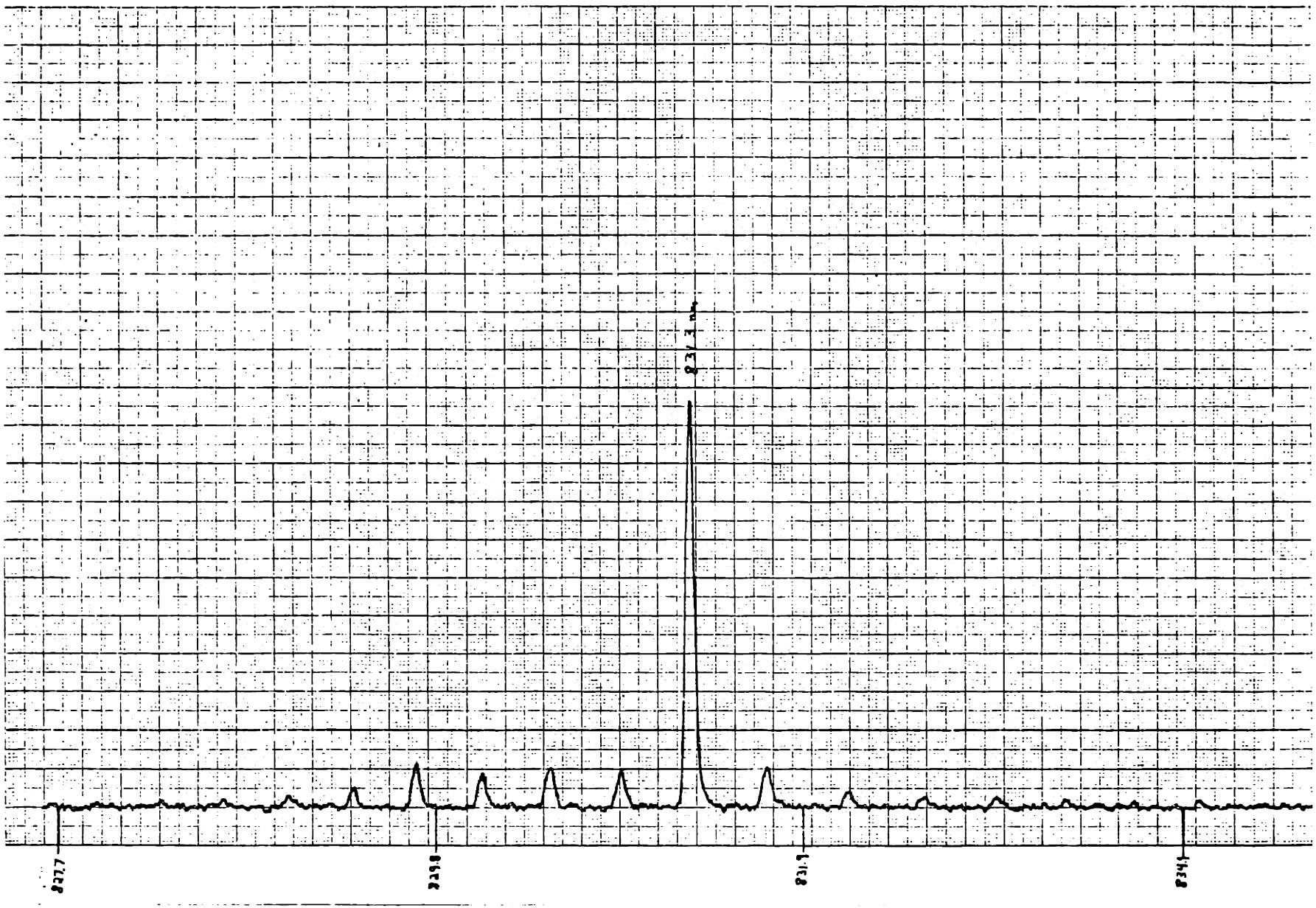

Figure 5.1. Typical spectrum of diode laser later converted to use as a gain element for the external cavity laser.

EXTERNAL CAVITY A = 20X MICROSCOPE OBJECTIVE + 90%R END MIRROR

EXTERNAL CAVITY B = 20X MICROSCOPE OBJECTIVE + 25 CM FL PRIMARY LENS
+ 8.75 CM FL SECONDARY LENS + 90%R END MIRROR

EXTERNAL CAVITY C = 20X MICROSCOPE OBJECTIVE + 25 CM FL PRIMARY LENS
+ 8.75 CM FL SECONDARY LENS + 50%R END MIRROR

EXTERNAL CAVITY D = 20X MICROSCOPE OBJECTIVE + 25 CM FL PRIMARY LENS
+ 8.75 CM FL SECONDARY LENS + 30%R END MIRROR

DIODE LASER NUMBER	EXTERNAL CAVITY TYPE	THRESHOLD CURRENT	ABOVE-THRESHOLD SLOPE	TYPICAL WAVELENGTH		CURRENT USED FOR SPECTRUM
1	A	80.0 mA	.011 mW/mA	830.1 nm	@	97.4 mA
2	A	92.5 mA	.019 mW/mA		-	
3	A	-	-		-	
4	A	86.0 mA	.011 mW/mA	836.7 nm	@	97.8 mA
5	A	89.0 mA	.021 mW/mA	831.1 nm	@	99.5 mA
1	B	91.0 mA	.008 mW/mA	831.8 nm	@	100.0 mA
2	B	83.0 mA	.008 mW/mA	834.7 nm	@	92.0 mA
3	B	94.0 mA	.005 mW/mA	835.1 nm	@	108.0 mA
4	B	93.0 mA	.007 mW/mA	837.9 nm	@	108.0 mA
5	B	80.0 mA	.008 mW/mA	833.6 nm	@	88.0 mA
1	C	-	-		-	
2	C	90.0 mA	.052 mW/mA	833.9 nm	@	105.0 mA
3	C	102.0 mA	.039 mW/mA	834.4 nm	@	123.0 mA
4	C	99.0 mA	.050 mW/mA	837.2 nm	@	115.0 mA
5	C	-	-		-	
1	D	-	-		-	
2	D	101.5 mA	.100 mW/mA	831.2 nm	@	112.0 mA
3	D	110.0 mA	.071 mW/mA	833.9 nm	@	126.0 mA
4	D	108.5 mA	.085 mW/mA	835.3 nm	@	120.0 mA
5	D	-	-		-	

Table 5.2. Operating characteristics, after antireflection coating, of gain elements used in various external cavities. Values were obtained at ambient temperatures and were sensitive to changes in cavity alignment.

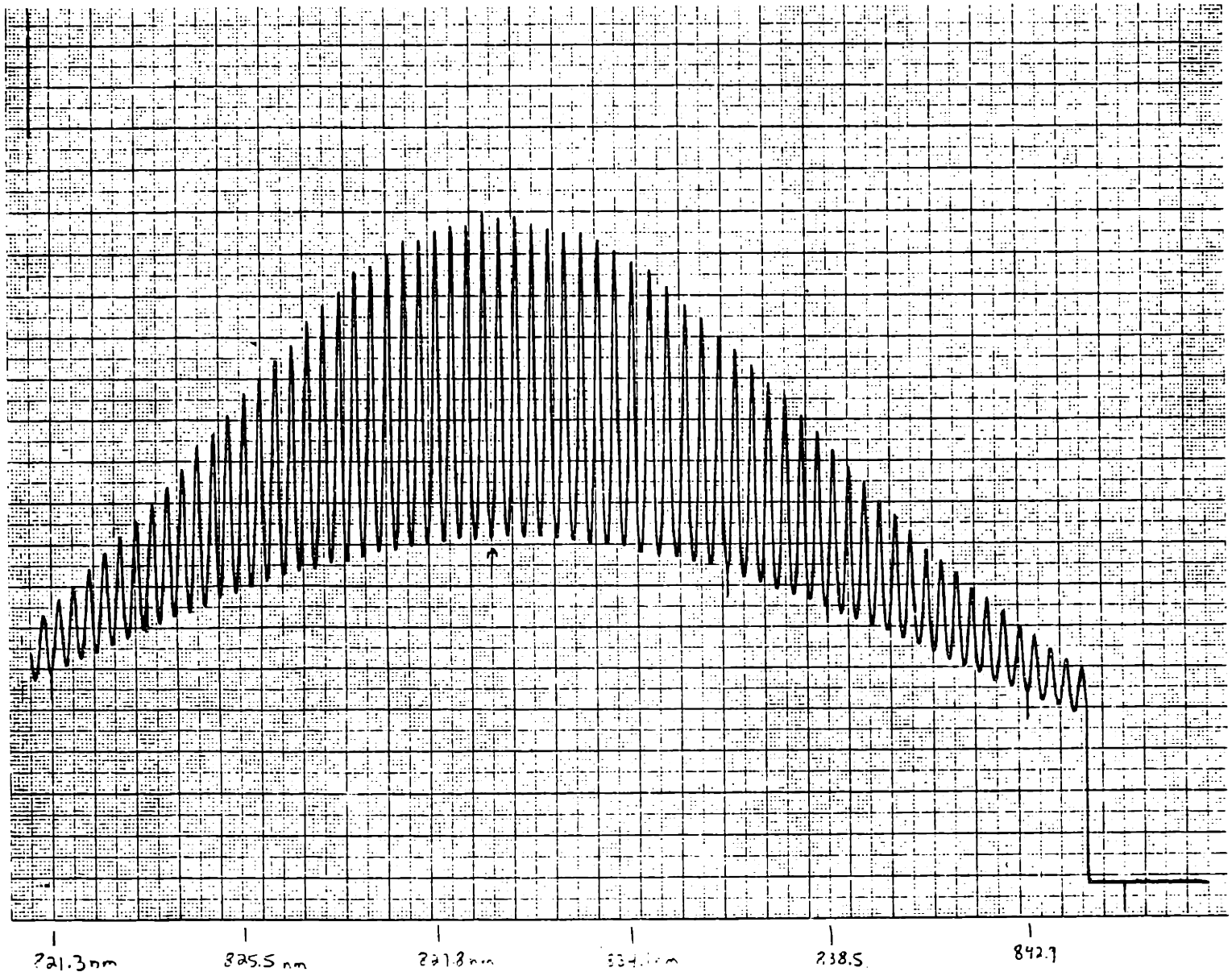

Figure 5.2. Example of superluminescent diode spectrum measured to determine dependence of unsaturated gain on diode current.

GAIN ELEMENT NUMBER	LOG $[(PMAX/PMIN)^{.5}-1]/[(PMAX/PMIN)^{.5}+1]$				
	@ 60 mA	@ 80 mA	@ 100 mA	@ 120 mA	@ 140 mA
1	-4.644	-3.447	-2.506	-1.740	-1.093
2	-4.656	-4.025	-3.176	-2.345	-1.541
3	-4.836	-4.052	-3.138	-2.262	-1.551
4	-4.857	-3.684	-2.702	-1.816	-1.076
5	-4.373	-3.476	-2.769	-1.976	-1.184

Table 5.3. Data from analysis of superluminescent diode spectra. For each diode the spectrum is recorded at five different currents. Figure 5.2 is a typical result. Near linecenter, the maximum and minimum values of the spectrum are measured. The analyzed data can be related to the internal gain of the diode, as discussed in Chapter 6. From this data the normalization current which appears in the theoretical model is determined to be 24 mA.

Occasionally, precise temperature control was used. The necessity for this control, with stability measured in millidegrees, was assumed from the outset, but was abandoned soon after the first successful operation of the device. On the one hand, the external cavity laser can be thought of as a frequency locking experiment, and as such, it may be necessary to accurately control the temperatures of the gain elements in order to "near-tune" the free-running wavelengths so that subsequent interaction (supplied by the spatial filter) will lock them. On the other hand, the gain of each gain element is inherently broad, so that the problem of obtaining overlap of the gain spectra ceases to be an issue. It is the latter view that prevails.

As originally received, and at a single-ended power output of about 1 mW, diode laser output spectra consisted of 1-3 modes separated in wavelength by intervals consistent with the 250 um length of the diode (Figure 5.1). After anti-reflection coating, and with the gain elements operating uncoupled in the external cavity, this situation persisted, namely, spectra consisting of 1-3 modes separated by the original Fabry-Perot spacing of the diode. The presence of a feature traceable to the optical length of gain element is evidence of a less than perfect anti-reflection coating. Residual reflectivity of the front facet is tantamount to an etalon being placed inside the external cavity. Although the finesse of a passive etalon with reflectivities of 32 percent at one facet and 0.5 percent, for example, at the other facet, is indeed low, it must be remembered that in the case of a gain element, the medium between the facets is not passive, and the overall finesse can be considerable [28]. This leads to modulation of gain spectrum and definition of isolated islands of gain in wavelength space. Although the spectra were multimode,

temperature tuning behavior was comparable to single frequency diode lasers [29], for which the modes shift at typically .06 nm/^{o}C while the average wavelength shifts at typically .25 nm/^{o}C.

5.2 Operation with Prototype Spatial Filter

The protocol leading up to the first successful operation of the external cavity laser dictated coincident free running wavelengths; but since without a spatial filter the five uncoupled lasers produced multimode spectra, the concept of coincidence was meaningless. Therefore, 300 um etalons were inserted into cavity, one per gain element. By using etalons it was possible to obtain single-mode (to the resolution of the spectrometer) free-running spectra. The etalons were able to select modes but not tune them. Temperature control could tune a mode wavelength, but without re-tilting an etalon to keep one of its passbands centered on this wavelength, a mode-hop would ensue. However, by iterating temperature control with etalon tilting, tunable single-mode spectra were obtained.

After tuning the single-mode spectra into coincidence the prototype spatial filter was inserted. The duty cycle of this filter, that is, the ratio of slit width to slit period, was later judged to be about .38. With little trouble single-mode lasing was obtained, but a subsequent spectrum indicated that the wavelength had shifted 3.2nm, corresponding to four free spectral ranges of the etalons. It was then suspected that etalons and temperature control were not essential to the external cavity laser. The etalons were removed, the free-running spectra resumed their distinct multimode character, and temperature control was used only to stabilize operating points, not to tune. Successful operation was obtained without these measures previously used to influence the behavior of the uncoupled

lasers. It should be stressed, though, that the gain elements were all from the same wafer, and the active regions were undoped in order to broaden the gain curve, in anticipation of gain-overlap requirements. It is reasonable to assume that these latter considerations aided significantly in obviating the need for the former tuning facilities.

Further results utilizing the prototype spatial filter have appeared in the literature [30]. Appendix A is a reprint of this work. The reader is strongly urged to refer to this appendix for the physical and operational summaries of the external cavity laser which have been omitted here. One of the most important qualities of any laser, along with spectral content and differential quantum efficiency, is power output. As noted in Appendix A , there was a power loss of 60 percent upon insertion of the spatial filter into the free-running system. This is clearly a concern since one of the major goals of the project under which this research was conducted is the development of a high power optical source. As such, any source of power loss is undesirable and must be avoided, if possible. Therefore, power loss must be studied and understood.

The above cited figure of 60 percent loss must be seen for what it is, namely, a single datum which is a function of a multitude of factors. Some of these factors are related to the dimensions of the filter or the alignment of the system. To consider another factor, the following digression is made in the form of an analogy:

For a typical laser at constant drive, the change in power induced by the insertion of a loss is well understood. The loss changes the laser threshold, and lasing ceases. Loss insertion also changes the external differential quantum efficiency, proportional to the slope of the output versus drive characteristic above threshold. If the loss is not so great

as to cause cessation of lasing, the loss in power would equal the shift in threshold times some average of the new and old slopes.

In the case of the external cavity laser with multiple gain elements and a spatial filter, the matter is not so simple. It would be desirable to say that power loss is a combination of changes in threshold and changes in slope. However, the meanings of these terms are brought into question. In a simple laser, the term "threshold" implies a minimum value for the single drive supplied to the device, above which stimulated emission is the predominant mode of transition; and the slope is the derivative of output with respect to this drive. In the external cavity laser, one of the degrees of freedom is individual control of gain element drive. Depending on the values of four gain element currents, the onset of stimulated emission can take place at different values of the fifth current. Similarly, the derivative of output with respect to any one current depends on the other four as well. In summary, although a drop in power is one of the easiest measurements to make, its interpretation is one of the most difficult.

5.3 Advanced Spatial Filters

The prototype spatial filter was necessary in order to debug various technological issues concerned with its manufacture; also to verify at the earliest possible opportunity the feasibility of obtaining coherent output from a multiplicity of diode lasers by utilizing a spatial filter. After this it was topical to explore the effects of different spatial filters on the operation of the external cavity laser. Using the same technology as for the prototype, two wafers, each consisting of ninety-six spatial filters, were produced. A redundancy of three was used to increase the

odds of obtaining at least one filter of each variation, in the face of random defects which would disqualify that wafer from use. Also some filters which appeared on one wafer also appeared on the other, because since the wafers were processed separately, the possibility of systematic variations was great. However, if filters on distinct wafers, nominally identical, gave identical performances, the entire filter group on one wafer would "connect" with the filter group on the other wafer. In addition, several "filters" were actually apertures of assorted dimensions, useful in system alignment. All told, there were approximately fifty distinct spatial filters which could theoretically be used for locking, split over two wafers.

Parameters for the spatial filters were verified as follows: Spatial filter periods could be checked under a microscope with an accurate reticle using a vernier type observation (e.g. 9 filter periods=19 reticle divisions at 5 um per division; so 1 period = 10.56 um). The duty cycle could be estimated by observing the diffraction pattern of these spatial filters under spontaneous emission illumination from the on-axis gain element, and noting which maxima were "missing" (e.g., a 50 percent duty cycle filter will be missing the $\pm 2, \pm 4, \pm 6, \ldots$ orders in the diffraction pattern).

The basic design criterion for the spatial filter is to match, to a greater or lesser degree, the interference pattern formed in the focal plane between the primary and secondary lens under coherent operation. Ideally, the interferance pattern is periodic, with narrow bright fringes alternating with broad dark fringes delimited by an area corresponding to the focal spot produced by the emission of any one gain element. Accordingly, many of the spatial filters fell into one or more filter

progressions: constant duty cycle and number of slits, variable period; constant period and number of slits, variable duty cycle; and, constant period and duty cycle, variable number of slits.

One progression of seven filters (30 percent nominal duty cycle, 41 slits, period ranging from 10.42 um to 10.78 um) systematically failed in this early effort. At the very least, underetching resulted in duty cycles that were close to half the specified value; in worse cases, underetching resulted in large areas of unremoved silicon substrate, obscuring central portions of filters and rendering them useless. This problem could be remedied by changing the wafer processing in the future. Another subset of filters was designed to pass some of the secondary maxima within the dark fringes of the interferance pattern. This necessitated slit widths and slit separations (edge-to-nearest-edge) of approximately 1 um. These filters too, failed, but in this case it was because of breaks in the strips of silicon nitride film defining the spatial filter slits, or because of adhesions between adjacent strips. The integrity of the technology had not been guaranteed for film strip widths narrower than 2 um, so it was not surprising when these structures were defective.

Of the remaining spatial filters, three progressions in particular are discussed. All had sufficient numbers of slits to amply cover the illuminated area of the focal plane. Series A had a constant 70 percent duty cycle, with periods ranging from 10.42 um to 10.78 um in steps of .06 um. Series B had a constant period of 10.60 um with nominal duty cycles ranging from 30 to 80 percent (a filter with a 20 percent duty cycle was not used because of vestigial substrate obscuring the central area). Series C had a constant 50 percent duty cycle, with periods ranging from 10.36 um to 10.96 um in steps of .12 um. Series A and B were produced on

one wafer with a silicon nitride thickness of 0.27 um; series C was produced on another wafer with a film thickness of 0.55 um.

5.4 Five-element Array Operation with Advanced Spatial Filters

Up to this point, whenever lasing took place with a spatial filter inside the external cavity, it was accompanied by a monochromatic spectrum recorded on the spectrometer. This seemed quite natural, since wavelength, array spacing and primary lens focal length determine interference pattern period; conversely, spatial filter period, primary lens focal length and array spacing define a specific wavelength. Reasoning with a quiet, homogeneous model of the laser would indicate that all things being equal, the laser wavelength should evolve to that unique value that results in an interference pattern with a period exactly equal to the spatial filter period. This implied the ability to tune the external cavity laser wavelength by using filters with different periods.

After considering the bandwidth of the gain elements though, it would not be reasonable to expect the laser wavelength to track over the entire series of filters. Assuming a 25 cm focal length and a 1.98 cm gain element spacing, the Series A spatial filters cover a range in wavelength from 825.3 nm to 853.8 nm in steps of 4.8 nm; Series C covers 820.5 nm to 868.0 nm in steps of 9.5 nm. However, it might be expected that the wavelength would track a limited number of filters in each sequence.

What was found , however, was very different from this. With a 90 percent reflectivity end mirror, and currents set so that without a spatial filter the uncoupled lasers produce 0.2 mW each out through the end mirror, the Series A spatial filters (70 percent nominal duty cycle) were inserted. The filter periods ranged from 10.42 um to 10.78 um. The duty cycle was

later empirically estimated to be close to 50 percent. As before, there was a drop in power, but only 40 percent as opposed to 60 percent. This made sense in that the previous filter was opaque over a greater fraction of its cycle. Also the previous filter consisted of only eleven slits covering slightly more than 100 um; this was sufficient for most of the focal spot but there was, in all likelihood, energy extending beyond this which was lost on opaque areas adjacent to the filter.

When the spectrum was recorded, the spectrum was multimode, as opposed to the single-mode spectrum recorded earlier (Appendix A) wherein a spatial filter with a smaller duty cycle was used. Although this result was unexpected at the time, it can be understood and explained by the discussion which follows in this chapter and the theory which appears in the next. Moreover, the spectrum was a strong function of the alignment.

Spectra resulting from individual spatial filters are shown in Figure 5.3. In Figure 5.4 the average wavelength, (i.e., centroid of the spectrum) is plotted against the spatial filter period. Initially after insertion of the spatial filter the average wavelength had a value consistent with Figure 5.3a. Peaking of the piezoelectric transducers resulted in the spectrum of Figure 5.3b. The spatial filter period had not changed but the average wavelength was now considerably shorter. As the spatial filter period was increased, the average wavelength jumped toward longer values and for the final two filters did not greatly change from this. It will be the rule rather than the exception in the remainder of thesis chapter to discuss the average wavelength of operation, since frequently the observed spectra are multimode.

Because the duty cycle was the same for the whole series, while the prototype filter yielded single-mode behavior, it was hypothesized that the

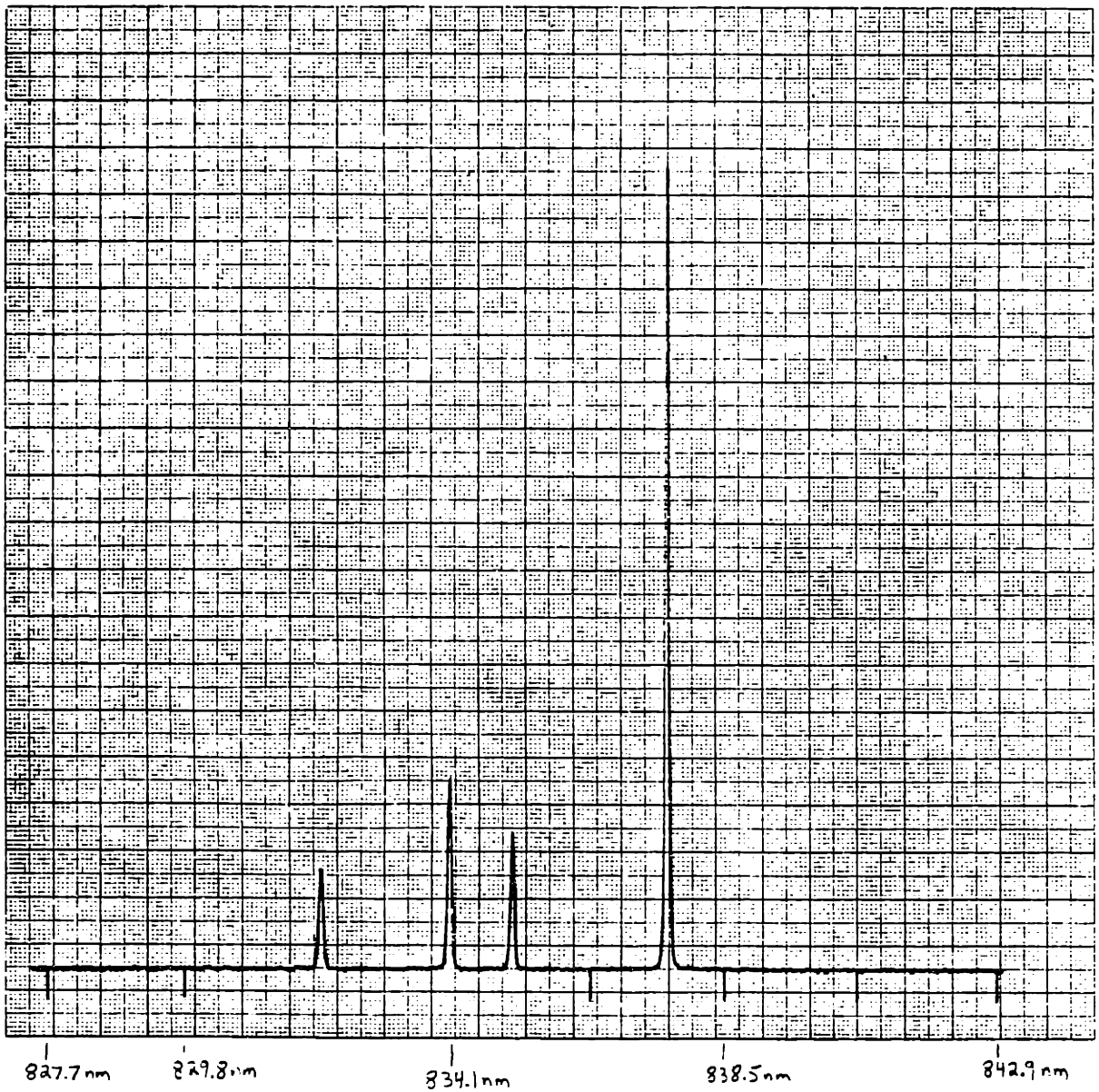

Figure 5.3a. Output spectrum of external cavity laser with five powered gain elements, 90 percent reflectivity end mirror, 70 percent (nom.) spatial filter duty cycle, 10.42 um spatial filter period. Average wavelength is 836.30 nm.

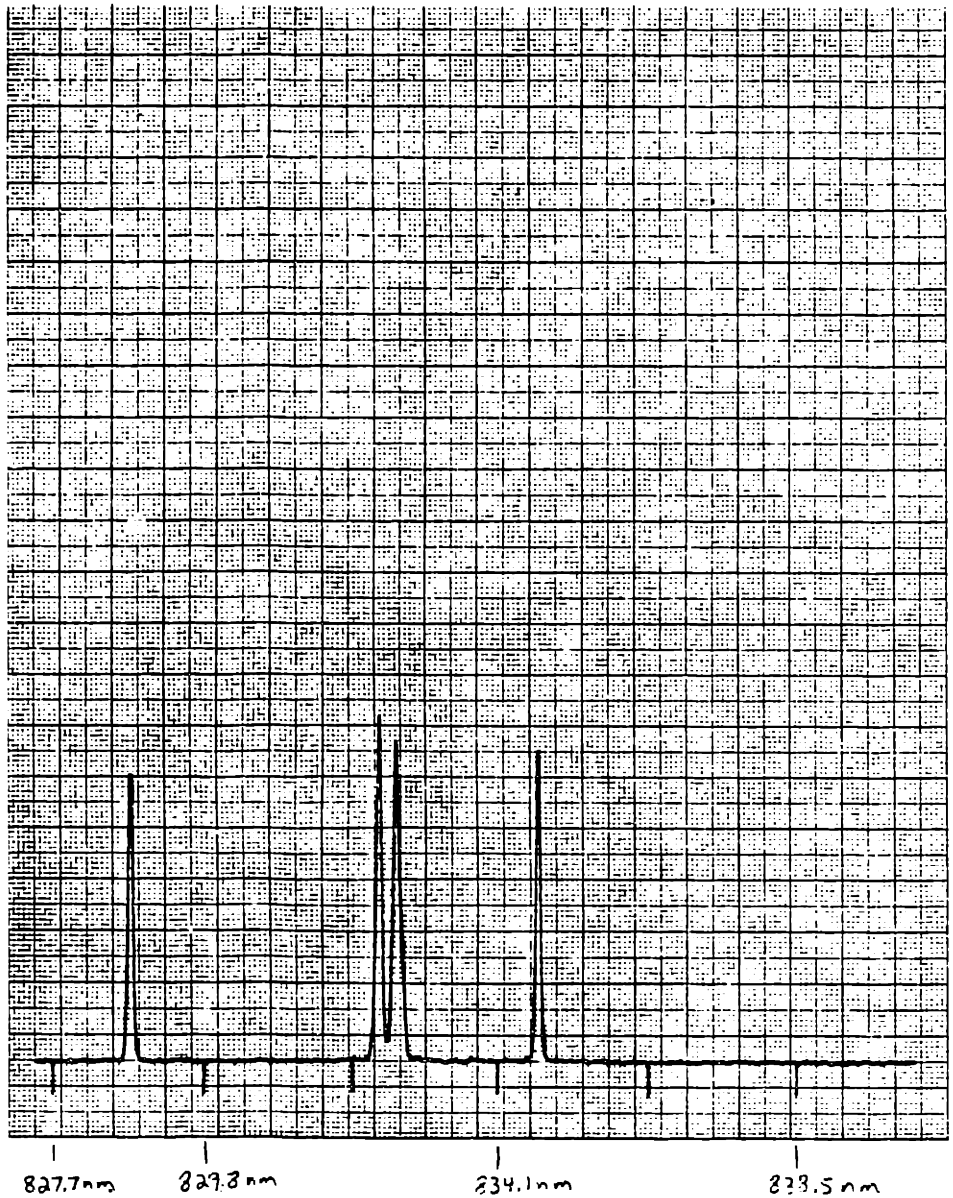

Figure 5.3b. Output spectrum of external cavity laser with five powered gain elements, 90 percent reflectivity end mirror, 70 percent (nom.) spatial filter duty cycle, 10.42 um spatial filter period. Average wavelength is 832.21 nm.

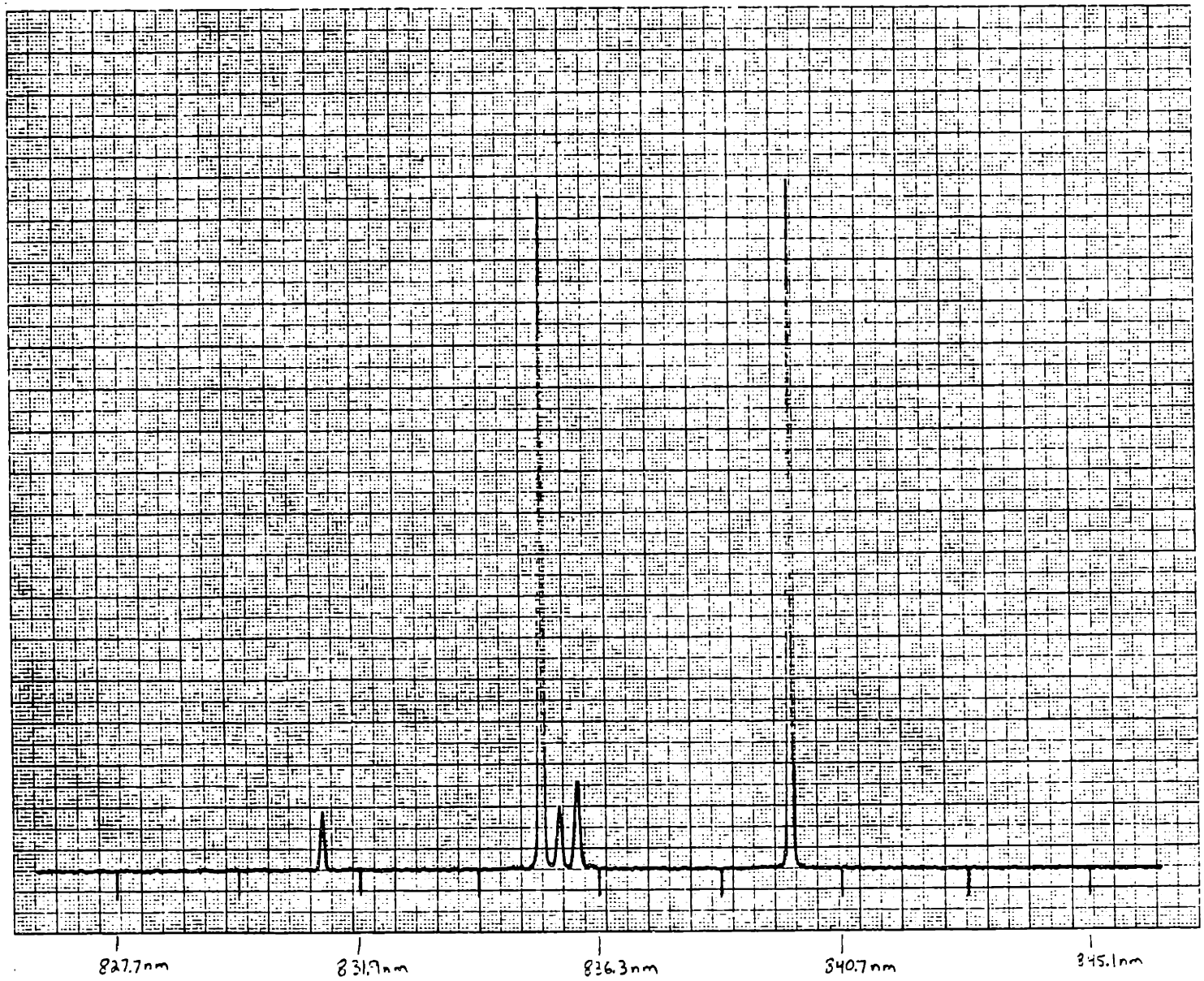

Figure 5.3c. Output spectrum of external cavity laser with five powered gain elements, 90 percent reflectivity end mirror, 70 percent (nom.) spatial filter duty cycle, 10.54 um spatial filter period. Average wavelength is 837.17 nm.

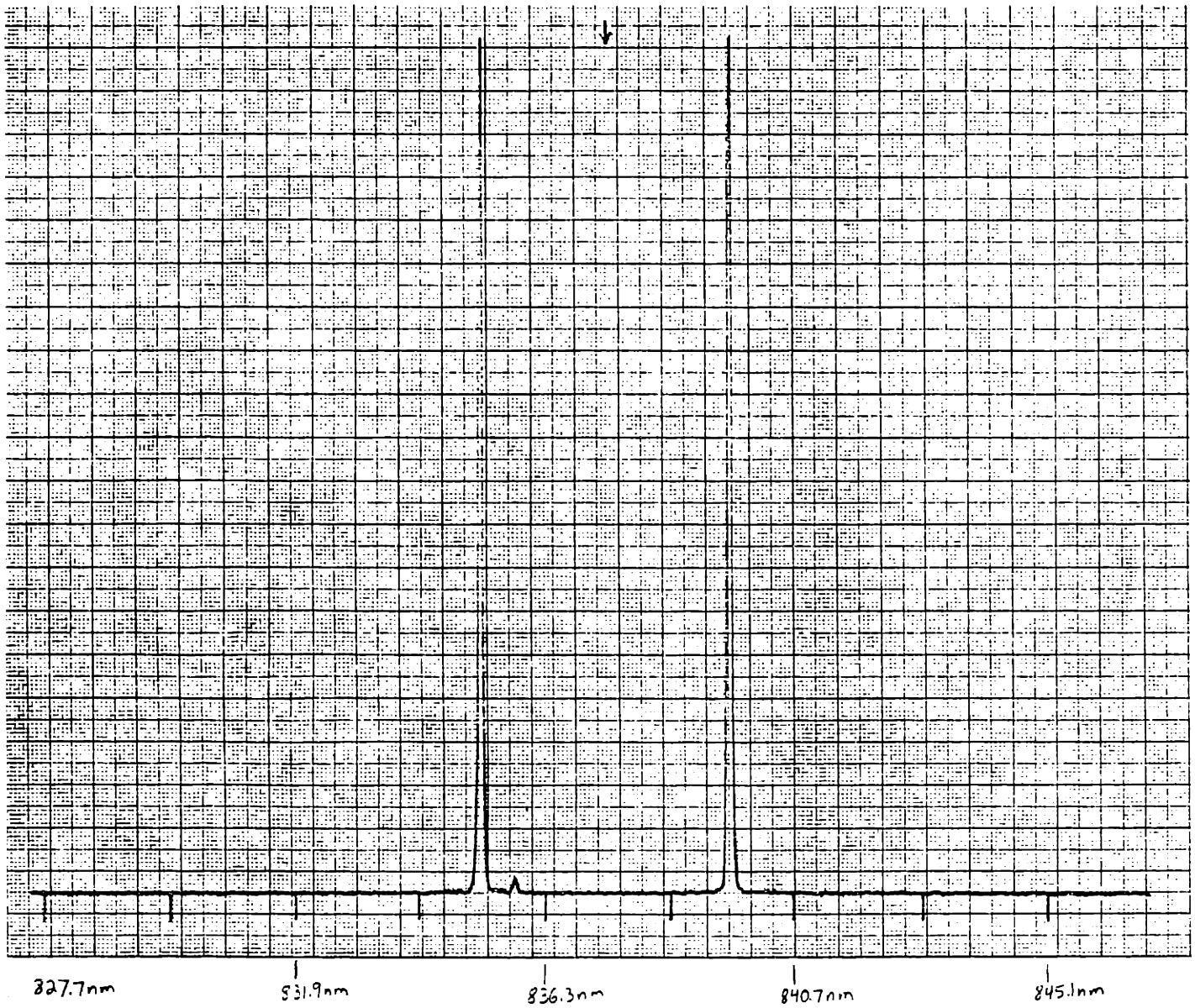

Figure 5.3d. Output spectrum of external cavity laser with five powered gain elements, 90 percent reflectivity end mirror, 70 percent (nom.) spatial filter duty cycle, 10.66 um spatial filter period. Average wavelength is 837.37 nm.

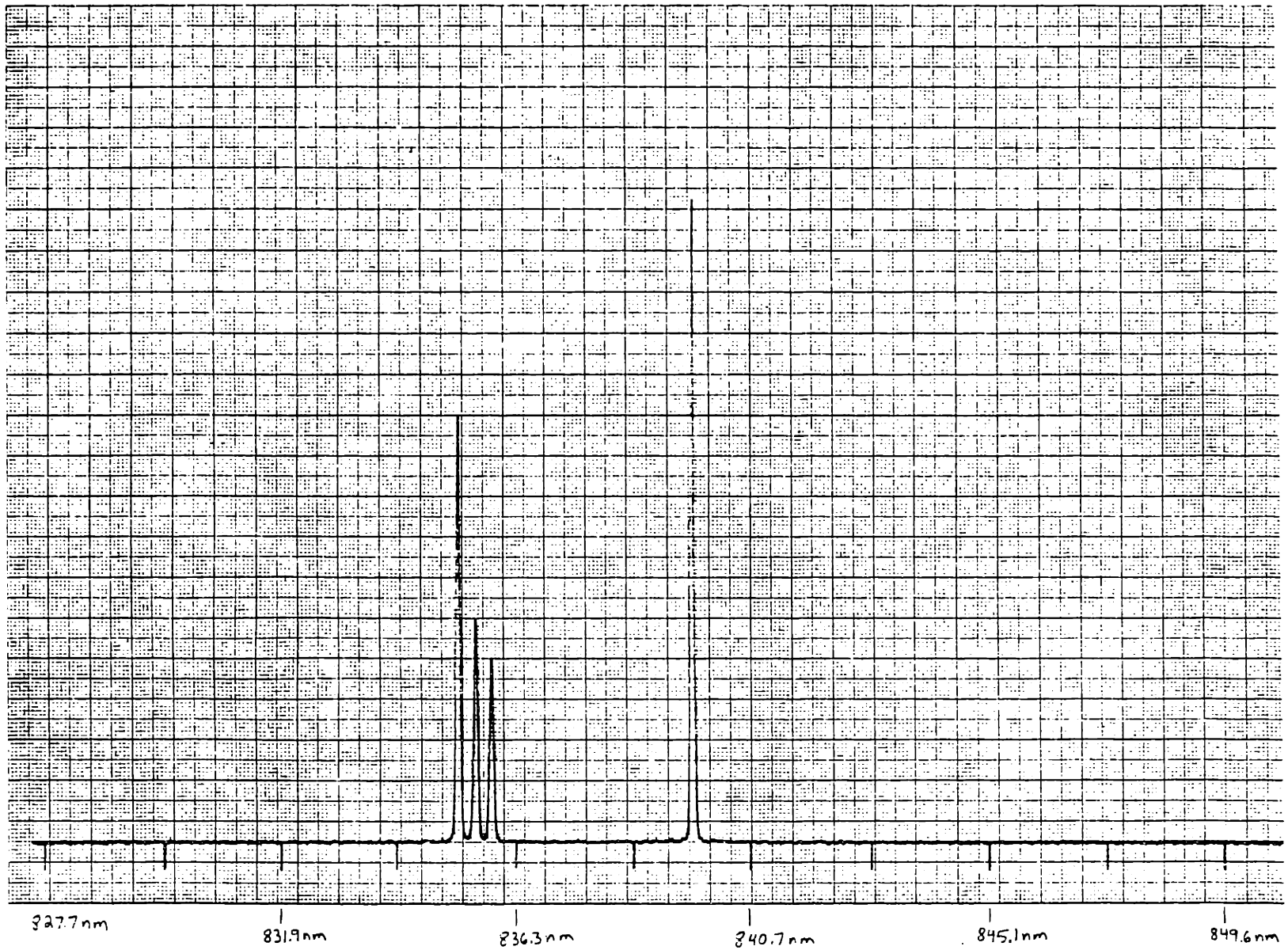

Figure 5.3e. Output spectrum of external cavity laser with five powered gain elements, 90 percent reflectivity end mirror, 70 percent (nom.) spatial filter duty cycle, 10.78 um spatial filter period. Average wavelength is 837.26 nm.

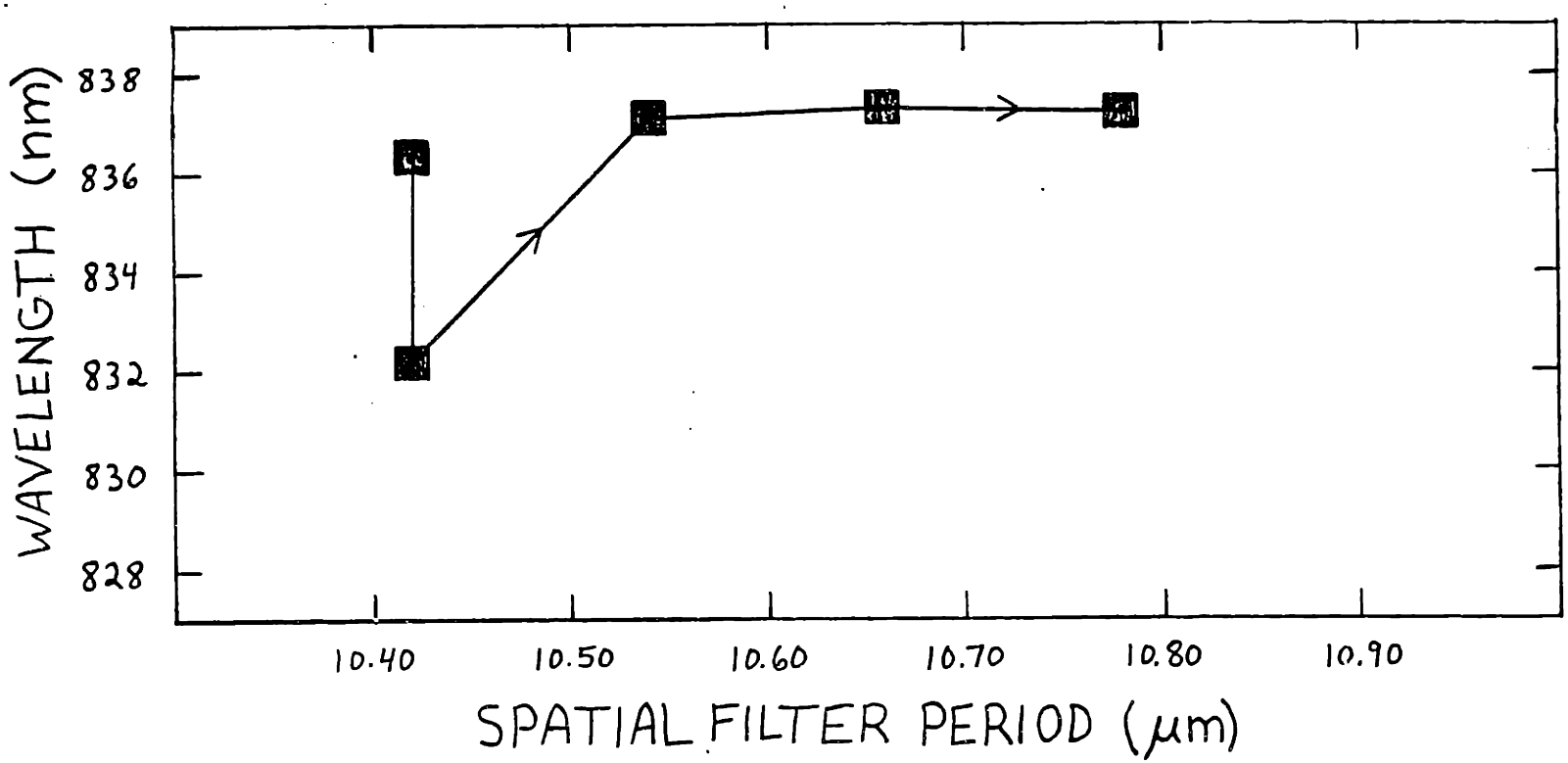

Figure 5.4. Summary of spectra in Figure 5.3a-e. Chronological order is indicated by arrows on lines connecting data points. The square boxes signify multimode spectra.

duty cycle might be contributory to the multimode nature of the spectra observed for filters from Series A. Series B, therefore, was a critical set of filters. It had filters as closed as the prototype filter which had yielded single-mode operation, and filters as open as the ones in Series A which had yielded multimode operation. When the 30, 40, and 50 percent (nom.) duty cycle spatial filters were used, the spectrum was found to be single-mode. This was significant since the prototype spatial filter was on a different wafer. Because it had been separately processed, it could have been argued that no direct comparison could be made; however, the behavior shown with that wafer was now repeated with the new wafer. When the 60, 70, and 80 percent duty cycle spatial filters were used, multimode spectra resulted. This connected with the behavior observed with the use of Series A, elsewhere on the same wafer. It should be mentioned in passing that the nominal duty cycles exceeded the values empirically determined (by visual estimation of the nulls in the diffraction pattern envelope) by approximately 10 percent. Still, this shifted range spans the duty cycles of both the prototype filter and the Series A filters.

Another possibility existed to explain this seemingly random behavior. In a non-rigorous analogy to master-slave frequency locking, it is well known that even though the master oscillator frequency may fall outside the lock-in range, it can still grossly perturb the waveform of the unlocked slave oscillator, producing beat notes in the slave oscillator output [1]. Combining this with imprecision in the value of primary lens focal length, or gain element spacing, or even nonuniformity in gain element spacing, it was logical to examine behavior for spatial filter spacings ranging over an even wider range than before. Thus Series C was introduced. In addition, with the failure of the "30 percent" filters, this series possessed the

smallest nominal duty cycle. The nominal duty cycle of 50 percent was consistent with empirical observations of the diffraction pattern. That the measured and nominal duty cycles were closer for Series C than for Series A or B can be partially explained by the fact that Series C appeared on a different wafer, with a different nitride layer thickness and processed later than the other wafer, i.e. with more experience. The period ranged from 10.36 um to 10.96 um, and the number of slits in each case was forty-one, sufficient to intercept all significant radiation in the focal plane. Operating currents were set as before.

Spectra resulting from individual spatial filters in Series C are shown in Figure 5.5. In Figure 5.6 the average wavelength is plotted against the spatial filter period. Of the six filters in the series, four produced single-mode spectra. In order of increasing filter period, the spectrum first hopped toward shorter wavelengths, then did not move at all for the next two filters. After that the spectrum broke up, but for the last three filters, including the last one to yield a single-mode spectrum, one could state that the average wavelength moved toward longer wavelengths.

The average wavelengths resulting from a second run attempted with Series C (50 percent nominal duty cycle) are illustrated in Figure 5.7 and bear little resemblance to the first run other than the attainment of single-mode spectra for the majority of the filters. In order of increasing spatial filter period, the spectrum increases in wavelength, then becomes multimode with an average wavelength of a value approximately equal to what the first filter yielded, and for the final three filters the spectrum retained single-modedness, but the wavelength was roughly constant at a value slightly shorter than the initial wavelength.

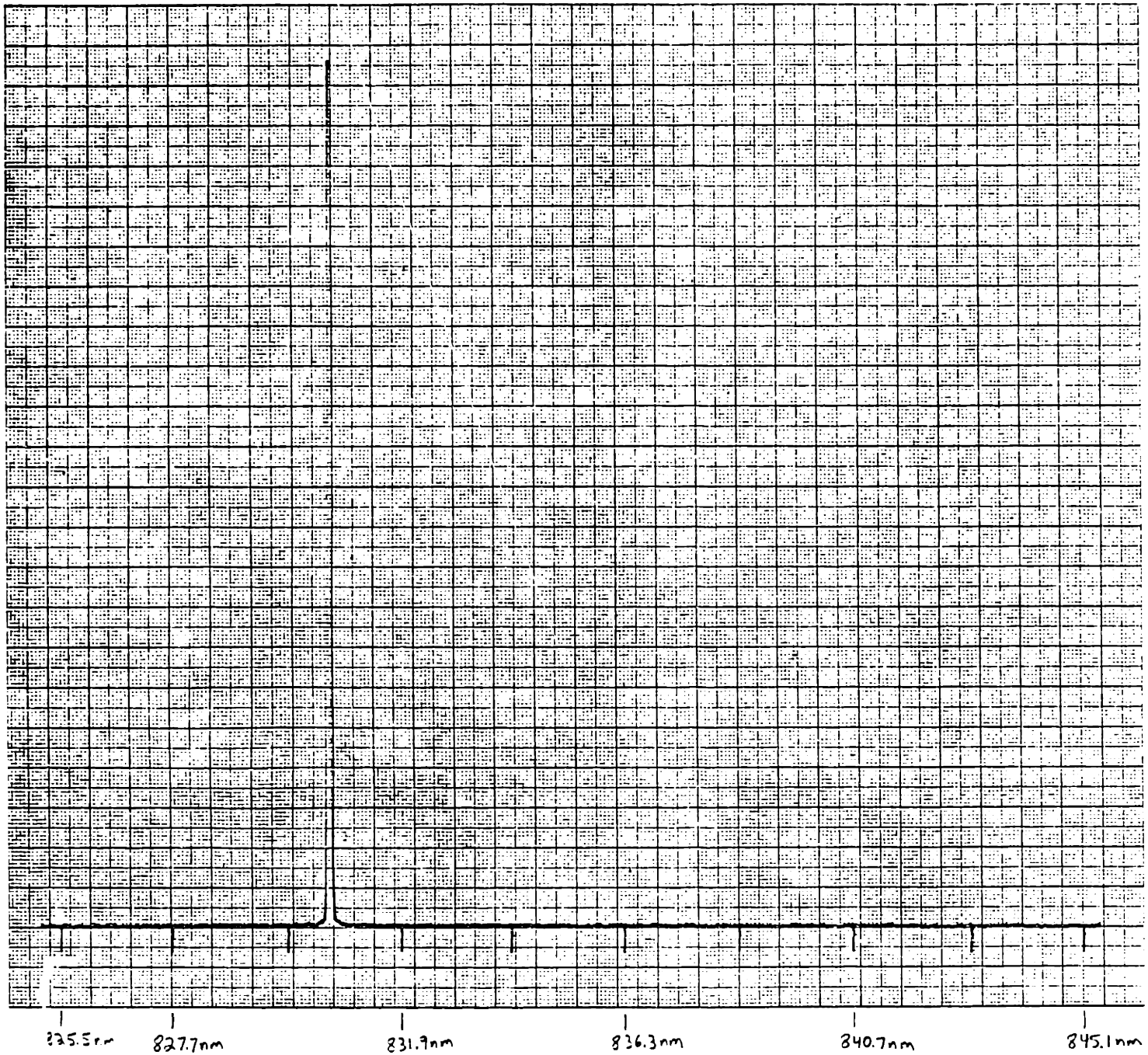

Figure 5.5a. Output spectrum of external cavity laser with five powered gain elements, 90 percent reflectivity end mirror, 50 percent (nom.) spatial filter duty cycle, 10.36 um spatial filter period. Average wavelength is 830.61 nm.

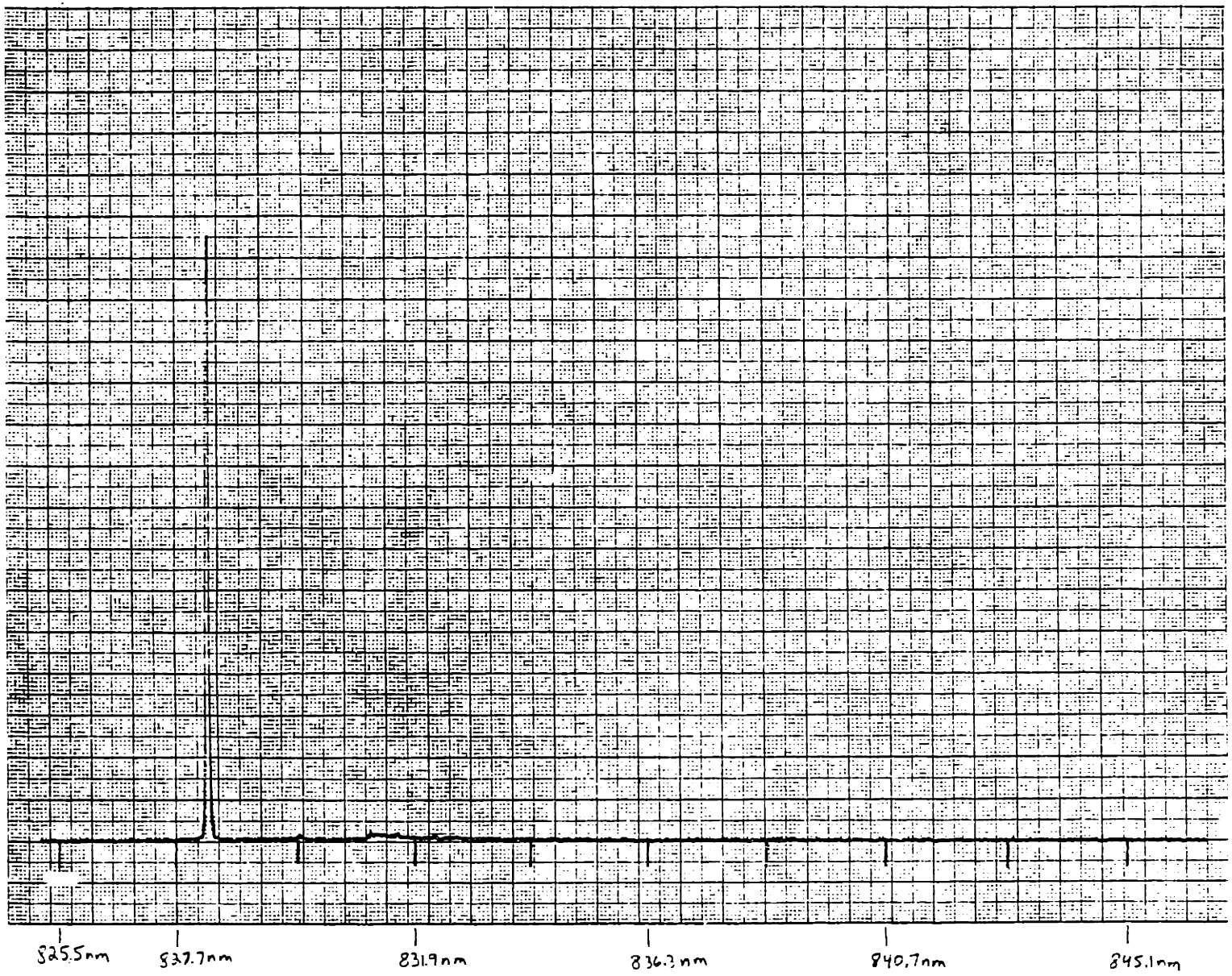

Figure 5.5b. Output spectrum of external cavity laser with five powered gain elements, 90 percent reflectivity end mirror, 50 percent (nom.) spatial filter duty cycle, 10.48 um spatial filter period. Average wavelength is 828.21 nm.

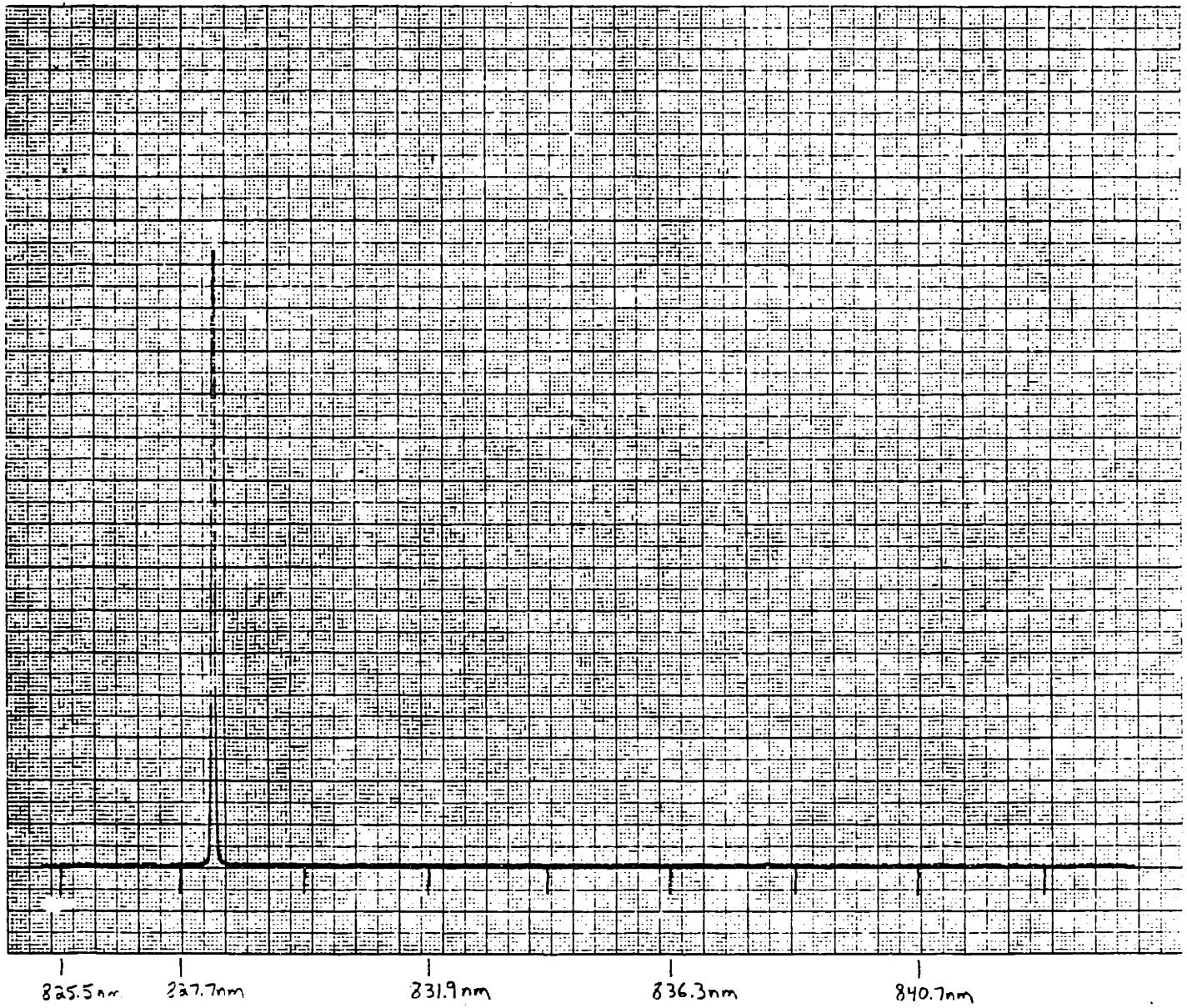

Figure 5.5c. Output spectrum of external cavity laser with five powered gain elements, 90 percent reflectivity end mirror, 50 percent (nom.) spatial filter duty cycle, 10.60 um spatial filter period. Average wavelength is 828.21 nm.

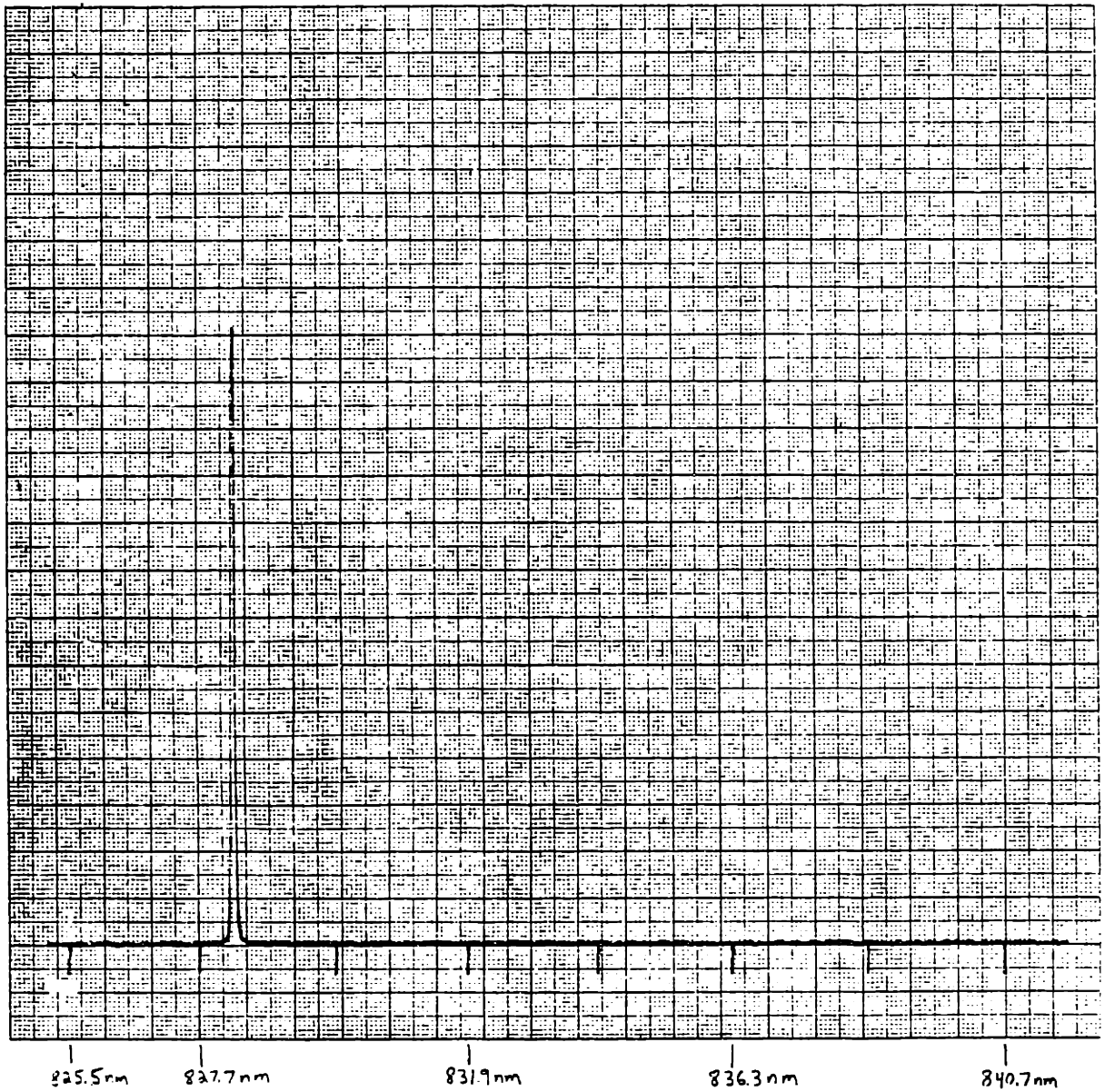

Figure 5.5d. Output spectrum of external cavity laser with five powered gain elements, 90 percent reflectivity end mirror, 50 percent (nom.) spatial filter duty cycle, 10.72 um spatial filter period. Average wavelength is 828.21 nm.

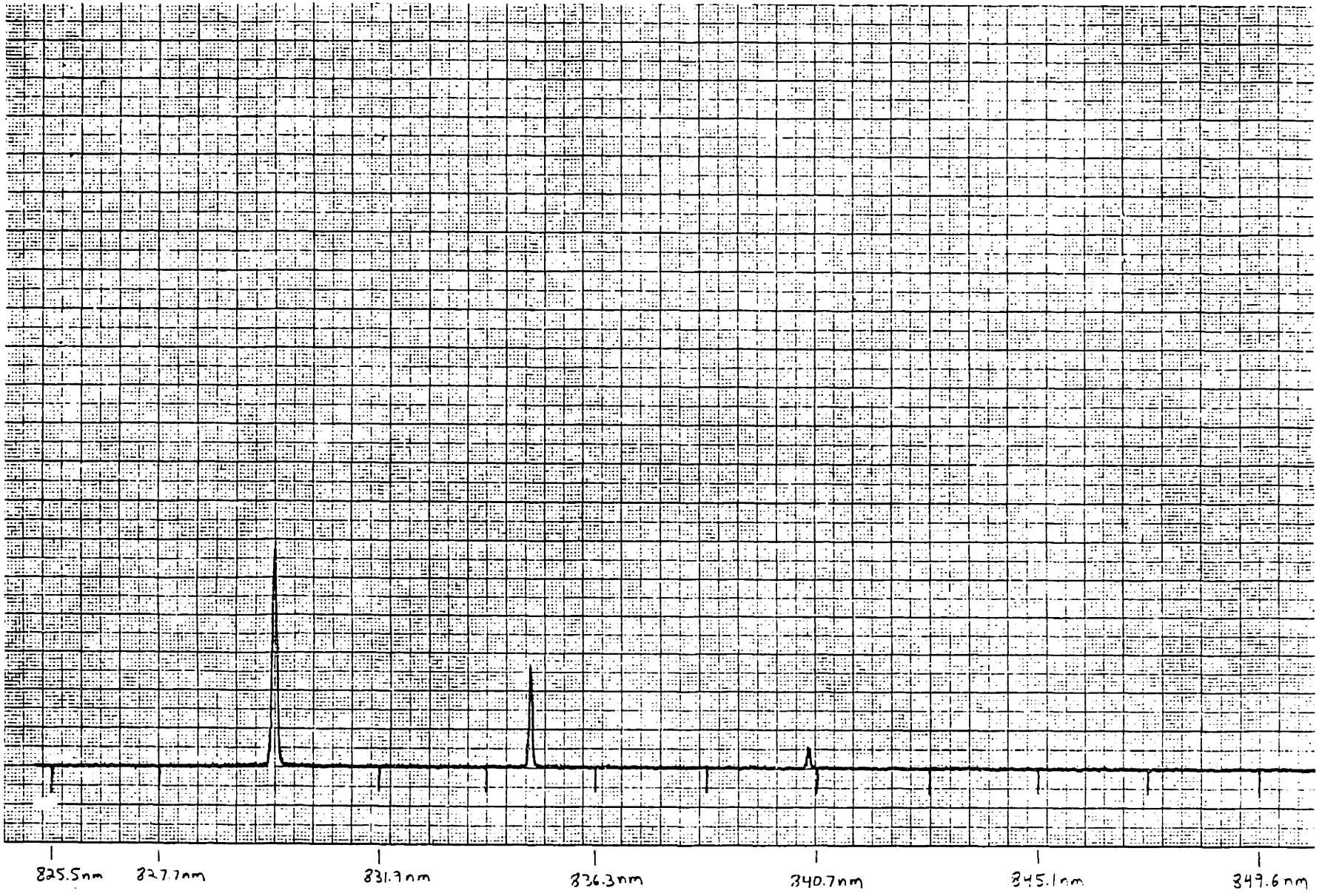

Figure 5.5e. Output spectrum of external cavity laser with five powered gain elements, 90 percent reflectivity end mirror, 50 percent (nom.) spatial filter duty cycle, 10.84 um spatial filter period. Average wavelength is 831.90 nm.

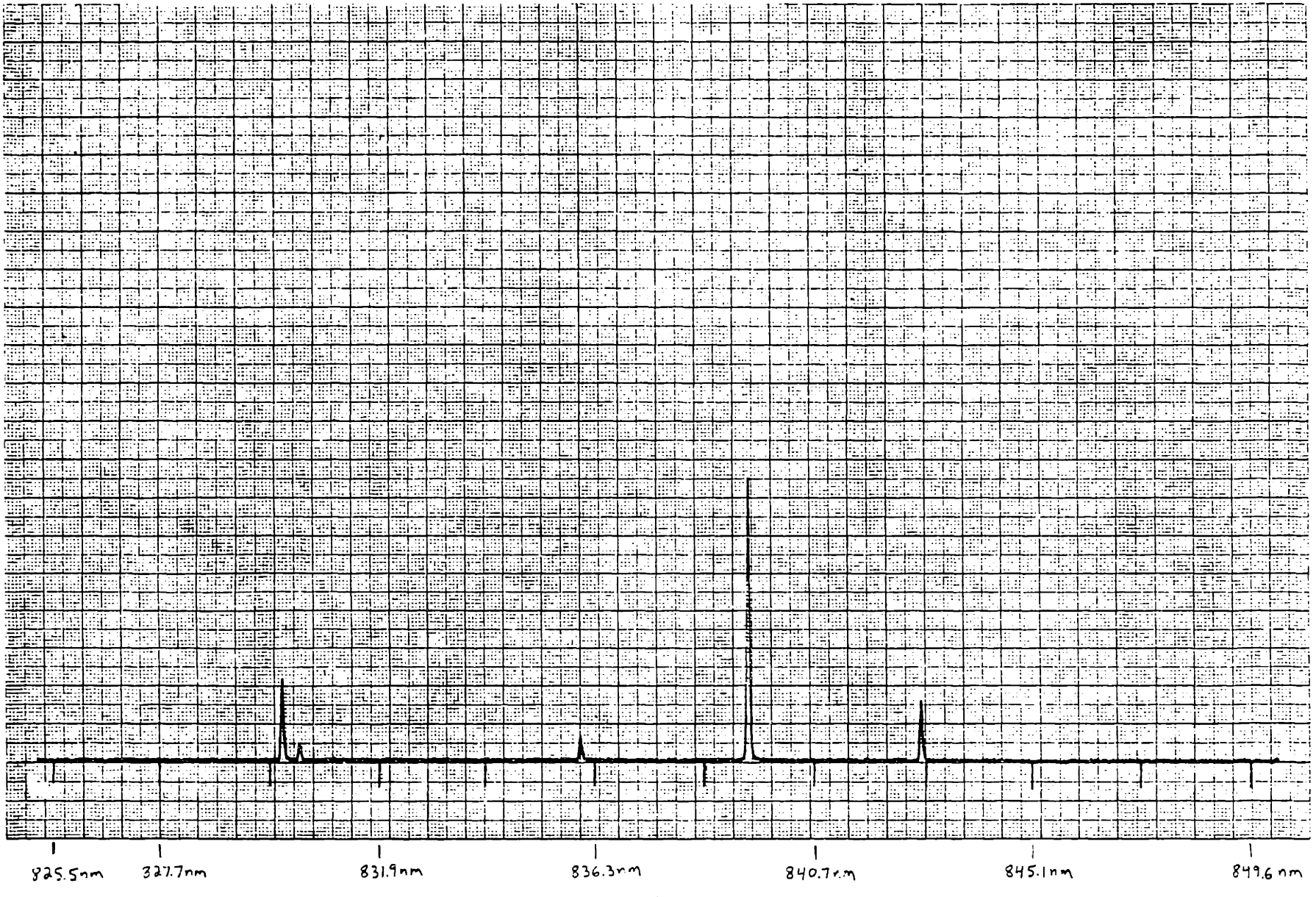

Figure 5.5f. Output spectrum of external cavity laser with five powered gain elements, 90 percent reflectivity end mirror, 50 percent (nom.) spatial filter duty cycle, 10.96 um spatial filter period. Average wavelength is 837.84 nm.

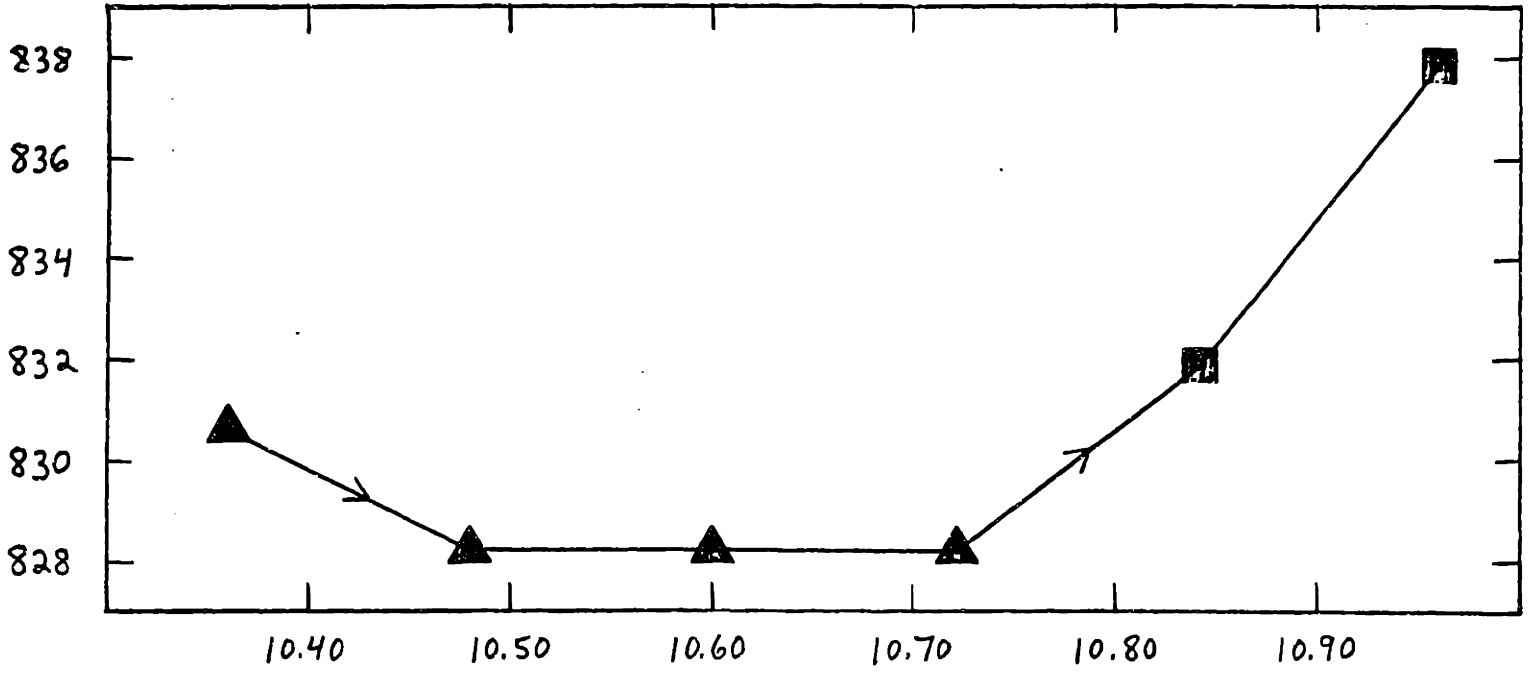

Figure 5.6. Summary of spectra in Figure 5.5a-f. Chronological order is indicated by arrows on lines connecting data points. The square boxes signify multimode spectra. The triangles signify single mode operation.

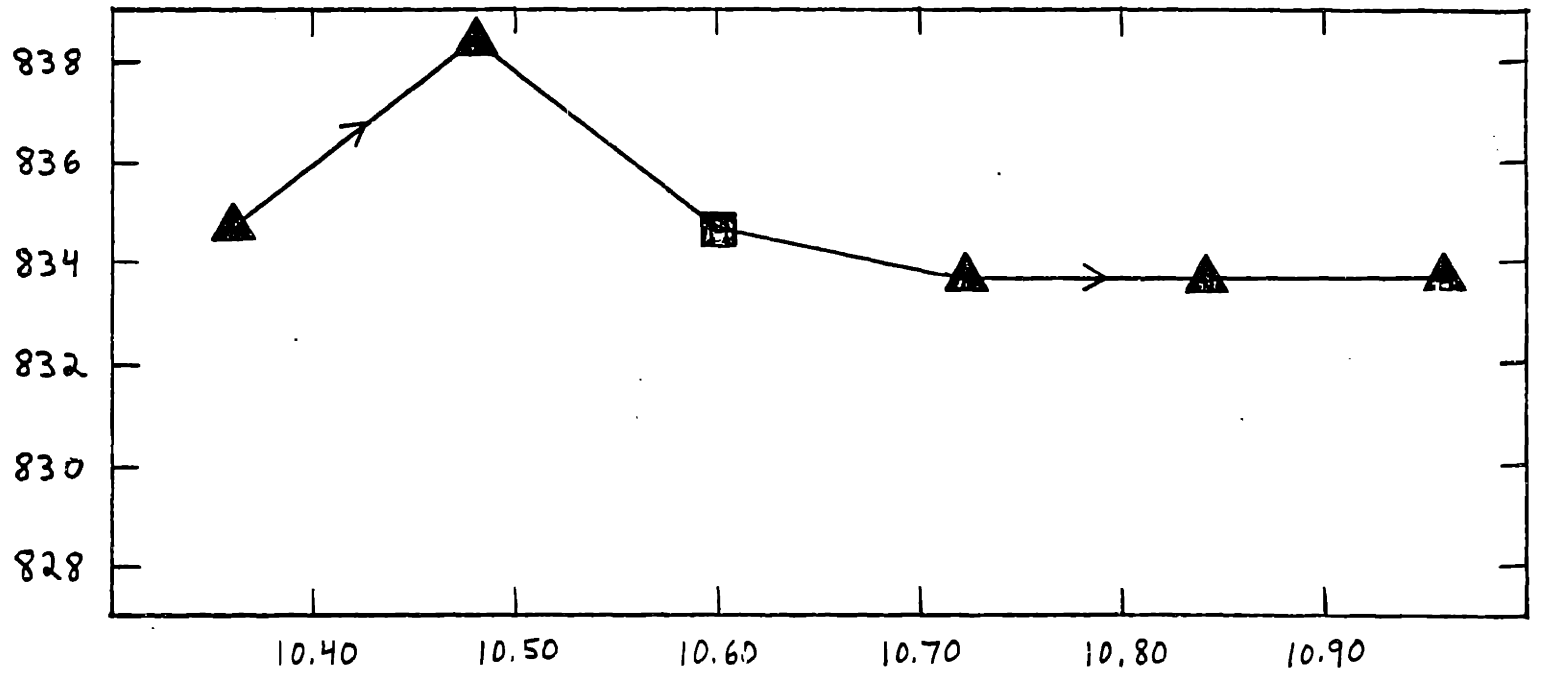

Figure 5.7. Summary of a second experimental study of output spectra of the external cavity laser with five powered gain elements, 90 percent reflectivity end mirror, 50 percent (nom.) spatial filter duty cycle. The square boxes signify multimode spectra. The triangles signify single mode operation.

5.5 Three-element Array Operation with Advanced Spatial Filters

Initial consideration of the wavelength selectivity of the spatial filter suggested that filters with slits narrow relative to the width of the bright fringes in the interference pattern would be more selective. This is because, as the wavelength changes, the transform (interference pattern), of the array output undergoes a scale transformation. Thus, off-axis bright fringes that previously had lined up with off-axis spatial filter slits would move relative to that slit. A narrow fringe with a relatively wide slit could suffer a greater displacement before it would miss the slit to a degree resulting in substantial power loss. Conversely, a wider fringe with a narrower slit would begin to suffer losses from the scale transformation almost immediately. Perhaps a more selective filter would yield a properly tunable single-mode spectrum.

Although filters with smaller duty cycles were not available, it was feasible to broaden the bright fringes of the interference pattern. It is well known from grating theory that the width of a grating order is inversely proportional to the number of illuminated lines in the grating. Reducing the number of lines broadens the order. In the case of the external cavity the analog was accomplished by only powering the three central gain elements. The element spacing remained the same, of course, so the spatial filter periods were still appropriate, but a bright fringe in the interference pattern from a three-element array is generally broader than one from a five-element array. (The disclaimer "generally" is necessary because merely specifying the number of elements in an array is not sufficient to determine the interference pattern; the relative weights of the elements must also be given.)

It should be kept in mind, however, that since the gain elements are coupled together by the spatial filter, turning off two of the five reduces the ensemble available gain in the cavity. In addition to the broadening of the bright fringes in the interference pattern, results must also be interpreted in light of the reduced gain.

Again Series A (70 percent nominal duty cycle) was introduced in an attempt to produce a tunable single-mode spectrum. Before filter insertion, currents were adjusted to yield the following powers out through the 90 percent reflectivity end mirror: .14 mW for the on-axis gain element; .11 mW for the adjacent gain elements. The remaining two elements were turned off. The average wavelengths obtained are shown in Figure 5.8. Power loss was typically 30 percent. In all seven cases a single-mode spectrum was obtained. The wavelength remained constant for the first three filters, then hopped to a shorter value for the fourth filter, but re-hopped to a wavelength longer than the first wavelength after peaking of the piezoelectric transducer, and remained at that value for the last three filters of the series.

The filters of Series C (50 percent nominal duty cycle) were also used in conjunction with the three-element array. Free-running powers were similar to the previous case; results were also similar (Figure 5.9). Spectra were predominantly single-mode. After initial alignment with the filter with the shortest period, the five filters with increasingly longer periods were substituted. A shift toward shorter wavelengths occurred as the second spatial filter was put in. The wavelength remained at this value for the remaining four filters, except for a slight drift due most probably to thermal effects.

In operation of the external cavity, powering only the three central

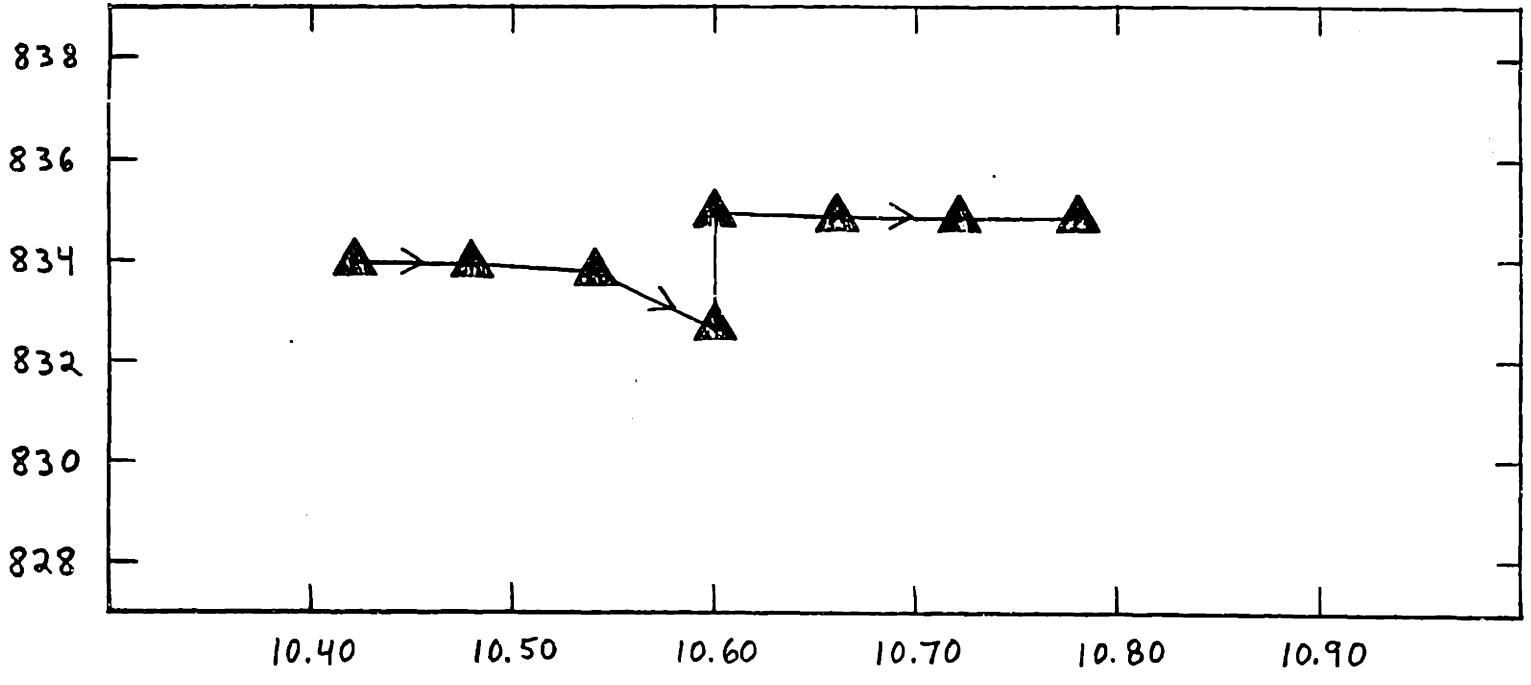

Figure 5.8. Summary of experimental study of output spectra of the external cavity laser with three powered gain elements, 90 percent reflectivity end mirror, 70 percent (nom.) spatial filter duty cycle. The triangles signify single mode operation.

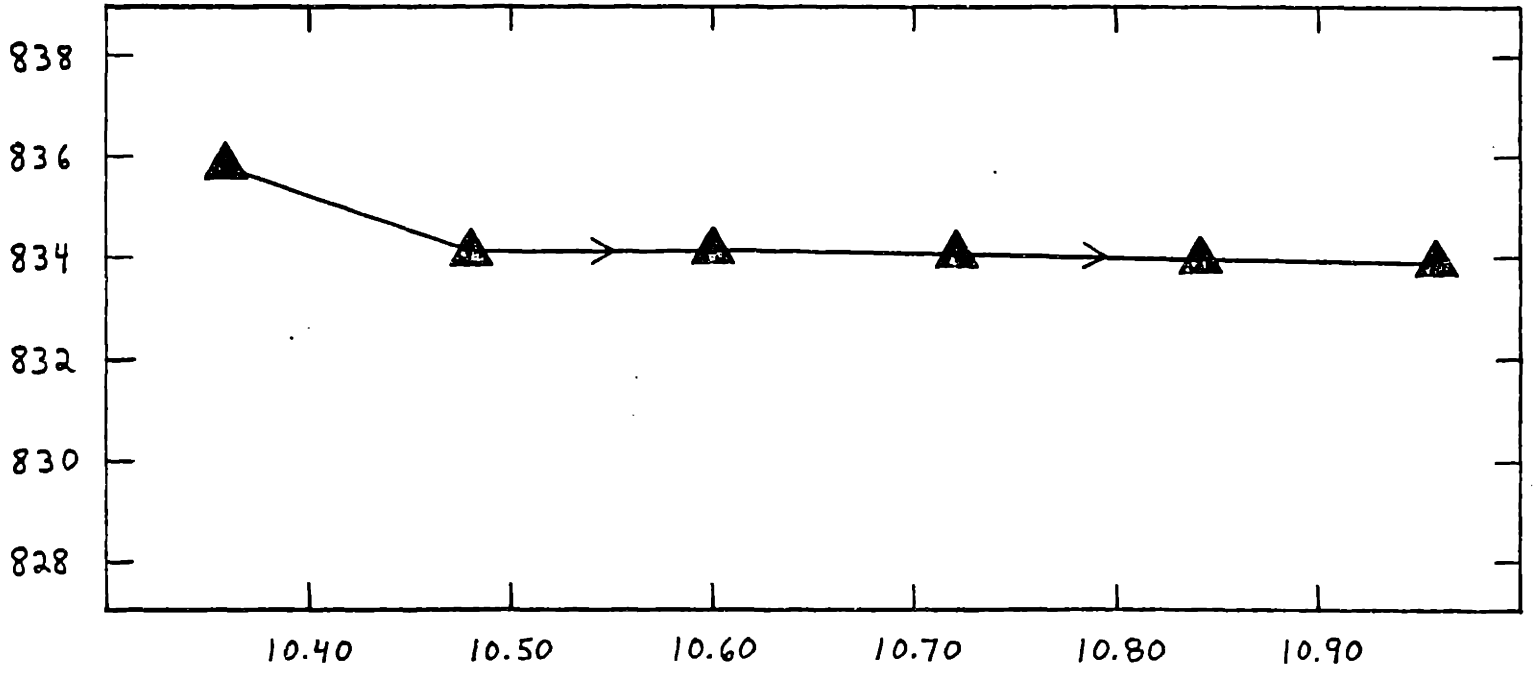

Figure 5.9. Summary of experimental study of output spectra of the external cavity laser with three powered gain elements, 90 percent reflectivity end mirror, 50 percent (nom.) spatial filter duty cycle. The triangles signify single mode operation.

gain elements usually leads to a single-mode spectrum to the resolution of the spectrometer. Five element operation often leads to multimode operation. It has been observed, however, that it is possible to intentionally or unintentionally raise multimode spectra for three-element operation. A "minor" misalignment is usually all that is needed. Often this is accompanied by a drop in power output. The point is that the system alignment plays a large role in determining the details of the output spectrum. Since re-alignment is usually done every time a new spatial filter is inserted, the depth of detail that can be compared between spectra recorded with different filters (or even the same filter at a different time) is necessarily limited.

5.6 Additional Experiments

Three additional experiments are presented which address topics not yet discussed:

(1) An end mirror with 50 percent reflectivity replaced the one used up to that point. Increased power output was of interest, even at the expense of increased injection currents, since a less reflective end mirror leads to a higher threshold. Three gain elements were used. Free-running powers out through the end mirror were 0.8 mW each. In comparison with operation with the 90 percent reflectivity end mirror, the power incident on the end mirror was ten times the throughput for the latter, but only two times the throughput for the former. The Series C filters were used (50 percent nominal duty cycle). A plot of average wavelength vs. spatial filter period appears in Figure 5.10. Power loss averaged around 65 percent. This was a greater loss than was suffered in previous experiments, but it is a questionable measurement without knowledge of the

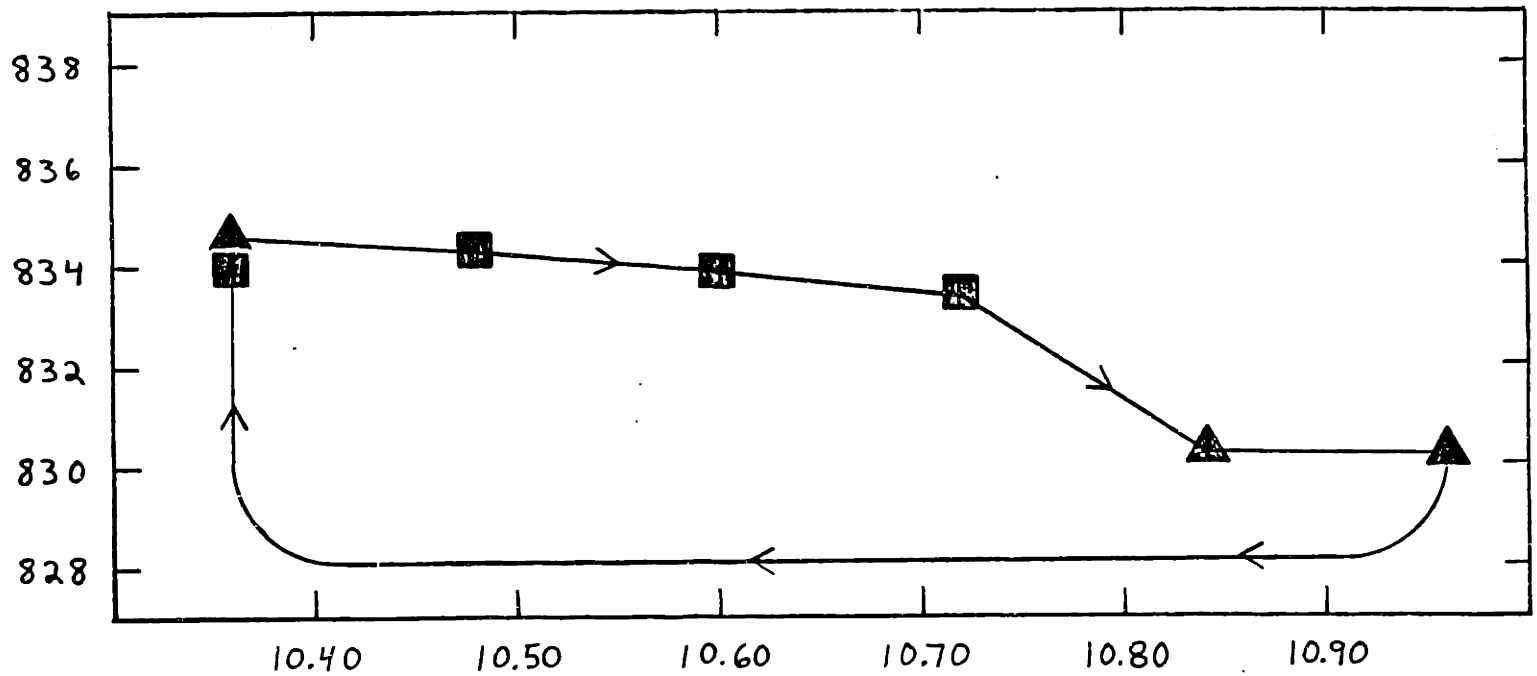

Figure 5.10. Summary of experimental study of output spectra of the external cavity laser with three powered gain elements, 50 percent reflectivity end mirror, 50 percent (nom.) spatial filter duty cycle. The triangles signify single mode operation.

ensemble threshold. The spectra were multimode for the most part. The average wavelength shifted to progressively shorter values as the six filters were inserted in order of increasing period; and when, after the last filter was used, the first was replaced, the average wavelength returned almost to what it had been initially for this filter, but the spectrum was now multimode.

(2) There could be no better demonstration of the operation of the external cavity laser than the output of a single-mode spectrum whose wavelength is dictated by the spatial filter period. Since the reality is far more complex than this, an alternate demonstration of coherent action was sought.

Using only the three central gain elements, threshold was measured for the central element operating current scanned, and the currents in the other elements fixed. A typical subset of data appears in Figure 5.11 and a table of measured thresholds appears in Table 5.4. For ease of measurement, the vertical offset was re-adjusted for each curve so that at zero current (for the on-axis gain element) the curve passed through the origin. The synergistic effect of coherent action is demonstrated, for example, by observing the reduction in threshold #3 (minimum current supplied to the on-axis element which will support stimulated emission) caused by non-zero current #2 alone; then with current #4 alone; finally with both currents #2 and #4 nonzero.

(3) For application requiring spectral bandwidths on the order of 0.1 nm, the situations that have been observed that resulted in multimode spectra are clearly undesirable. When spectral tolerances are several orders of magnitude tighter, many, if not all, commercially available grating spectrometers are incapable of accurately verifying the width of

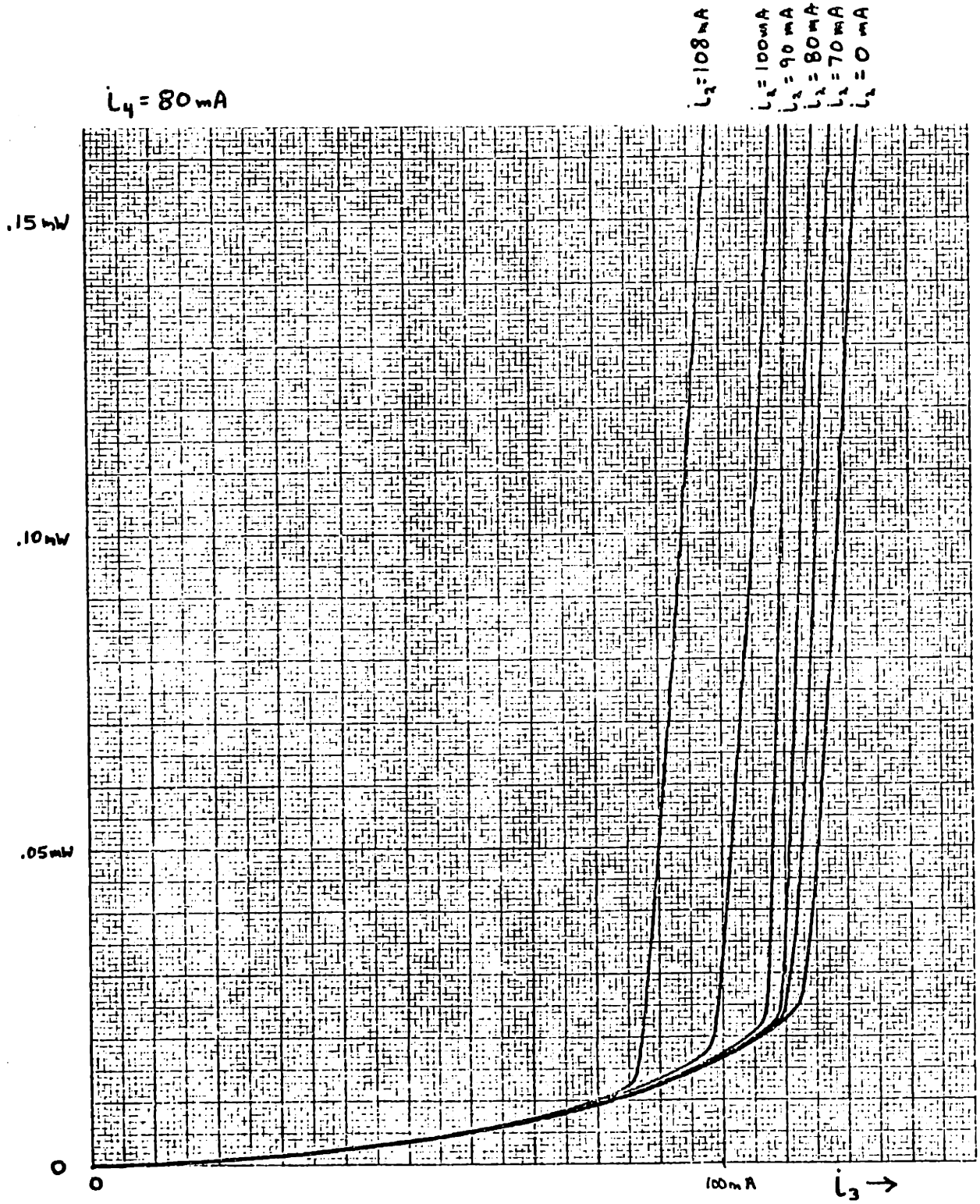

Figure 5.11. Demonstration of coherent action in the external cavity laser. Six curves of cavity output power vs. current in the on-axis gain element are superimposed with vertical offsets adjusted such that all curves coincide at zero (on-axis gain element) current. The current in one adjacent gain element is a parameter fixed at 0, 70, 80, 90, 100, and 108 mA, respectively, for the individual curves. The current in the other adjacent gain element is fixed at 80 mA for the entire set of six curves. The peripheral gain elements are not driven. The end mirror reflectivity is 90 percent. The spatial filter duty cycle and period are 50 percent and 10.72 um, respectively.

#4 GAIN ELEMENT CURRENT	#2 GAIN ELEMENT CURRENT					
	0 mA	70 mA	80 mA	90 mA	100 mA	108 mA
0 mA	114 mA	113 mA	111 mA	106 mA	99 mA	88 mA
70 mA	111 mA	111 mA	108 mA	104 mA	97 mA	86 mA
80 mA	112 mA	110 mA	108 mA	106 mA	98 mA	86 mA
90 mA	109 mA	108 mA	106 mA	104 mA	96 mA	84 mA
100 mA	104 mA	103 mA	103 mA	101 mA	91 mA	81 mA
110 mA	92 mA	92 mA	90 mA	86 mA	81 mA	75 mA

Table 5.4 Demonstration of coherent action in the external cavity laser. The threshold value of on-axis (#3) gain element current is measured with the currents in the adjacent (#2 and #4) elements fixed. The peripheral gain elements (#1 and #5) are not driven. The end mirror reflectivity is 90 percent. The spatial filter duty cycle and period are 50 percent and 10.72 um, respectively. Figure 5.11 is a subset of the raw data.

such spectra. In such cases it is preferable to use a scanning Fabry-Perot interferometer.

The three central gain elements were run at free-running powers of 0.8 mW each through a 50 percent reflectivity end mirror. A spatial filter with 50 percent duty cycle and 10.72 um period was inserted. Power loss was approximately 60 percent. According to the spectrometer, the output spectrum was single-mode. A sample of the output was then directed into the Fabry-Perot interferometer. The Fabry-Perot was a Tropel Model 240 Spectrum Analyzer, confocal mirror separation of 5 cm and a specified finesse of at least 200. The specified instrumental linewidth was 7.5 MHz or narrower. The external cavity laser had an optical length of approximately 75 cm and so would have a longitudinal mode separation of 200 MHz. It was clearly beyond the capability of the spectrometer to resolve intervals of this extent, but not beyond the ability of the Fabry-Perot.

Results are shown in Figure 5.12. It should be mentioned at the outset that obtaining single-mode spectra at the level of Fabry-Perot resolution is not a trivial undertaking; slight misalignments can cause the spectra to be multimode, despite being below the resolution limit of the grating spectrometer. The horizontal sensitivity on the upper and lower traces are equivalent to 405 MHz/div and 8.1 MHz/div, respectively, where "div" is one of the ten large divisions that span the photograph from left to right. The vertical sensitivity is .1 mV/div, where "div" is one of the eight large divisions that span the photograph from bottom to top.

Recalling that the interferometer is confocal, and defining a free spectral range to be the interval between two "pile-ups" of m+n=even modes, it can be seen that about one and one-half free spectral ranges are displayed in the top trace. Just right of center is a pile-up of m+n=odd

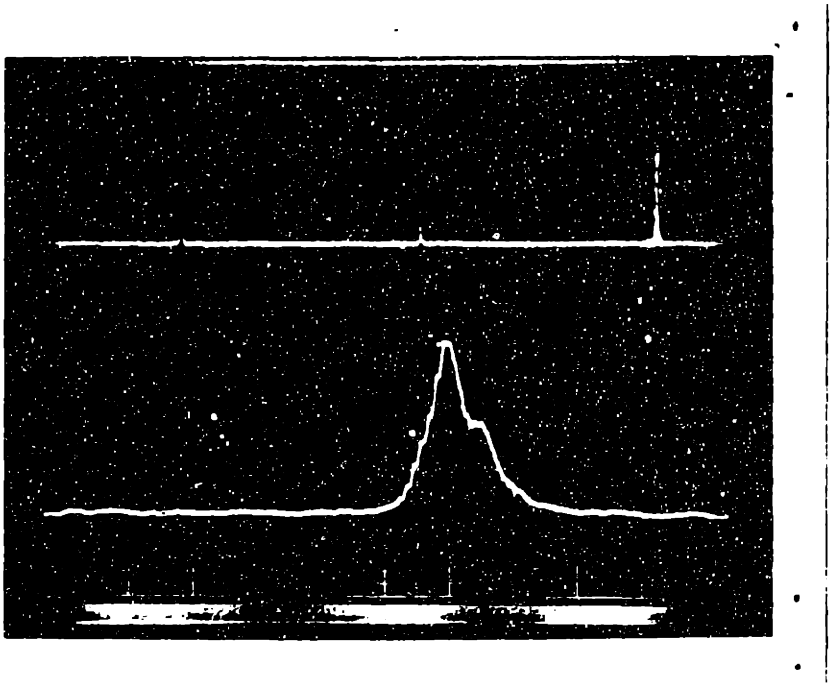

Figure 5.12. Spectrum of external cavity laser output recorded by confocal scanning Fabry-Perot interferometer. The horizontal sensitivity in the upper and lower traces are 405 and 8.1 MHz/div, respectively. The vertical sensitivity in both traces is .1 mV/div. The measurement appears to be instrument-limited.

modes; under precisely modematched conditions this peak vanishes, but the risk of feedback into the laser is too great. The peak on the right is intensified and expanded in the lower trace. On the left, the other m+n=even peak can be located by the break in the baseline of the upper trace.

The asymmetry in the lower trace, i.e., the hump on the right side of the peak, is evidence of imperfect alignment of the Fabry-Perot. The m+n=even modes do not perfectly pile up on top of each other, thus broadening the peak. Nevertheless, the measured spectral linewidth is clearly consistent with the 7.5MHz instrumental linewidth, and it could be stated with some confidence that this measurement is instrument limited.

5.7 Discussion

Some aspects of these experiments have supported intuitive notions of how the external cavity laser operates; some have refuted these preconceptions; and many have revealed insights into mechanisms that were not imagined before hand, so that no expectations had even been formed. It would be instructive first to examine those notions which seemed correct but which the experiments failed to support. Then these notions will be amended to more properly reflect reality.

Concerning basic processes governing laser output spectra: Given that the amplifying medium is homogeneous, it could be concluded that, via a "survival of the fittest" scenario for photon densities, the laser spectrum will be monochromatic , at that wavelength where the net round-trip gain is greatest. The many multimode spectra observed during operation of the external cavity with a five-element array and spatial filter are a flagrant violation of this picture. To a lesser degree, even for the original diode

lasers (Figure 5.1), the relatively small modes adjacent to the main peak are not consistent with the above notion of how a laser works.

What has been overlooked is the role of spontaneous emission in determining the laser spectrum. The spontaneous emission acts as a noise source that initially excites the laser. A perspective that ignores spontaneous emission concludes that the stimulated emission grows, saturating the gain until the peak round-trip gain is clamped equal to the round-trip loss (including output coupling and internal losses). This would in fact be the necessary condition if the situation was one where a fixed number of photons were "tossed" into the laser resonator at one time and that it was required that this number remains fixed, i.e., the photons survive. However, spontaneous emission is a constant source of photons, not just at one time. Thus, in the steady state the gain must clamp at a level less than the loss, but the difference (the net loss) must drain photons away at exactly the rate at which spontaneous emission supplies them.

This immediately allows for the existence of multimode spectra. It is easy to see that the intensity of a particular mode in the spectrum is qualitatively proportional to the rate of photons spontaneously emitted into that mode divided by the net loss for that mode [31]. Consequently, in order to understand the relative intensities of two modes in a spectrum, it is necessary to ascertain the relative rates of spontaneous emission for the two modes, and the relative net losses. Complicating the picture slightly is the fact that, although both gain and spontaneous emission in a semiconductor-diode laser are smooth single-humped functions of wavelength, their maxima generally do not occur at the same wavelength. To explain this discrepancy in as simple a way as possible, consider a two-level

system where f_2 is the probability of electron occupancy in the upper level and f_1 is the probability of electron occupancy in the lower level. Then $1-f_2$ and $1-f_1$ are the probabilities of electron vacancy in these levels, respectively. The spontaneous emission rate is proportional to the joint probability of an upper level occupancy and a lower level vacancy, or $f_2(1-f_1)$. Since the introduction of a photon into the system can result in either stimulated emission or stimulated absorption, gain is proportional to the difference in probabilities of downward (photon-emitting) versus upward (photon-absorbing) transitions or $f_2(1-f_1) - f_1(1-f_2) = f_2 - f_1$. If f_2 and f_1 are now wavelength dependent it is easy to see that $f_2(\lambda)(1-f_1(\lambda))$ and $f_2(\lambda) - f_1(\lambda)$ are in general shaped differently; in particular, these two expressions peak at different wavelengths.

Nevertheless, if five identical lasers were coupled together, it might be expected that the spectrum resulting from coherent operation would be no harder to fathom than the spectrum of an individual laser. After all, the forces governing the laser operation, e.g., gain or spontaneous emission, all fully overlap with regard to wavelength dependence.

Unfortunately the gain elements used in this thesis were not identical, even though they were all cut from the same wafer. There are many reasons that could be offered to explain differences between them, such as material defects, dust on a facet, a poorly bonded lead resulting in increased ohmic heating, intentionally running a different current through the gain element, or aberrations in the collimating lens used to couple light into the gain element. Whatever the cause, the effect is the same, namely, to change the gain and/or the spontaneous emission. In general, then, one has to consider that there are five sources of spontaneous emission exciting the external cavity laser, each with its own

dependence on wavelength, and five gain media, each with its own spectral behavior.

Despite the multimode character of the output spectrum of the external cavity laser, it could still be hoped that at least the average wavelength could be tuned as a function of spatial filter period. Of course this must be accomplished in respect of the wavelength selectivity of the spatial filter, but also in consideration of the spectral limits on the gain and spontaneous emission. No matter how selective the filter is, if there is no spontaneous emission to supply photons or gain to compensate internal losses and output coupling, lasing will not occur. On the other hand, returning to analogy with master-slave frequency locking, or in general with a system consisting of a variable frequency oscillator in the presence of an external stimulus with a specific frequency preference, some rather complex behavior can be described as the external signal or external resonance is tuned relative to the gain bandwidth; from very off-resonant to one side, to just short of a lock-in range, through the lock-in range, to beyond lock-in on the other side.

The observed behavior does not support the claim of an average wavelength grossly tunable according to the spatial filter period. Average wavelengths were observed over the range from 828.21 nm to 838.44 nm. Individual experiments were performed under differing circumstances, such as currents, end mirror reflectivity, filter series, and alignment. Nevertheless, the behavior indicative of tunability was the same in each case. For a given change in spatial filter period (in um), the wavelength that leads to the interference pattern with the same period changes at a rate of .079 nm/um. This translates to a 4.75 nm change between adjacent filters in Series A (70 percent nominal duty cycle), and a 9.50 nm change

between adjacent filters in Series C (50 percent nominal duty cycle). It is clear that, given the observed range of lasing wavelength in these experiments, hops of the indicated amount could appear only once (Series C) or twice in succession (Series A). Although some positive hops in wavelength did occur, the significance of such hops are severely diminished in light of the number of null and negative hops that occurred with respect to changes in filter period. Since no systematic behavior could be discerned, it is not possible to conclude at this time that tunability was demonstrated. The tunability of the spatial filter is considered in Chapters 6 and 7 and the observed absence of tunability will be seen to be consistent with the theoretical model.

One measurement made before was not mentioned and its inclusion now could be properly appreciated. But first it is necessary to review some aspects of the spatial filter. In a sense, the mechanism by which the spatial filter couples the gain elements together is diffraction. The spatial filter is essentially a grating, and like all gratings has a diffraction pattern composed of grating orders of varying strengths. As a result, when the filter is illuminated with the focussed output of the gain element array, whether the array is composed of one element, five elements., or any number in between, a spray of beams (in the far field) exits the filter. The numerical aperture of the secondary lens excludes all but five of these beams, and collimates these remaining ones onto the end mirror. There, they reflect and act as sources for the return pass. Each source receives a contribution form each gain element weighted by the strength of an appropriate diffraction order of the spatial filter. (Similarly the beam returned to each gain element receives a contribution from each source at the end mirror weighted by an appropriate diffraction

order.)

Assume that the gain elements are labelled -2,-1,0,+1,+2 and the sources at the end mirror are similarly labelled. It is important that the order of the labelling reflect the image inversion in the system due to the primary and secondary lenses used afocally. The weights used to calculate the strength of the -1st source at the end mirror, for example, from the strengths of the gain elements would be proportional to the strength of the spatial filter's +1,0,1,2,3 orders for the -2,-1,0,1,2 gain elements, respectively. For the spatial filters used the 0 order is always strongest and ± 1 orders next so. Also, each source at the end mirror gives rise to a reflected beam. A proportional transmitted beam constitutes part of the laser output, and can be labelled after the associated reflected beam. Thus it can be said that the -1 cavity output beam arises predominantly from the output of the -2,-1, and 0 gain elements. The +2 cavity output beam arises predominantly from the +1 and +2 gain elements (there is no +3 gain element). Similar identifications can be made for the other cavity output beams.

Up to this point, the external cavity laser output had been regarded as an indivisible entity. Now it is recognized as being composed of five separate beams. Moreover, each beam can be regarded as arising predominantly from three of the gain elements, or two for the ± 2 cavity output beams. For the arrangement in Figure 5.3b, with filter period 10.42 um and average observed wavelength of 832.21 nm, the following experiment was performed: Rather than collect all five cavity output beams and imput them to the spectrometer, the beams were input individually. Surprisingly, the beams showed different spectral contents. Results of the measurement are shown in Figure 5.13. The data indicate that there is a short

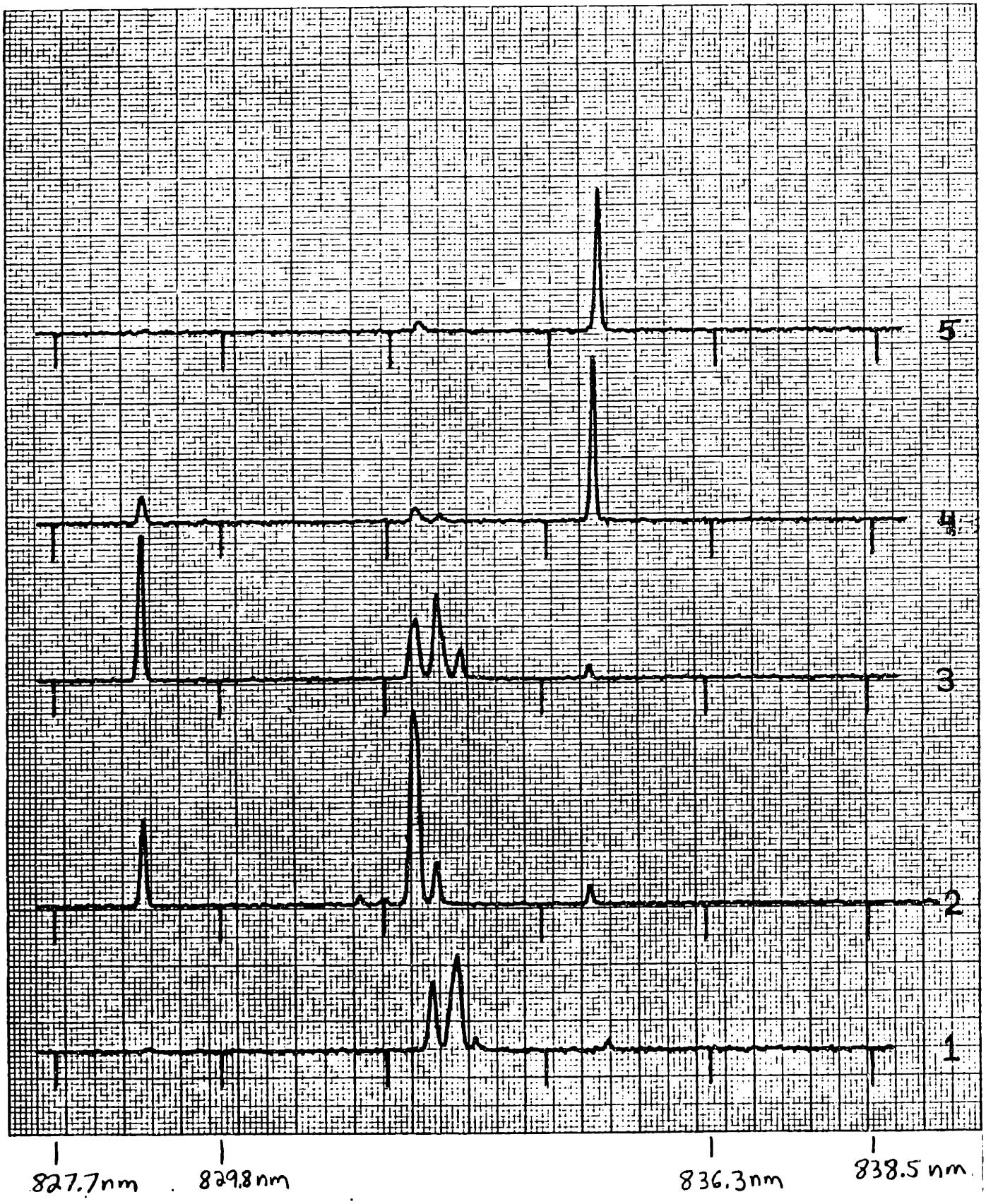

Figure 5.13. Spectra of the individual beams exiting the external cavity laser under multimode operation. The measurement points to the possibility of different wavelengths arising predominantly from distinct subsets of gain elements, a breakdown of a simple view of coherent action.

wavelength component arising from gain elements -1,0, and +1; a medium wavelength component attributable to gain elements -2, -1, and 0; and a long wavelength component coming from gain elements +1 and +2. When the five "sub-spectra" are summed, the spectrum of Figure 5.3b is recovered. Discrepancy can be traced to the half hour it took to record the five sub-spectra.

The important possibility that this brief measurement points to is that multimode operation of the laser may occur when the gain element ensemble is not acting fully coherent, but instead breaks up into several subgroups, probably overlapping, composed of adjacent gain elements. Since the spatial filter and the primary lens focal length is the same for each subgroup, different wavelengths could be explained by different average element spacings for each subgroup. The fractional width of multimode spectra typically run from 1 to 5 percent. This would be the necessary spread in average element spacing between subgroups. This translates to spacing variations of 0.02 cm to 0.10 cm around an average of 1.98 cm. Given the inherent imprecision of the pre-alignment of the gain elements relative to their collimating lenses, and the lack of facility of correcting this after installation into the cavity, the cited variation is a definite possibility.

Another issue influencing the spectrum of the external cavity laser combines several effects. The simpler of the two concerns residual front facet reflectivity persisting after anti-reflection coating. According to the witness sample that accompanied the diode lasers in their transition of gain elements, the residual reflectivity was on the order of 0.5 percent, down considerably from the initial 32 percent facet reflectivity, but still nonzero. From the standpoint of the large passive part of the laser

resonator, each gain element became an amplifying medium incorporated into a resonant reflector.

For the moment assume that the amount of gain in each gain element was comparable to the amount of gain necessary in the original diode laser. From the laser threshold condition $R_a R_b G^2=1$, the gain is determined to be $G=(.32)^{-1}$ when the facet reflectivities R_a and R_b are each 32 percent. Now assume this same amount of amplification between facets of 0.5 and 32 percent reflectivity. The less reflective facet is the one that is coupled to the external cavity while the more reflective facet couples out of the cavity. The reflectivity of a plane-parallel, resonant reflector with unequal reflectivities and encompassing a specified gain can be easily shown to be:

$$R_{eff} = \frac{\left(\sqrt{R_a}-\sqrt{R_b G^2}\right)^2+4\sqrt{R_a R_b G^2}\sin^2\phi}{\left(1-\sqrt{R_a R_b G^2}\right)^2+4\sqrt{R_a R_b G^2}\sin^2\phi}$$

where light is introduced through the facet with reflectivity R_a, and ϕ is the phase shift upon propagation between facets. It is not intended that this expression vigorously represent the use of an AR-coated diode laser as a resonant reflector but merely to suggest general behavior. For the given values the effective reflectivity varies between a maximum of 3.76 (376 percent) and a minimum of 2.67 (267 percent). The period of the variation (i.e., phase shift differences converted to wavelength differences) is the same as the free spectral range of the original diode laser, or

$$\Delta\lambda = \frac{\lambda^2}{2n_g L} = \frac{\lambda}{2L\left(\frac{n}{\lambda}-\frac{\partial n}{\partial\lambda}\right)}$$

where the meanings of the variables are obvious. For the diode laser

used, the following values are appropriate: λ=830 nm, L=250 um, n=3.6 nm. If the linewidth of a reflectivity resonance were defined at the average of maximum and minimum reflectivities (rather than at simply half-maximum) then the resonant reflector has a finesse of 2.4. In other words, the reflectivity falls to 3.22 (322 percent) when the wavelength shifts $\pm$.065 nm away from linecenter. It is interesting to note that for a passive resonant reflector (G=1) the effective reflectivity in Eq. 5.1 obtains its minimum value when the phase shift is a multiple of pi; for the resonant reflector with sufficient internal gain, the effective reflectivity obtains its maximum value instead. Also, in actual usage, the gain supplied by the gain elements is higher than what was assumed. The necessity of the higher gain is evident from the increased thresholds in Table 5.2 relative to Table 5.1. The external cavity laser has greater round-trip loss, so the gain must be accordingly higher. This means that the maximum effective reflectivity of the gain element is higher, the contrast between maximum and minimum is greater, and the finesse increases as well.

The presence of the residual front facet reflectivity has a profound effect on the operation of the laser. The gain, which previously had been expressed in terms of occupation probabilities, was inherently a smooth, single-humped, function of wavelength. By encasing the gain medium inside a resonant reflector, however, a deep periodic modulation is impressed upon the gain lineshape. The implications with regard to laser output spectra are important. Without this etalon (resonant reflector) effect, the determination of ensemble or modal gain at a particular wavelength is relatively straightforward, and is a smooth function of wavelength since the individual gains are smooth; likewise for the spontaneous emission. The modulation of the individual gains due to residual facet reflectivity,

conversely, complicate this determination. The problem is somewhat analogous to superimposing five hair combs and finding positions where the teeth from the separate combs line up. As will be discussed shortly, the combs in general are shifted with respect to one another, and may not have uniform spacing.

There is some resemblance between this problem and the operation of the cleaved-coupled-cavity (C^3) laser [32]. The C^3 laser integrates two resonant reflector, with one or both reflectors having gain. The reflectors are of different lengths so that the periods of the two sets of reflectivity resonances are different. The superimposed combs can line up at one wavelength, but the next coincidence of teeth may not occur until a wavelength at which the internal gain is substantially lower. The C^3 structure, meanwhile, has performed the task of discriminating against lasing close to the desired mode (e.g. 0.3 nm away). In this way, stable single-mode emission can be obtained. For the external cavity laser, there are five combs, and there may not be a perfect line-up of comb teeth anywhere. The problem is much more complex. However, the C^3 effect, that is, the notion of lined-up teeth in order to have lasing at that wavelength, is a valuable idea to keep in mind and may explain much of the "inertia" of the spectrum (non-tunability with respect to changes in the spatial filter period).

There is one critical process which has been omitted up to this point. Although it seems innocuous enough, its influence on the laser operation is far-reaching. Gain dependent phase shift is a consequence of the Kramers-Kroenig relations [33]. A little less rigorously, if an electron oscillator model of the gain medium is used, the gain is proportional to the imaginary part of a complex dielectric susceptibility, while the real

part gives rise to the gain-dependent phase shift. It is not entirely accurate to say that the phase shift is gain-dependent since they both derive, rather, from a common source; what is indicated is the phase shift in the medium that is due to the same source as the gain, as opposed to other phase shifts that are also present and contribute to the total phase shift.

A major complication arises due to gain saturation. The small-signal gain of a gain element can be set by adjusting the diode current, but the act of stimulated emission tends to decrease the inversion responsible for the gain. Thus the eventual gain, and therefore phase shift, of a gain element depends on the intensity of the field it is amplifying. This feature can be both beneficial and deleterious.

On the positive side, gain-dependent phase can supply a form of self-compensation for optical path length differences inside the resonator. The classical Fabry-Perot type laser has a standing wave inside with nodes (approximately) at the mirrors. The resonant frequencies are derived from this assumption. Similarly, an early critique of the external cavity laser design implied that at any wavelength of operation it would be necessary to have nodes of the internal fields at all mirrors, of which there are six (the one common end mirror and the five individual rear gain element facets). This suggested that phase adjustment was necessary, which took the form of a piston type degree of freedom being included into the design of each collimator pen mounting. It was found that the phase adjustments were not critical to the successful operation of the laser. Assuming that the system was operating initially in a situation where nodes existed at all mirrors, and then path length differences were introduced, the nodes-at-mirrors condition could be regained by postulating slightly different

fields around the cavity. The revised fields would induce new phase shifts that would satisfy the nodes-at-mirrors condition. Of course, this must be done consistently since the field in one part of the laser is linked via the spatial filter to fields elsewhere in the laser. The wavelength may also need to change in order to satisfy the resonance condition with the new path length differences. In fact, multimode spectra may be an indication that it is impossible (or less efficient) to satisfy the nodes at mirrors condition with only one wavelength, and at the same time be consistent with the gains of the gain elements and the constraints imposed by the presence of the spatial filter. On the other hand, if multiple wavelengths are circulating in the cavity, gain is divided up among the competing wavelengths. Now there is a phase shift in each gain element for each wavelength. Also, the spatial filter couples each wavelength to the same wavelength elsewhere in the cavity. The spatial filter does not couple different wavelengths together, since diffraction is linear in field; the different wavelengths do couple in the gain elements, where they compete for a limited gain. All told, it may not be possible for any one wavelength to satisfy all the constraints in the external cavity laser, but it may be possible to satisfy them when multiple wavelengths are present. The fields at each wavelength would be proportioned consistent with the mixing effect of the spatial filter and the amount of gain "allotted" to that wavelength in each gain element, and would separately satisfy the nodes-at mirrors condition; together the fields at all wavelengths would use up all the available gain.

On the negative side of gain-dependent phase is its impact on the C^3 effect discussed earlier. The resonant reflector created by the imperfect antireflection coating of the front facet was treated in terms of a

specified gain and yielded an effective reflectivity that was not explicitly dependent on the incident or reflected powers. In the external cavity laser, however, only the small signal gains are specified by the selection of current. Power internal to the resonant reflector saturates the gain to a greater or lesser degree, which in turn affects the gain dependent phase, which in turn shifts the comb of effective reflectivity (versus wavelength), which finally affects the amount of incident power coupled into the internal power, and the process then repeats. This is also known as a nonlinear Fabry-Perot, and its behavior can be quite complex. There can be hysteresis or bistability, for example, in the dependence of reflectivity versus incident power. The phase of the reflected wave will also have a nonlinear dependence on incident power. All this serves to further cloud the amount of gain in the external cavity laser available to a particular wavelength and how it is distributed. And while the effective gains and phases are complicated functions of the fields, the fields are complicated functions of the gains and phases. It is even conceivable that temporal instability can occur; as a particular wavelength builds in intensity inside the laser, whatever configuration of gains and phases that had been beneficial to such growth may suddenly cease as a result of the nonlinearities discussed here, and instead the laser may favor the growth of a different wavelength that was not preferred earlier. The spectrum could then become a function of time, with dynamic behavior not yet determined. There are many challenging problems in predicting the spectrum of the external cavity laser, and the relevance of gain-dependent phase cannot be overstated.

Of a more practical nature, two final effects are discussed which influence laser operation through straightforward shifting of the resonant

reflector combs and adding fixed phase shifts which may require new field strengths and wavelengths in order to self-consistently satisfy all the constraints imposed. First, as Eq. 5.2 indicates, the free spectral range of the resonant reflector depends on the length of the diode. Length variation between diodes can be subtle, as might arise from temperature changes. Second is the effect of fine pitch-yaw adjustment on the collimator pens. The angles involved are not severe enough to affect overlap of the beams in the focal plane of the primary lens. However, the change in angles is sufficient to move the position on the front facet illuminated by the focussed spot from the beam returned to the collimator pen. This changes the launching condition into the gain element waveguide. Considering that the active region is surrounded by cladding regions of lower refractive index, altered launching conditions may cause the launched field to "see" a little more or less of the index of the cladding layers. The effect may allow some phase shift difference to accrue without severely altering the power coupling into the waveguide. Although the phase shift difference might be small, just as the shift in the reflectivity comb of the resonant reflector induced by length variations might be small, it could require a drastic re-shuffling of powers around the cavity, and even changes in the spectral content of the laser output, in order to satisfy the boundary conditions. A shift in the reflectivity comb of one resonant reflector (i.e., gain element) may force laser operation at two wavelengths with satisfactory coincidence of combs, rather than operation at one with good coincidence of all combs. Similarly, adding or deleting some phase shift at a crucial position may force laser operation to go multimode. Conversely, <u>not</u> changing phase shifts can fix the operating wavelength, even though the design wavelength

of the spatial filter changes.

This discussion has attempted to clarify various aspects of the external cavity laser operation, as suggested by the outcome and interpretation of preliminary experiments. Simple models to the contrary, multimode spectra are easily, though not desireably, produced. Mechanisms have been suggested to motivate non-tunability of the spectrum as well as spectral changes dependent on factors other than the spatial filter period, such as the alignment.

Chapter 6. Theory

Preliminary experimental studies have pointed out, only too well, how little is known with certainty about the principles by which the external cavity laser operates. In particular the frequently observed multimode output spectra are cause for much speculation. Nevertheless, a model is developed in this chapter based upon the assumption of monochromaticity. This can certainly be justified as a stepping stone to a multimode theory, but for certain situations, the monochromatic model itself is a sufficiently faithful representation of reality. The rationale is based upon the observation that the spectrum is an extremely sensitive function of alignment and spatial filter period, while at the same time the total power exiting the laser through the end mirror barely varies. To see that this is reasonable, the following two scenarios should be considered: In both cases the amount of internal power is expressed in terms of the number of photons passing a given plane. In one case the photons all have the same wavelength, situated at the peak of the gain curve and monopolizing all the available gain. In the other case, the photons are split among two wavelengths in competition for the available gain. Each receives a share of the gain, so that the amount of photons (determined by the loss and the spontaneous emission) at each wavelength is less than in the previous case. However, the sum of the photons at the two wavelengths is comparable to the former situation. It can also be shown from the rate equations that, so long as the spontaneous emission factor [34] is small and the cross-section of the inversion with each wavelength is comparable, then the total number of photons is not a strong function of the number of modes over which the photons are split. In this sense the photon number, and hence the cavity output power, is a global quantity of the external cavity, not strongly

dependant on how the photons are distributed in wavelength. It is with this caveat that the model is developed.

A technical description of the operation of the Laser, as for any oscillator, must consider characteristics of the amplification mechanism as well as the feedback mechanism. The Laser system may be cut, so to speak, at the left focal plane of the five collimating lenses in Figure 3.1 and the action of the two resulting sub-systems considered separately. The feedback is supplied by the passive subsystem to the left of this cut and the amplification by the active subsystem to the right.

6.1 Analysis of Passive Part of the External Cavity Laser

The passive part of the cavity is now considered. Light leaving the active subsystem makes a leftwards pass through the passive subsystem and strikes the output mirror. Some of the light is transmitted and constitutes the cavity output, the remainder is reflected and makes a rightwards pass through the subsystem and re-enters the active subsystem. Figure 6.1a illustrates the leftwards pass through the Laser's passive subsystem. The active subsystem input/output plane, the primary lens, the spatial filter, the secondary lens, and the output mirror are positioned where the exact Fourier transform relation holds for the lenses. Given that $U(x,y;z=-2f_p)$ is the output of the active subsystem, (suppressing the $e^{j(\omega t-kz)}$ dependence) and the $T(x,y)$ is the transmission of the spatial filter, then in the plane of output mirror, we have

$$U(x,y;z=2f_s) = \mathcal{F}_s\{T(x,y)\cdot\mathcal{F}_p\{U(x,y;z=-2f_p)\}\} \quad (6.1a)$$

$$= \mathcal{F}_s\{T(x,y)\} * \mathcal{F}_s\{\mathcal{F}_p\{U(x,y;z=-2f_p)\}\} \quad (6.1b)$$

$$= \mathcal{F}_s\{T(x,y)\} * \frac{f_p}{f_s}U\left(-\frac{f_p}{f_s}x, -\frac{f_p}{f_s}y, z=-2f_p\right) \quad (6.1c)$$

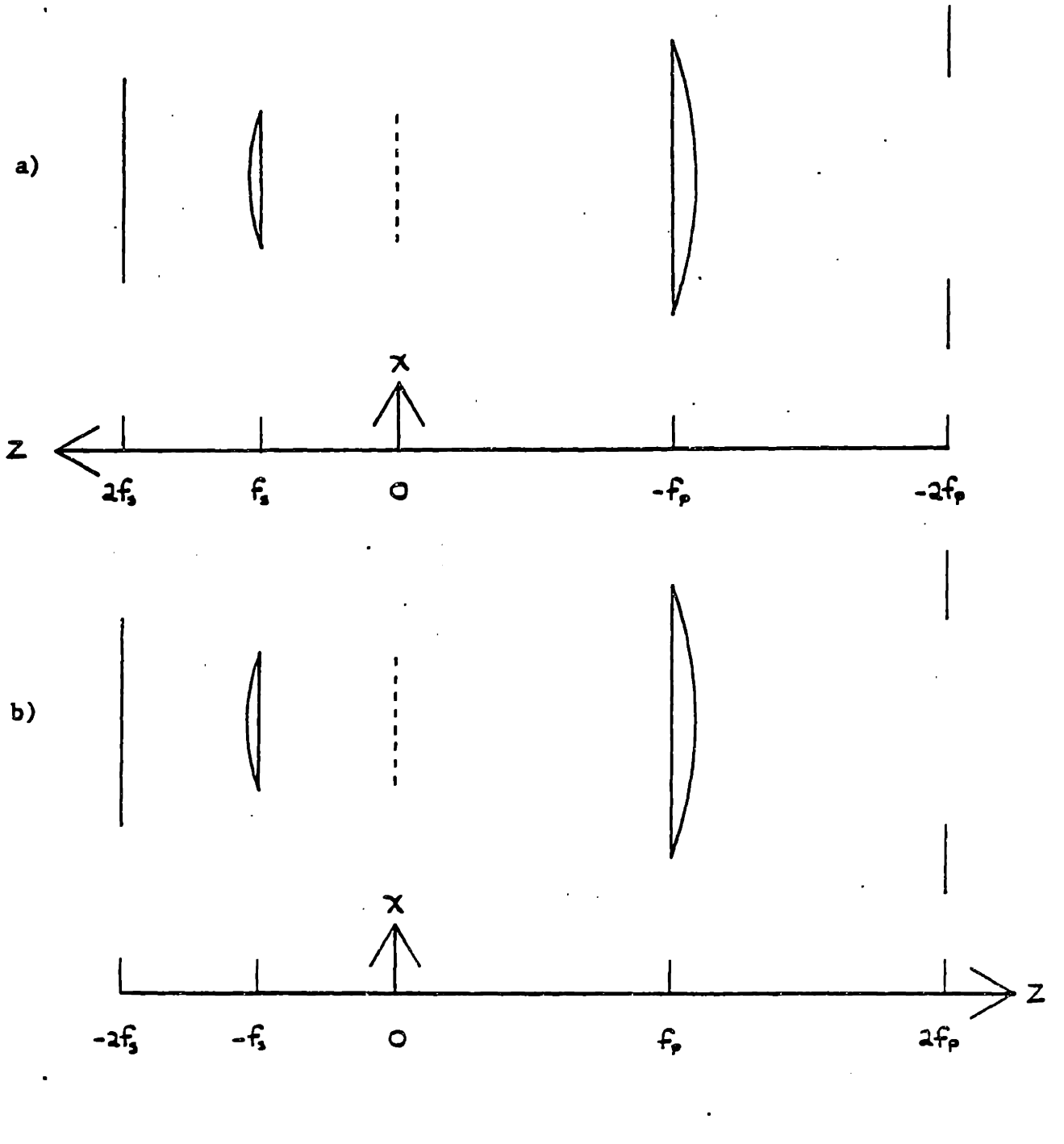

Figure 6.1. Optical diagram of passive part of the external cavity laser.
a) Leftwards pass. b) Rightwards pass.

where $F_p\{*\}$ and $F_s\{*\}$ are the functionals indicating the action of the primary and secondary lenses. The argument is the field at the right focal plane and the value is the field at the left focal plane. In Eqs. 6.1b,c the convolution operation is used. The gain elements and collimating lenses that constitute the active subsystem are identical and uniformly spaced along the x-axis, so that, to within a multiplicative constant and a shift, the active subsystem output is an array composed of five identical fields:

$$U(x,y;z=-2f_p)=\sum_{n=-2}^{n=2}\psi_n\, u(x-nD,y) \qquad (6.2)$$

where D is the distance between gain elements, ψ_n is a weighting factor and u(x,y) represents the collimated emission of a gain element.

The spatial filter, as discussed in Section 3 is composed of transmitting strips alternating with opaque strips. Now, given that u(x,y) is approximately of width d_x and height d_y, then $F_p\{U(x,y;z=-2f_p)\}$, the field that illuminates the spatial filter, is approximately of width $2\lambda f_p/d_x$ and height $2\lambda f_p/d_y$. As long as the spatial filter, in actuality, is significantly larger than the bounds of $F_p\{U(x,y;z=-2f_p)\}$, then we may treat it as being infinite in extent. The spatial filter is aligned parallel to the y-axis but is not necessarily centered with respect to it (i.e. even about x=0):

$$T(x,y)=\sum_{m=-\infty}^{m=\infty}\mathrm{rect}\left(\frac{x-\alpha\Delta-m\Delta}{\epsilon\Delta}\right) \qquad (6.3)$$

The function T(x,y) is plotted in Figure 6.2. The filter period is Δ, the width of the transparent strips of the filter is ϵ, and the offset is α. The rect{*} notation follows that of Goodman [35]. The filter transmission can be expanded in a Fourier series. The mathematics is straightforward

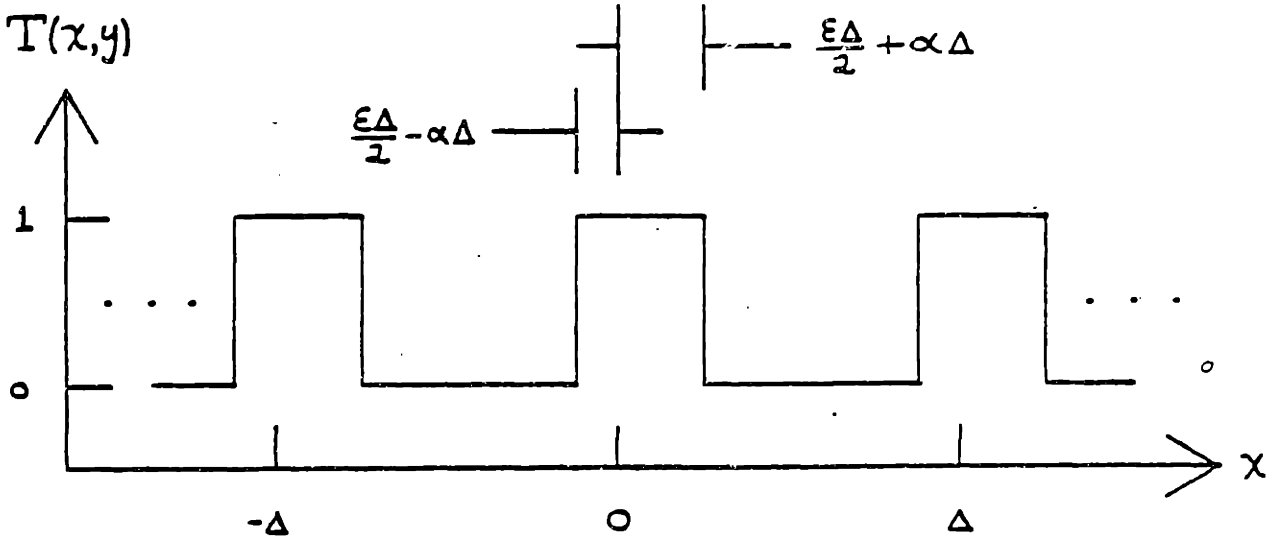

Figure 6.2. Plot of spatial filter transmission T(x,y). Slit period is Δ, duty cycle (fractional slit width) is ϵ, and the fractional offset from the optic axis is α.

and only the results are stated:

$$T(x,y) = \sum_{m=-\infty}^{m=\infty} \gamma_m \exp(2\pi j m x/\Delta) \tag{6.4a}$$

$$\gamma_m = \epsilon \exp(-2\pi j m \alpha) \operatorname{sinc}(\pi m \epsilon) \tag{6.4b}$$

Note that the magnitude of γ_m is a function only of (m and) the spatial filter duty cycle, ϵ.

The value of $F_S\{\exp(2\pi j m x/\triangle)\}$ will need to be determined. Clearly, if the spatial filter is removed, that is, it is everywhere transmitting, then the field at $z=2f_s$ must be the inverted image of the field at $z=-2_p$. This image is precisely $(f_p/f_s)U(-(f_p/f_s)x,-(f_p/f_s)y;z=-2f_p)$. Referring to Eq.6.1c, it must be the case that $F_S\{T(x,y)\}=\delta(x,y)$ when $T(x,y)=1$, or $F_S\{1\}=\delta(x,y)$. Appealing to the nature of the Fourier transform it is possible to show

$$\mathcal{F}_s\{\exp(2\pi j m x/\Delta)\} = \delta(x-\lambda f_s m/\Delta, y) \tag{6.5}$$

where λ is the wavelength of operation. Equation 6.5 equivalently expresses the thought that the secondary lens will focus a tilted plane wave down to an off-axis point. It is further assumed that the filter period is equal to the period of the interference pattern of the array (assuming coherence);

$$\triangle = \lambda f_p/D \tag{6.6}$$

This condition will be relaxed in a later section. Combining Eqs. 6.1-6 and making use of properties of $\delta(x,y)$, the field at $z=2f_s$ is preliminarily determined to be

$$U(x,y;z=2f_s) = \sum_{m=-\infty}^{m=\infty} \gamma_m \delta\left(x - m\frac{f_s}{f_p}D, y\right) * \frac{f_p}{f_s}\sum_{n=-2}^{n=2} \psi_n u\left(-\frac{f_p}{f_s}x - nD, -\frac{f_p}{f_s}y\right) \tag{6.7a}$$

$$= \frac{f_p}{f_s}\sum_{m=-\infty}^{m=\infty} \gamma_m \sum_{n=-2}^{n=2} \psi_n u\left(-\frac{f_p}{f_s}x + (m-n)D, -\frac{f_p}{f_s}y\right) \tag{6.7b}$$

$$= (f_p/f_s)\sum_{p=-\infty}^{p=\infty}\left(\sum_{n=-2}^{n=2}\gamma_{n-p}\psi_n\right)u\left(-(f_p/f_s)x - pD, -(f_p/f_s)y\right) \quad (6.7c)$$

where terms in u(x,y) have been collected by introducing the summation variable p=n-m. The summation in parenthesis in Eq.6.7c is a discrete convolution of the "functions" v_n and ψ_n (and for convenience is called B_p). Whereas in the plane $z=-2f_p$ the field consisted of only five weighted and shifted versions of u(x,y), in the plane $z=2f_s$ the field consists of an infinite number of weighted, shifted, and inverted images of u(x,y), the weights being convolutions of the original weights with five consecutive Fourier coefficients of T(x,y).

Up until now, no numerical aperture for the system has been assumed. At the very least, the size of the gain element array (for the rightwards pass through the passive subsystem), defines an aperture; so does the size of the output mirror. In this realization of the Laser, the limiting aperture is presented by the lenses. The primary and secondary lenses are of f/2.5 design. Together with the spatial filter spacing and the wavelength of operation this implies a limitation of

$$|p| \leq 2 \text{ (realization dependant)} \quad (6.8)$$

Thus the field completing a leftward pass through the passive subsystem of the Laser is exressed by

$$U(x,y;z=2f_s) = \frac{f_p}{f_s}\sum_{p=-2}^{p=2} B_p\, u\left(-\frac{f_p}{f_s}x - pD, -\frac{f_p}{f_s}y\right) \quad (6.9a)$$

$$B_p \equiv \sum_{n=-2}^{n=2}\gamma_{n-p}\psi_n \quad (6.9b)$$

Equation 6.9b is expressible in matrix form as

$$\bar{B} = \bar{\gamma}\,\bar{\Psi} \tag{6.10a}$$

$$\bar{B} = \begin{bmatrix} B_{-2} \\ B_{-1} \\ B_0 \\ B_1 \\ B_2 \end{bmatrix} \tag{6.10b}$$

$$\bar{\gamma} = \begin{bmatrix} \gamma_0 & \gamma_1 & \gamma_2 & \gamma_3 & \gamma_4 \\ \gamma_{-1} & \gamma_0 & \gamma_1 & \gamma_2 & \gamma_3 \\ \gamma_{-2} & \gamma_{-1} & \gamma_0 & \gamma_1 & \gamma_2 \\ \gamma_{-3} & \gamma_{-2} & \gamma_{-1} & \gamma_0 & \gamma_1 \\ \gamma_{-4} & \gamma_{-3} & \gamma_{-2} & \gamma_{-1} & \gamma_0 \end{bmatrix} \tag{6.10c}$$

$$\bar{\Psi} = \begin{bmatrix} \Psi_{-2} \\ \Psi_{-1} \\ \Psi_0 \\ \Psi_1 \\ \Psi_2 \end{bmatrix} \tag{6.10d}$$

Figure 6.3a summarizes consideration of the leftward pass by using this matrix notation. The output of the Laser by the vector $t\bar{B}$ where t is the field transmission of the output mirror. The vector $r\bar{B}$, where r is the field reflectivity of the output mirror, represents the field that begins the rightwards pass through the passive subsystem. After reversing the direction of propogation and re-defining the z-axis per Figure 6.1b, the following relations are obtained from previously derived ones, by interchanging f_p , f_s and using Eq.6.9a:

$$(6.1c) \longrightarrow U(x,y;z=2f_p) = \mathcal{F}_p\{T(x,y)\} * \frac{f_s}{f_p} U\left(-\frac{f_s}{f_p}x, -\frac{f_s}{f_p}y; z=-2f_s\right) \tag{6.11a}$$

$$(6.4a,5,6) \longrightarrow \mathcal{F}_p\{T(x,y)\} = \sum_{m=-\infty}^{m=\infty} \gamma_m \delta(x-\lambda f_p m/\Delta, y) = \sum_{m=-\infty}^{m=\infty} \gamma_m \delta(x-mD, y) \tag{6.11b}$$

$$(6.9) \longrightarrow U(x,y;z=-2f_s) = r\frac{f_p}{f_s}\sum_{p=-2}^{p=2} B_p\, u\left(-\frac{f_p}{f_s}x - pD, -\frac{f_p}{f_s}y\right) \tag{6.11c}$$

These equations are easily combined, and introducing the summation variable n=p+m gives the result:

$$U(x,y;z=2f_p) = r\sum_{m=-\infty}^{m=\infty}\gamma_m \sum_{p=-2}^{p=2} B_p\, u(x-(m+p)D, y) \tag{6.12a}$$

$$= \sum_{n=-2}^{n=2}\left(r\sum_{p=-2}^{p=2}\gamma_{n-p}B_p\right) u(x-nD, y) \tag{6.12b}$$

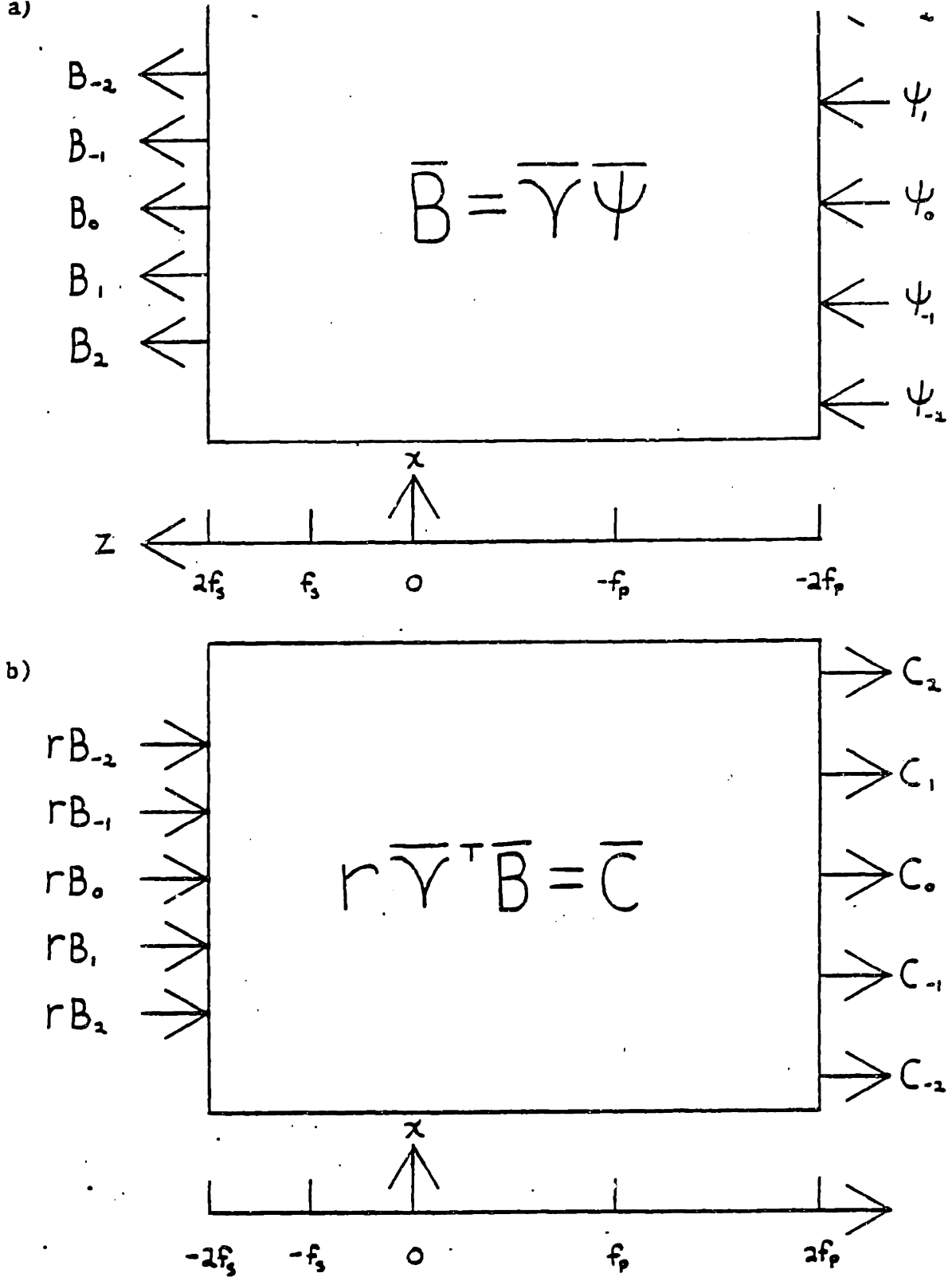

Figure 6.3. Matrix representation of passive part of the external cavity laser. a) Leftwards pass. b) Rightwards pass.

$$= \sum_{n=-2}^{n=2} C_n \, u(x-nD, y) \qquad (6.12c)$$

$$C_n \equiv r \sum_{p=-2}^{p=2} \gamma_{n-p} B_p \qquad (6.12d)$$

In Eq.6.12b the f/2.5 design of the primary lens has been invoked to truncate the n-summation, in analogy to the argument used to go from Eq.6.7c to Eqs.6.9a,b. Equation 6.12d can be put into matrix form as follows:

$$\bar{C} = r \bar{\gamma}^T \bar{B} \qquad (6.13a)$$

$$\bar{C} = \begin{bmatrix} C_{-2} \\ C_{-1} \\ C_0 \\ C_1 \\ C_2 \end{bmatrix} \qquad (6.13b)$$

$$\bar{\gamma}^T = \begin{bmatrix} \gamma_0 & \gamma_{-1} & \gamma_{-2} & \gamma_{-3} & \gamma_{-4} \\ \gamma_1 & \gamma_0 & \gamma_{-1} & \gamma_{-2} & \gamma_{-3} \\ \gamma_2 & \gamma_1 & \gamma_0 & \gamma_{-1} & \gamma_{-2} \\ \gamma_3 & \gamma_2 & \gamma_1 & \gamma_0 & \gamma_{-1} \\ \gamma_4 & \gamma_3 & \gamma_2 & \gamma_1 & \gamma_0 \end{bmatrix} \qquad (6.13c)$$

$$\bar{B} = \begin{bmatrix} B_{-2} \\ B_{-1} \\ B_0 \\ B_1 \\ B_2 \end{bmatrix} \qquad (6.13d)$$

A schematic equivalent is shown in Figure 6.3b. Equation 6.10a and Eq.6.13a are combined to specify the result of propagating the output of the active subsystem of the Laser around the passive subsystem and retuning to act as input to the active subsystem:

$$U(x,y;z=2f_p) = \sum_{n=-2}^{n=2} C_n \, u(x-nD, y) \qquad (6.14a)$$

$$\bar{C} = r \bar{\gamma}^T \bar{\gamma} \bar{\Psi} \qquad (6.14b)$$

where the elements of $\bar{\gamma}^T\bar{\gamma}$ are from Eq.6.2.

The active subsystem of the Laser, pictured in Figure 6.4, is handled in a simplified manner for purposes of brevity. It consists of five uncoupled sub-subsystems of a gain element and a collimating lens each. Each such sub-subsystem is termed a collimator pen. A rightwards traveling

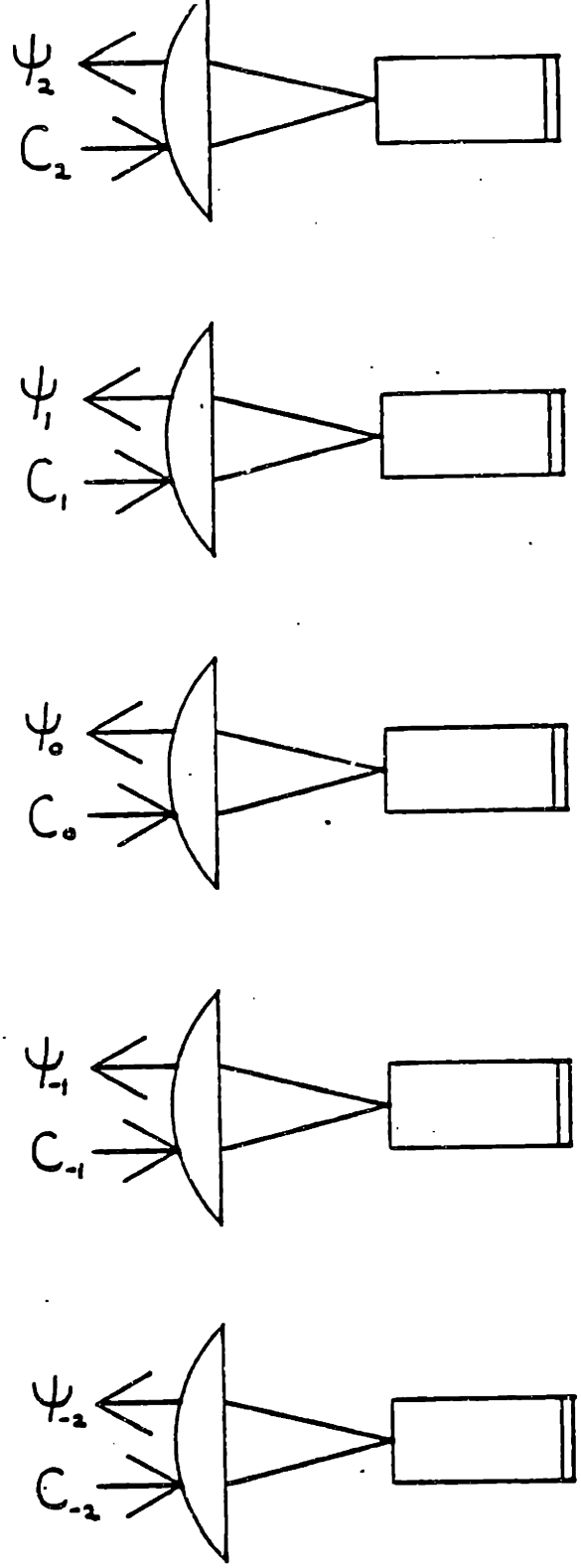

Figure 6.4. Optical diagram of active part of external cavity laser.

wave of the form $C_n u(x-nD,y)$ is present at the left focal plane of the nth collimating lens. This couples into the nth gain element through the antireflection coated left facet, is amplified, reflected at the right facet, amplified, couples out, and is present at the left focal plane of the collimating lens as a leftwards travelling wave of the form $\Psi_n u(x-nD,y)$. The effective field gain of the collimator pen is G_n, where effective gain includes both passes through the gain element and coupling and reflection coefficients. The most important qualitative feature of the amplification mechanism is that it saturates. That is, the gain decreases as the intensity of the radiation passing through the collimator pen increases. The exact nature of this saturation will be discussed shortly; here, the nonlinear dependence is merely indicated:

$$\Psi_n = G_n(\Psi_n)C_n \tag{6.15}$$

A solution for the behavior of the Laser must self consistently determine the modal amplitudes Ψ_n and the gains G_n. Therefore, Eq.6.14b and Eq.6.15, describing the passive and active subsystems, are combined to yield

$$\left(r\,G(\bar{\Psi})\bar{V}^T\bar{V} - \bar{1}\right)\bar{\Psi} = 0 \tag{6.16a}$$

$$G(\bar{\Psi}) = \begin{bmatrix} G_{-2}(\Psi_{-2}) & 0 & 0 & 0 & 0 \\ 0 & G_{-1}(\Psi_{-1}) & 0 & 0 & 0 \\ 0 & 0 & G_0(\Psi_0) & 0 & 0 \\ 0 & 0 & 0 & G_1(\Psi_1) & 0 \\ 0 & 0 & 0 & 0 & G_2(\Psi_2) \end{bmatrix} \tag{6.16b}$$

where $\bar{1}$ is the identity matrix. Equation 16a is the basic result of this section. Its solution entails consistently determining the gains of the collimator pens $G_n(\Psi_n)$ (after specifying the exact dependence of G_n on Ψ_n),

and the modal amplitudes Ψ_n themselves. In general, because Eq.6.16a is a system of nonlinear equations, such a task is best performed by a computer using iterative numerical techniques. This is discussed in Chapter 7.

In summary, a matrix equation that models the behavior of the Laser is given. Its derivation entails expressing the spatial filter transmission a Fourier series, recognizing spatial bandwidth limitations, and acknowledging the nonlinear character of the amplification mechanism.

6.2 Analysis of Active Part of the External Cavity Laser

The theoretical treatment of the gain elements closely follows that of Cassidy [36] in his model of the injection laser. In this case, however, monochromaticity is assumed, as well as one perfectly AR-coated facet. The approach has been termed a "Fabry-Perot" model and it assumes forward and backward travelling waves inside the gain medium. This is in distinction to the so-called "rate equation" approach in which spatial dependence is omitted and instead the variables include the photon population (of a particular mode) and the total injected carrier population inversion. Equivalently, one can divide by the mode volume in order to speak in terms of photon densities and inversion density. With appropriate assumptions, either model will conform to reality [37], but the Fabry-Perot model is the more natural one to use. If the rate equations are restricted to an infinitesimal section through the gain element, however, and then integrated over length, the Fabry-Perot model would be immediately obtained.

One crucial assumption is made in the following derivation, that the gain medium can be modeled as a homogeneous two level system with negligible lower level population. As discussed in Chapter 5, the gain and

spontaneous emission have different dependencies on upper and lower level occupation probabilities . Both quantities increase for increasing upper level occupation, but for negligible lower level occupation the gain and spontaneous emission are proportional. This simplification results in a model which can be solved exactly. It also implies that situations involving absorption cannot be considered; since absorption is negative gain, the proportionality would dictate a negative spontaneous emission, which is unphysical. On the other hand, lower level population can be included by scaling system parameters [38] in order to reflect the additional pumping necessary to attain a specified gain and the additional spontaneous emission that would accompany the new upper and lower level populations.

There are two differential equations necessary to describe the model, one for the inversion density at a particular point along the length of the gain element waveguide, and one for the photon fluxes I^+ and I^- of the mode travelling in each direction. The solution is assumed integrated over the (effective) cross section of the waveguide. The former equation is a rate equation with respect to time, the latter a propogation equation with respect to distance:

$$\frac{dn}{dt} = N - Sn - \sigma n\left(I^+ + I^-\right) \qquad (6.17a)$$

$$\frac{dI^{\pm}}{dz} = \pm gn\left(I^{\pm} + c\right) \qquad (6.17b)$$

where N is the inversion pumping per unit length, S is the inverse of the spontaneous carrier lifetime, σ describes the coupling of the mode to the inversion, gn is the gain coefficient per unit length for the mode, and gnc is the spontaneous emission per unit length input to the forward or backward travelling mode. The two variables σ and g have values that are

very close [36], and it should not be too blatant an approximation when, later, their equality is assumed. Equation 6.17a is first solved in the steady state, and then substituted into Eq. 6.17b. After an appropriate change of variables, Eq. 6.17b becomes:

$$\frac{d\phi^{\pm}}{dz} = \pm g \frac{\phi^{\pm}}{1+\phi^{+}+\phi^{-}} \qquad (6.18a)$$

$$\phi^{\pm} = \frac{\sigma(I^{\pm}+C)}{S-2\sigma C} \qquad (6.18b)$$

$$g = \frac{gN}{S-2\sigma C} \qquad (6.18c)$$

where $\phi^{\pm}$ is the adjusted flux. The objective is to determine the forward travelling photon flux output from the front facet of the gain element, assuming that the backward travelling photon flux input at the same facet is known. Equation 6.18a is transformed into an equation in one variable by noting that $\phi^{+}\phi^{-}=K$ is a constant of motion. Specifically, the equation for the adjusted flux ϕ^{-} becomes:

$$\frac{d\phi^{-}}{dz} = -g \frac{\phi^{-}}{1+\frac{K}{\phi^{-}}+\phi^{-}} \qquad (6.19)$$

The gain medium can be visualized as extending from the plane z=0 to the plane z=-L. Equation 6.19 is integrated from end to end and subscripts are appended to the adjusted fluxes to denote the end at which each is measured:

$$\ln\frac{\phi^{-}_{-L}}{\phi^{-}_{0}} = gL-(\phi^{-}_{-L}-\phi^{-}_{0})-\left(\frac{K}{\phi^{-}_{0}}-\frac{K}{\phi^{-}_{-L}}\right) \qquad (6.20)$$

The constant K is determined at the partially reflecting facet at z=-L. The rear facet reflectivity is R_b. The reflected adjusted flux from the rear facet is related to the incident adjusted flux onto the rear facet by

$$\Phi_{-L}^{+} = R_b \Phi_{-L}^{-} + \frac{\sigma C}{S - 2\sigma C}(1 - R_b) \qquad (6.21a)$$

$$K = \Phi_{-L}^{-}\left[R_b \Phi_{-L}^{-} + \frac{\sigma C}{S - 2\sigma C}(1 - R_b)\right] \qquad (6.21b)$$

By using the definition 6.18b, it can be shown that Eq. 6.21a is the familiar proportionality between reflected and incident photon fluxes. This proportionality does not hold for the adjusted fluxes. Finally, Eq. 6.21b is substituted into Eq. 6.20 to yield

$$V = \exp\left\{\frac{gNL}{S - 2\sigma C} - (V-1)\left[\Phi_o^{-}(1 + R_b V) + \frac{\sigma C}{S - 2\sigma C}(1 - R_b)\right]\right\} \qquad (6.22a)$$

$$V = \Phi_{-L}^{-} / \Phi_o^{-} \qquad (6.22b)$$

This is an important result. It is a transcendental equation in v, the ratio of the backward travelling adjusted flux at the rear of the gain medium to that at the front. The latter quantity is known. Once Eqs. 6.22 are solved (assuming a solution exists), then K can be determined from Eq. 6.21. Then the forward travelling adjusted flux at the front of the gain medium is easily determined and likewise the modal photon flux exiting the front antireflection-coated facet:

$$\Phi_o^{+} = K / \Phi_o^{-} \qquad (6.23a)$$

$$I^{+}(0) = \frac{S - 2\sigma C}{\sigma} \Phi_o^{+} - C \qquad (6.23b)$$

Multiplying by the energy per photon yields the modal power exiting the gain element. The antireflection coating is assumed perfect for simplicity. Coupling from the front facet to the rear focal plane of the collimating lenses is straightforward and is not discussed here. The aforementioned plane marks the division between the active and passive subsystems of the laser. It should also be noted that Eq. 6.22a is amenable to solution by iterative numerical techniques and the rate of

convergence can be accelerated significantly by using, for example, the Newton-Raphson method rather than a simpler successive substitution method [39]. Such considerations were included in the design of the computer simulation (Chapter 7). Having determined the output photon flux as a function of the input photon flux, it is now necessary to calculate the phase shift for fields amplified by the gain element. Two approximations are made at this point. The first is that the gain-dependent phase shift is proportional to the logarithmic field gain, being related, as it were, to the real and imaginary parts of the refractive index. That a general proportionally exists between the two has been shown experimentally [40]. According to the preceeding analysis, the modal photon fluxes are a function of position inside the gain medium; although the inversion pumping may be uniform, the gain saturation is not. Hence the phase shift per unit length is not constant. It is difficult to calculate the total accrued gain-dependent phase shift resulting from two passes through the gain element (down and back) interrupted by a reflection from the rear facet. To circumvent this problem, as a second assumption, the gain coefficient is assumed constant , at a level consistent with the derived output photon flux. Thus the "average" logarithmic power gain is

$$\bar{g} = \frac{1}{2L} \ln \frac{I_o^+ / I_o^-}{R_b} \qquad (6.24a)$$

$$= -2(\omega^2 n_o / c^2 k_o) \Delta n'' \qquad (6.24b)$$

where ω is the angular frequency, n_o and k_o are the real index of refraction and wavevector, respectively, that are gain independent, c is the speed of light, and $\Delta n''$ is the imaginary part of the complex gain-dependent contribution to the index of refraction [40]. The average logarithmic power gain is -2 times the imaginary part of the gain-dependent

contribution to the wavevector. To obtain the phase shift per unit length, the -2 is divided out and the imaginary part of the gain-dependent index is replaced by the real part:

$$\beta = (\omega^2 n_o / c^2 k_o) \Delta n' \qquad (6.25)$$

where $\Delta n'$ is the real part of the gain-dependent refractive index. Invoking the proportionality between real and imaginary parts, and using Eq. 6.24b to solve for the term in parentheses in terms of $\bar{g}$, it is easy to show that:

$$\beta = -\bar{g}\beta_c/2$$

where β_c is the ratio of real to imaginary parts of the gain dependent refractive index. The phase shift accrued over the down-and-back trip through the gain element is obtained by multiplying by 2L. The phase shift from reflection from the rear facet is ignored, since it is mostly gain-independent. Lastly, the average logarithmic field gain is $\bar{g}/2$.

The tractability of computing the action of the resonator on internal fields has been shown. Beginning with fields exiting the collimator pens, Eqs. 6.14 determine what returns. After finding the associated photon flux and adjusted flux input to each gain element through its antireflection coated facet, Eqs. 6.23 determine the output fluxes. This information is sufficient to fix the magnitude of the field gain but not its phase. The latter is supplied via the proportionality of real and imaginary parts of the gain-dependent index of refraction (Eq.6.26). Thus the fields exiting the collimator pens are determined, completing one round trip of the laser.

6.3 Empirical Determination of Theoretical Parameters

One of the major applications of the theoretical treatment of the external cavity laser is as an expediant alternative to experimentation.

It is possible to use theory to indicate the outcome of proposed engineering changes to the laser for example. If theory predicts deleterious results, the proposed change can be aborted and time and money saved. Of course, theories can be wrong. In order to merit any confidence at all, the theory must be consistent with a foundation of empirically known behavior. This requires that the parameters of the theory take on realistic values. The topic of this section is to show how those values can be obtained from convenient measurements of observable quantities. The parameters peculiar to the passive part of the laser are not discussed. To the accuracy of the theory, they are few in number and well known: focal lengths, numerical apertures, spacings, reflectivities, spatial filter periods and duty cycles. Lens aberrations, misalignments, etc., are not discussed. On the other hand, the parameters governing the action of the gain elements are less well known. They are the focus of attention.

(1) The quantity gNL/S is related to measurable quantities. To do this Eqs. 6.17 are taken to the limit of negligible gain saturation:

$$\frac{dI^{\pm}}{dz} = \pm \frac{gN}{S}(I^{\pm}+C) \qquad (6.27)$$

This can be integrated to yield

$$I_o^+ = C(G-1)+G\,I_{-L}^+ \qquad (6.28a)$$

$$I_{-L}^- = C(G-1)+G\,I_o^- \qquad (6.28b)$$

$$I_{-L}^+ = R_b\,I_{-L}^- \qquad (6.28c)$$

$$I_o^- = R_a\,I_o^+ \qquad (6.28d)$$

$$G = \exp gNL/S \qquad (6.28e)$$

The gain element has been removed from any external cavity and stands isolated. Recall that the gain medium extends from z=0 to z=-L. The facet at z=0 is assumed to have a reflectivity R_a (not necessarily zero) and the facet at z=-L is assumed to have a reflectivity R_b. All photons are

internally generated. The photon fluxes in Eqs. 6.28 are measured inside the gain medium at the respective facet and in the respective direction.

In an ad hoc fashion, the distributed spontaneous emission flux in Eqs. 6.28 can be lumped into a single forward travelling flux outside the facet at z=-L , and a single backward travelling flux outside the facet at z=0. The two lumped fluxes are assumed uncorrelated. It is important to note that these virtual external fluxes may only be used to determine the flux at a point internal to the gain medium.

Having eliminated the internal spontaneous emission, the gain element becomes a Fabry-Perot etalon with gain. The governing differential equation is simply:

$$\frac{dI^{\pm}}{dz} = \pm \frac{gN}{S} I^{\pm} \qquad (6.29)$$

Restating Eqs. 6.28 in light of the lumping of the spontaneous emission:

$$I_0^+ = G I_{-L}^+ \qquad (6.30a)$$

$$I_{-L}^- = G I_0^- \qquad (6.30b)$$

$$I_{-L}^+ = (1-R_b) C_b^+ + R_b I_{-L}^- \qquad (6.30c)$$

$$I_0^- = (1-R_a) C_a^- + R_a I_0^+ \qquad (6.30d)$$

$$C_b^+ = C(1-G^{-1})/(1-R_b) \qquad (6.30e)$$

$$C_a^- = C(1-G^{-1})/(1-R_a) \qquad (6.30f)$$

The boundary conditions Eqs. 6.28c,d have changed to conform with the interpretation that the spontaneous emission is incident from the outside of the gain medium rather than the first picture where all photons were generated inside the medium. An additional assumption is that the power transmitted into the gain medium due to the flux incident on a facet from the outside adds to flux reflected from the facet due to the flux incident on that facet from the inside. The fact that the lumped spontaneous fluxes

in Eqs. 6.30e,f go to zero for G=1 or gNL/S=0 reflect the assumption of proportionality of spontaneous emission and (logarithmic) gain. It can be seen that with the relations Eqs. 6.30, the ad hoc interpretation leads to the same result for I_o^+ as Eqs. 6.29. The value of the latter flux is the immediate objective.

Typically one calculates the transmitted or reflected flux from a Fabry-Perot etalon due to an incident flux or fluxes. In this case, it is an internal flux which must be calculated from two external fluxes and the formulae are not the usual ones. The photon flux incident on the facet at z=0 from the inside is a sum of two terms over a common denominator:

$$I_o^+ = \frac{C_a^-(1-R_a)R_bG^2 + C_b^+(1-R_b)G}{(1-\sqrt{R_aR_bG^2})^2 + 4\sqrt{R_aR_bG^2}\sin^2\phi} \qquad (6.31)$$

using the definitions for the virtual external input fluxes, Eq. 6.31 reduces to

$$I_o^+ = \frac{C(G-1)(R_bG+1)}{(1-\sqrt{R_aR_bG^2})^2 + 4\sqrt{R_aR_bG^2}\sin^2\phi} \qquad (6.32)$$

to obtain the superluminescent output power into the region z>0, it is necessary to multiply Eq. 6.32 by the transmission of the facet at z=0 and also the energy per photon:

$$P_a = \frac{\hbar\omega(1-R_a)C(G-1)(R_bG+1)}{(1-\sqrt{R_aR_bG^2})^2 + 4\sqrt{R_aR_bG^2}\sin^2\phi} \qquad (6.33)$$

(Again, the result of P_a=0 for G=1 derives from the assumed proportionality of spontaneous emission and gain.) The phase shift ϕ depends on the wavelength of operation.

In seeming contradiction to one of the basic assumptions of the theory, it is now assumed that a continuous spectrum of wavelengths is circulating inside the gain element. As long as the assumption of

negligible gain saturation persists there is no competition between different wavelengths, so for each wavelength in the superluminescent spectrum Eq. 6.33 is applicable, with ϕ adjusted for that wavelength. It is assumed also that the basic parameters of the gain element are negligibly varying in wavelength relative to $\sin\phi$.

The superluminescent diode spectrum varies between maximum and minimum values of

$$P_{amax} = \frac{\hbar\omega(1-R_a)C(G-1)(R_bG+1)}{(1-\sqrt{R_aR_bG^2})^2} \qquad (6.34a)$$

$$P_{amin} = \frac{\hbar\omega(1-R_a)C(G-1)(R_bG+1)}{(1+\sqrt{R_aR_bG^2})^2} \qquad (6.34b)$$

The square root of the ratio of maximum to minimum defines the quantity w. Using Eqs. a,b, it can be shown that

$$W = \sqrt{P_{amax}/P_{amin}} \qquad (6.35a)$$

$$\ln\left(\frac{W-1}{W+1}\right) = gNL/S + \ln\sqrt{R_aR_b} \qquad (6.35b)$$

where the definition of G, Eq. 6.28e, has been used. Many models have been proposed to treat the dependence of gain on inversion, and thereby on current. Here, the logarithmic gain is assumed to have a linear dependence on current [27]. (Regardless of the precise dependence, a linearization would be permissible over a limited range.) Therefore Eq. 6.35b becomes

$$\ln\left(\frac{W-1}{W+1}\right) = (i-i_o)/i_n + \ln\sqrt{R_aR_b} \qquad (6.36)$$

where i_n and i_o are normalization and offset parameters that describe the dependence of gNL/S on the gain element current i. By plotting ln((w-1)/(w+1)) versus current I and fitting a line to the data, the normalization current i_n is determined as the inverse slope of the fit line.

The offset current is determined in a slightly different manner. Up to this point there was negligible gain saturation and the gain element was presumed to be run below threshold. Also, the facet reflectivities were left general. However, by assuming that the facet reflectivities were unchanged from the original diode laser reflectivities and stretching the assumption of negligible gain saturation, the offset current i_o is determined. For the original symmetric diode laser at threshold, Eq. 6.36 is evaluated. The ratio of maximum to minimum for the superluminescent diode-spectrum becomes infinite ($\ln((w-1)/(w+1))=0$). The current is the known threshold current ($i=i_{th}^o$). The facet reflectivities are known ($R_a=R_b=R_L$). The normalization current can be determined from the superluminescent diode spectra in two ways; either for the original diode laser at lower currents or at the same currents but for the gain element with reduced facet reflectivity due to antireflection coating. Then i_o is determined to be

$$i_o = i_{th}^o + i_n \ln(R_L) \tag{6.37}$$

By plugging the values for i_n and i_o into Eq. 6.36, it is possible to estimate the value for R_aR_b; and if R_b is not changed from its value on the original diode laser, the value of R_a can be ascertained [27]. For the experiments performed measurements were taken from superluminescent diode spectra (Table 5.3). Linear fits to the data were made for each gain element. the average inverse slopes (the normalization current) was taken to be i_n=24mA. The average diode laser threshold current (i.e., before antireflection coating) was 86mA. Original facet reflectivity, based on the Fresnel reflection between media of indices 1 and 3.6, was R_L=32. Thus, using Eq. 6.37, the offset current was fixed at i_o=59mA. One implication of the proportionality of spontaneous emission and gain, or equivalently,

neglect of lower level population, is that the operating current must not fall below 59mA, or else the (gain and) spontaneous emission would become negative. This is due to the range limitation of the linearization. However, the superluminescent spectra were recorded for 60mA to 140mA, which <u>is</u> appropriate for the experiments performed.

The linearization that was used to go from Eq.6.35b to 6.36, namely,

$$gNL/S = (i-i_o)/i_n \tag{6.38}$$

is the basic result of this subsection. The variables i, i_o, i_n are easily determined from measurements, as described. It is not necessary to separately determine the values of the four parameters on the left hand side of Eq.6.38, since gNL (but not S) always appears in combination in the theory. For the spontaneous carrier lifetime 1/S, no independent determination was made. Rather, a typical value of 3nS has been obtained from the literature [41,42].

The values of three additional parameters are to be found. The cross section σ, which accounts for the coupling of the photons to the inversion when saturation is included, is obtained from previously determined parameters and the measured slope of the output power versus input current for the original diode laser. The factor C, denoting the ratio of spontaneous emission to gain in the flux propogation equations (Eqs. 6.17,27), will be indirectly obtained from a reference based on a rate equation model. Finally, the coupling efficiency between gain element and end mirror is estimated, independent of spatial filter effects.

(2) To determine the cross section σ, Eq. 6.20 is rewritten as

$$\left(\frac{K}{\Phi_o^-} - \Phi_o^-\right) + \left(\Phi_{-L}^- - \frac{K}{\Phi_{-L}^-}\right) = gL + \ln\left(\frac{\Phi_o^-}{\sqrt{K}}\,\frac{\sqrt{K}}{\Phi_{-L}^-}\right) \tag{6.39a}$$

$$(\Phi_o^+ - \Phi_o^-) + (\Phi_{-L}^- - \Phi_{-L}^+) = gL + \ln\sqrt{\frac{\Phi_o^-}{\Phi_o^+}\,\frac{\Phi_{-L}^+}{\Phi_{-L}^-}} \tag{6.39b}$$

where the definition of K at both ends has been used to obtain the latter equation. In the limit of very large photon flux such that C<<I, using the definition of ϕ, Eq. 6.18b, yields

$$(I_0^+ - I_0^-) + (I_{-L}^- - I_{-L}^+) = \frac{gNL}{\sigma} + \frac{S}{\sigma} \ln \sqrt{\frac{I_0^-}{I_0^+} \frac{I_{-L}^+}{I_{-L}^-}} \qquad (6.40)$$

Assume that the diode laser is isolated so that no photons impinge on the facets from the outside, and that facet absorption is negligible. Then the differences between the internal fluxes incident and reflected from the facets are the output fluxes. The ratio of reflected to incident fluxes are the facet reflectivities. Multiplying by the energy per photons leads to the following expression for the output powers:

$$P_a + P_b = \frac{\hbar\omega}{\sigma} \left(gNL + S \ln \sqrt{R_a R_b} \right) \qquad (6.41)$$

For the original symmetrical diode, there are the simplifications $P_a = P_b = P_{se}$ and $R_a = R_b = R_L$. Equation 6.41 becomes:

$$2P_{se} = \frac{\hbar\omega S}{\sigma} \left(\frac{i - I_0}{i_n} + \ln R_L \right) \qquad (6.42)$$

where Eq. 6.42 is obtained by using Eq. 6.38 to express gNL in terms of S and i. By differentiating Eq. 6.42 with respect to current and solving for σ, one obtains

$$\sigma = \hbar\omega S \left(2 i_n \frac{dP_{se}}{di} \right)^{-1} \qquad (6.43)$$

The derivative dP_{se}/di is simply the slope of the (single-ended) power versus current curve for the diode laser. The other parameters have been previously determined. For the experiments performed, the average slope of the output power versus current (Table 5.1) was taken to be 0.13 mW/mA. This leads to a value of $\sigma = 1.3 \times 10^{-8}$.

(3) To determine the spontaneous emission flux C, Eq. 6.17b is taken to the limit of very low photon flux:

$$\frac{dI^{\pm}}{dz} = \pm gnC \qquad (6.44)$$

where n is the inversion per unit length. Integrating Eq. 6.44 in each direction and multiplying by the energy per photon, one finds

$$\hbar\omega I_0^+ - \hbar\omega I_{-L}^+ = \hbar\omega gnLC \qquad (6.45a)$$

$$\hbar\omega I_0^- - \hbar\omega I_{-L}^- = -\hbar\omega gnLC \qquad (6.45b)$$

As for the superluminescent diode, the medium is isolated, producing its own photons. There is no external illumination. By subtracting the second equation from the first, and realizing that the difference between incident and reflected power is the transmitted power (neglecting surface absorption), an expression is obtained for the total power output of the diode, both for z>0 and z<-L:

$$P_{tot} = 2\hbar\omega g(nL)C \qquad (6.46)$$

This result is compared to the rate-equation model of Suematsu, et. al. [34]. In the low photon flux limit their model reduces to

$$\frac{dn}{dt} = \frac{j}{ed} - \frac{n_s}{T_s} \qquad (6.47a)$$

$$\frac{dS_s}{dt} = -\Gamma S_s + C_s n_s / T_s \qquad (6.47b)$$

where n_s is the inversion density (inversion per unit volume), S_s is the photon density (photons per unit volume), j/ed represents the pumping for the inversion density, T_s is the spontaneous carrier lifetime (=1/S), Γ is the inverse of the photon lifetime, assumed due solely to output coupling, and C_s is the spontaneous emission factor. The subscript "s" specifying "Suematsu" has been appended to various parameters to prevent confusion with symbols used in the Fabry-Perot model.

In the steady state, Eq. 6.47b can be solved for photon density in the diode. Multiplying by the mode volume yields the total photon population

in the diode. Multiplying this by Γ gives the rate at which photons are being output from the laser. Multiplying this by the energy per photon gives the output power of the diode:

$$P_{tot} = \hbar\omega\Gamma S_s V = \hbar\omega(n_s v)C_s/T_s \qquad (6.48)$$

where v is the modal volume. Comparing Eq. 6.46 with Eq. 6.48, it is seen that the term in parentheses in each case, nL or $n_s v$, represents the total inversion of the diode. The energy per photon is the same in each case. Therefore, in order to result in the same total output power for each model, the following relationship is surmised between the spontaneous flux and the spontaneous emission factor:

$$2gC = C_s/T_s \qquad (6.49)$$

It is approximately the case that $g=\sigma$ [36]. If S is used for the inverse inversion lifetime and Eq. 6.43 replaces g, then the spontaneous flux is determined to be

$$C = C_s\left(\frac{i_n}{\hbar\omega}\frac{dP_a}{di}\right) \qquad (6.50)$$

The spontaneous emission factor is the fraction of the spontaneously emitted photons going into the guided mode in question. To exactly calculate this would involve treating both the guided and radiation modes. An approximate value may be obtained by mode counting techniques [43,44]:

$$C_s = \frac{\lambda^4}{8\pi n^2 n_g V \Delta\lambda} \qquad (6.51)$$

where n is the refractive index of the material n_g is the group index, V is the <u>effective</u> mode volume, and $\triangle\lambda$ is the effective bandwidth into which the spontaneous emission is emitted. Effective volume includes the effect of incomplete confinement of the mode to the active region of the diode laser. Effective bandwidth is explained with the following example: a

lorentzian with half-width half-maximum (HWHM) equal to a, and with unit height at center is meant to represent the spontaneous line. The integral under the line is πa. This is identical to the integral under a rectangle function of unit height (agreeing with the lorentzian at linecenter) with full width πa. This resolves two expressions by Marcuse that seem to differ by a factor of pi; one expression using bandwidth in the rectangular sense [43], the other using the HWHM of a lorentzian [44]. Using manufacturer supplied far-field intensity scans of the original diode lasers the effective width and height of the active region is estimated. The HWHM angular divergences were 4.8^{o} and 12^{o} is planes parallel and perpendicular to the active region, respectively. Assuming a wavelength of 834 nm and a sinc-squared intensity dependence:

$$\mathrm{sinc}^2\left(\frac{\pi}{\lambda b}\sin\theta_{HWHM}\right) = \frac{1}{2} \qquad (6.52)$$

where b represents the appropriate dimension of a rectangular aperture, one obtains <u>effective</u> values of width and height of 4.41 um and 1.78um, respectively. With a specified diode length of 250um, the effective volume obtains 1961 um^3. A refractive index of 3.6 and a group index of 3.9 is assumed. The group index is inferred from Eq. 5.2, the longitudinal mode spacing in the original diode laser spectra (0.36nm) and the given diode length.

From spectra recorded from the anti-reflection coated diodes, at low currents (60 mA) the HWHM of the spontaneous line was estimated to be approximately 13 nm, which leads to an effective bandwidth pi times larger or 41 nm. Inserting the values for wavelength, index, volume, and bandwidth into Eq. 6.51, a value of $5x10^{-6}$ is obtained for the spontaneous emission factor. Using Eq. 6.50 the spontaneous flux is determined to be $6x10^{10}$ sec^{-1}.

(4) Up to this point, in this section, only simple gain medium geometries have been considered. At the end of the gain medium there is a facet with no absorption. Whatever is not reflected is transmitted. In a single gain element external cavity laser, however, there is no reflector at one end of the gain medium. Instead, at that end the facet is antireflection coated and an external mirror lies beyond. There is generally less than unity coupling from the non-reflecting facet to the external mirror and from the external mirror back to the non-reflecting facet. The flux reflected back into the non-reflecting end of the gain medium and the flux output form the cavity are related to the flux exiting the non-reflecting end of the gain medium as follows

$$I_o^- = k^+ k^- R_x I_o^+ \tag{6.53a}$$

$$P_x / \hbar\omega = k^+ (1-R_x) I_o^+ \tag{6.53b}$$

where k^+ and k^- are the forward and backward coupling coefficients between the non-reflecting facet and the external mirror, R_x is the reflectivity of the external mirror, and P_x is the power output past the external mirror. The external mirror is assumed to have no absorption and the reflectivity of the non-reflecting facet is taken to be zero. With the new boundary condition on I_o^- and the definition of P_x, Eq. 6.41 is modified (with the help of Eq. 6.38) to

$$\left[\frac{1-k^+k^-R_x}{k^+(1-R_x)}\right] P_x + P_b = \frac{\hbar\omega S}{\sigma}\left(\frac{i-i_o}{i_n} + \ln\sqrt{k^+k^-R_xR_b}\right) \tag{6.54}$$

The output powers P_x and P_b are non-negative, and the coupling efficiencies k^+ and k^-, and the external mirror reflectivity can only take on values between zero and unity. Clearly, then, the left-hand side is non-negative. This directly leads to the definition of threshold current

$$i_{th} = i_o - i_n \ln\sqrt{k^+k^- R_x R_b} \qquad (6.55a)$$

$$= i_{th}^o + i_n \ln \frac{R_L}{\sqrt{k^+k^- R_x R_b}} \qquad (6.55b)$$

where Eq. 6.37 has been used to replace i_o. Equation 6.55b implies that knowledge of the normalization current i_n and the shift in threshold current $i_{th}-i_{th}^o$ is sufficient information to determine the coupling product to and from the external mirror (of known reflectivity). In fact, if the normalization current was not known, but the threshold shift for a second external mirror reflectivity was known, the two shifts would provide enough information to determine both i_n and k^+k^-.

For simplicity, equality of forward and backward coupling coefficients is assumed. As indicated by Table 5.2, the use of the 90% reflectivity end mirror with the antireflection coated gain elements in uncoupled external cavities resulted in essentially unchanged laser thresholds relative to the original diode lasers. Thus, using Eq. 6.55b, it may be concluded that $k^+k^-R_x=R_L$ from which an estimate of $k^+=k^-=0.60$ is obtained.

The preceeding values for i_n, i_o, σ, C, and $k^{\pm}$ are regarded as essential quantities (along with S) for applying a theoretical treatment of external cavity laser operation. Methods to determine these values have been detailed which are based on convenient measurements. To be sure, there are many more variables which exert influence on the laser; but to reiterate the sentiment expressed earlier, parameters specific to the passive part of the laser, including the spatial filter, are better known than the parameters quantifying the action of the active part. It is the latter group which has merited attention in this section.

6.4 Frequency Detuning

In connection with the observed multimode behavior of the external cavity laser, one of the most salient questions that can be asked is what is the frequency selectivity of the spatial filter. Empirically, the selectivity must be quite broad or else the observed spectra would have been inconsistent. On the other hand, the spatial filter is designed to match the interference pattern of a coherent phased array operating at a specific wavelength and, intuitively, some deleterious effects must arise as a consequence of operation at wavelengths different than the design wavelength. There are many other things that can go wrong, such as arrays that are only approximately uniform in spacing, or gain elements that have spatially dissimilar outputs. It is the question of wavelength that is at issue here.

In a natural way, the problem at hand is divisible at the boundary between the passive and active parts of the laser. It is then attacked from two perspectives. First, given the output of the array at a non-design wavelength, the fields returned to the array are calculated. Second, the behavior of the array towards the returned field is considered. In order to obtain a feel for the effect of frequency detuning, it is not necessary to consider the realistic limitations of numerical aperture as pertains to the primary or secondary lenses or the size of the end mirror. In the non-detuned treatment of Eqs. 6.1-14, this implies that the field at the end mirror consists of an infinite number of evenly spaced (scaled, inverted) images of the array element. As before, the amplitude of each image is a weighted sum of the amplitudes of the five array elements, the weights for each image being a distinct set of five coefficients from the Fourier series representing the spatial filter transmission. The field returned to the array consists of an infinite number of (unscaled, erect)

images of the array element. Only five images enter the array of gain elements; the others are lost beyond the bounds of the array. The five that are captured each have an amplitude which is a weighted sum of the amplitudes of the infinite number of images at the end mirror, a distinct set of weights being used in each case.

The non-apertured assumptions made imply that the Fourier transformations are exact. Therefore, the field returned to the gain element array may be calculated directly from the output of the array without the ad hoc limitations imposed by numerical aperture (Eq. 6.8). The passive part of the laser can be unfolded at the end mirror. The field input to the passive part of the laser undergoes four Fourier transformations and two spatial filterings. Using the notation of Eqs. 6.1,7, but moving the z-origin to the end mirror instead of at the spatial filter, the relation of returned field to input field is expressed by

$$U(x,y;z=2f_p+2f_s)=r\mathcal{F}_p\{T(x,y)\mathcal{F}_s\{\mathcal{F}_s\{T(x,y)\mathcal{F}_p\{U(x,y;z=-2f_p-2f_s)\}\}\}\} \quad (6.56)$$

By using theorems of Fourier transformation [35], Eq. 6.56 is simplified to

$$U(x,y;z=2f_p+2f_s)=r\mathcal{F}_p\{T(x,y)T(-x,-y)\}*U(x,y;z=-2f_p-2f_s) \quad (6.57)$$

Put into words, Eq. 6.57 states that the action of the passive part of the laser is to perform a convolution on the output of the gain element array and reflect this back into the array. The function which is convolved (with the output of the array) is the Fourier transform through the primary lens of the product of the spatial filter transmission with its inverted image. No assumptions have been made regarding the form of the spatial filter transmission or the composition of the array output.

Equation 6.2,3 are now assumed. That is, the array consists of five

uniformly spaced elements and the array consists of an infinite number of parallel slits aligned parallel to the y-axis. An interesting corollary to Eq. 6.57 is that for spatial filters with duty cycles less than 50 percent, it is possible to have an offset such that the product of T(x,y) and T(-x,-y) is everywhere zero. The field returned to the array drops to zero and so stimulated emis ion would cease. (There would still be spontaneous emission passing from the array through the passive part of the laser and exiting through the end mirror, so that cavity output would not drop entirely to zero) This effect is observed experimentally: as the spatial filter is translated in the x-direction, the output power undulates deeply and periodically (as a ranges through several spatial filter periods). Another way of seeing this is to consider a spatial filter with an offset as discussed. Assume one is looking at the spatial filter from a vantage point between the filter and the primary lens. The solid areas of the filter, of course, look dark. Looking through an open area of the filter to one side of the y-axis, however, one sees (via the action of the secondary lens and the end mirror) the back side of a solid area on the opposite side of the y-axis. The back of a solid area also looks dark. Therefore the entire spatial filter is effectively opaque to radiation making a round trip through the passive part of the laser.

For the periodic binary filter considered, alternating between 0 and 100 percent transmission, the product transmission T(x,y)T(-x,-y) can be expressed as a sum of two transmissions of the form given in Eq. 6.3. Both of the component transmissions are even in x, one being a "center-on" transmission with zero offset (α=0) and one being a "center-off" transmission with a half-period offset (α=.5). The duty cycle of the component transmissions are e_1 and e_2, both less than or equal to the

original filter duty cycle and generally not equal to each other. The exact value of ϵ_1 and ϵ_2 depends on the duty cycle and offset of the filter.

$$T(x,y)T(-x,-y) = \sum_{m=-\infty}^{\infty} \text{rect}\left(\frac{x-\alpha\Delta-m\Delta}{\epsilon\Delta}\right) \cdot \sum_{m=-\infty}^{\infty} \text{rect}\left(\frac{-x-\alpha\Delta-m\Delta}{\epsilon\Delta}\right) \qquad (6.58a)$$

$$= \sum_{m=-\infty}^{\infty} \text{rect}\left(\frac{x-m\Delta}{\epsilon_1\Delta}\right) + \sum_{m=-\infty}^{\infty} \text{rect}\left(\frac{-x-(m+1/2)\Delta}{\epsilon_2\Delta}\right) \qquad (6.58b)$$

$$\epsilon_1 = \begin{cases} \epsilon + |1-2\alpha| - 1 & , |1-2\alpha| > 1-\epsilon \\ 0 & , |1-2\alpha| < 1-\epsilon \end{cases} \qquad (6.58c)$$

$$\epsilon_2 = \begin{cases} \epsilon - |1-2\alpha| & , |1-2\alpha| < \epsilon \\ 0 & , |1-2\alpha| > \epsilon \end{cases} \qquad (6.58d)$$

It is assumed that ϵ and α, the duty cycle and offset of the spatial filter are restricted to lie on the interval [0,1]. It can be shown, for example, that for a 30 percent duty cycle filter, the product transmission is equivalent to a center-on type transmission only, as long as the offset is between 0 and 15 percent or between 85 and 100 percent. For an offset between 35 and 65 percent the product transmission is representable by a center-off type transmission only. For the remaining values of offset the product is zero. On the other hand, for a 60 percent duty cycle filter, there is a center-on transmission component for offsets between 0 and 30 percent and between 70 and 100 percent. There is a center-off transmission component for offsets between 20 and 80 percent. There is no offset range for which the product transmission is zero, and there are two ranges wherein both center-on and center-off transmissions are present.

It is also interesting to note that for duty cycles exceeding 50 percent and at offsets of 25 and 75 percent, the duty cycles of the

component transmissions are equal, that is $\epsilon_1=\epsilon_2=\epsilon-.5$. The period of the original filter is effectively halved. In order to obtain the coefficients in the Fourier series expansion of Eq 6.58b, it is necessary to add together two instances of Eq. 6.4b, with ϵ_1 and ϵ_2 replacing ϵ, and 0 and 0.5 replacing α. It would then be found that the odd components of the sum series (based on periods of $\triangle$) vanish. Only even harmonics remain, consistent with the period halving.

In general, however, it would not be too inaccurate to state that the product of the two transmissions T(x,y) and T(-x,-y), each with a period $\triangle$, itself is periodic with period $\triangle$. The worst that can be said for this generalization is that in specific cases (as discussed in the previous paragraph) the odd harmonics have values of zero and are therefore superfluous.

The Fourier series expansion of T(x,y)T(-x,-y) can be substituted into Eq. 6.57 along with the form of the array output, Eq. 6.2, and the return of the array can be calculated. Instead, a general approach will be outlined. The period of T(x,y)T(-x,-y) is $\triangle$. Therefore, in analogy with the left and center expression of Eq. 6.11b, the transform of the series is an infinite sum of delta functions spaced by $\lambda f_p/\triangle$, where λ is the operating wavelength. However, replacing Eq. 6.6 is the following expression

$$\triangle = \lambda_d f_p/D \tag{6.59}$$

saying that the spatial filter period is designed for a design wavelength λ_d, an array of element spacing D, and a primary lens focal length f_p. Then the delta function spacing in the transform of T(x,y)T(-x,-y) becomes $(\lambda/\lambda_d)D$.

According to Eq. 6.2, the array output consists of five collimated

uniformly spaced beams. Each beam serves as a generatrix upon which the comb of delta functions operates. The result in each case is an infinite array of returning beams spaced by the delta function spacing, which equals the gain element spacing for zero detuning. Ideally, the various images in the returned array (generated from one beam of the array output) are colinear with the output beams of neighboring elements, second nearest neighbors, third nearest neighbor, etcetera. In case of detuning, it is straightforward to show that for two elements, the ith and jth, the shear between the intended image diffracted by the passive part of the laser from the jth element and the output field of the ith element is expressed by

$$d_{ij} = (i-j)(1-\lambda/\lambda_d)D \tag{6.60}$$

The basic question that must be answered as a key to explain spatial filter tunability, is what is the sensitivity of a gain-element/collimator-lens combination with respect to the shear of a returned image. The answer depends on the shape of the collimated beam u(x,y).

To a reasonable approximation, the normalized output of the collimating lens of the ith element of the array is an elliptical gaussian beam given by

$$E_i^+ = u(x,y) = \sqrt{\frac{2}{\pi w_x w_y}} \exp -\frac{x^2}{w_x^2} \exp -\frac{y^2}{w_y^2} \tag{6.61}$$

where the x-origin has been shifted to the center of the ith element, the beam radii are w_x and w_y, and where the beam waists occurs at the rear focal plane of the collimating lens on the dividing plane between the active and passive parts of the laser. The field u(x,y) arises from an elliptical gaussian beam exiting the antireflection-coated gain element facet. This field is given by

$$\sqrt{\frac{2}{\pi w_{ox} w_{oy}}} \exp -\frac{x^2}{w_{ox}^2} \exp -\frac{y^2}{w_{oy}^2} \tag{6.62a}$$

$$w_{0x} = \lambda f_c / w_x \qquad (6.62b)$$

$$w_{0y} = \lambda f_c / w_y \qquad (6.62c)$$

The field at the rear focal plane of the collimating lens is Fourier-transform-related to the field at the front focal plane . Therefore one is effectively a scaled far-field diffraction pattern of the other and it cannot matter where (in z) one calculates the coupling between two beams. Instead of directly calculating the fraction of returning power coupled into the backward travelling mode in the gain element waveguide, the coupling is calculated by projecting the returning field evaluated at the rear focal plane of the collimating lens onto the transform of the gain element mode at the same plane, given by Eq. 6.61. The returning field is a summation of terms contributed by the collimated output of each of the five gain elements. Individually, each contribution is of the same shape as Eq 6.61, except for a shear in x given by Eq. 6.60. Thus the total returned field relative to the center of the ith element is

$$E_i^- = r \sum_j (\bar{V}^T \bar{V})_{ij} \psi_j \sqrt{\frac{2}{\pi w_x w_y}} \exp - \frac{(x-d_{ij})^2}{w_x^2} \exp - \frac{y^2}{w_y^2} \qquad (6.63)$$

In the absence of aperturing limitations $\bar{V}^T$ and $\bar{V}$ are infinite dimensional generalizations of the matrices given in Eqs. 6.13c and 6.10c. In the limit of vanishing shear, Eqs 6.14 are recovered.

Because of distinct shears, the coupling of an individual contribution to E_i^- is different and is handled separately. For the contribution from the jth element the coupling coefficient is given by the projection integral [45,46]

$$k_{ij} \approx \iint \left[\sqrt{\frac{2}{\pi w_x w_y}} e^{-\left(\frac{x^2}{w_x^2} + \frac{y^2}{w_y^2}\right)} \right] \left[\sqrt{\frac{2}{\pi w_x w_y}} e^{-\left(\frac{(x-d_{ij})^2}{w_x^2} + \frac{y^2}{w_y^2}\right)} \right] dx\,dy \qquad (6.64a)$$

$$= \exp \frac{-d_{ij}^2}{2w_x^2} \qquad (6.64b)$$

$$= \exp -2(i-j)^2 \left(\frac{D}{2w_x}\right)^2 \left(1 - \frac{\lambda}{\lambda_d}\right)^2 \qquad (6.64c)$$

where Eq. 6.60 has been used. The ratio $D/2w_x$ approximates the reciprocal fill factor of the array. The detuning-dependent coupling may be incorporated into an effective matrix element, and shear thereafter ignored, according to

$$(\bar{V}^T\bar{V})_{ijeff} = k_{ij}(\bar{V}^T\bar{V})_{ij} \quad . \qquad (6.65)$$

with k_{ij} given by Eq. 6.64c. These effective matrix elements are then used in Eq. 6.16.

It is assumed that the coupling of the y-dependent part of the returning field is constant with respect to shear. This is an approximation since the area of integration in Eq. 6.64a is bounded by the rear aperture of the collimating lens. The length of a vertical chord of a circle is certainly a function of the x-coordinate of the chord. Thus the vertical aperturing of the returning field changes with shear and the coupling efficiency drops more rapidly than is given by Eqs. 6.64. This inaccuracy is ignored in the interests of simplicity.

It can be shown that Eq. 6.65 is also a reasonable way to handle detuning in a numerically apertured system. The numerical aperture of the secondary lens effectively truncates the Fourier series for the second term of the product in Eq. 6.58a. The resulting product, is still periodic in $\triangle$ and will transform through the primary lens to a comb of delta functions. The comb is truncated due to the numerical aperture of the primary lens. However, the remaining delta functions induce detuning-dependent shears just as before.

For the specific realization of external cavity laser for this thesis, the ratio $D/2w_x$ is approximately 8. This figure is based on an element spacing of 1.98 cm, a half-power divergence half-angle of 4.8^o parallel to the active region, and a collimating lens focal length of .875 cm. For a wavelength detuning of 1 percent, or 8.34 nm, the coupling coefficients given by Eq. 6.64c take on values of 1, .99, .95, .89, and .81 for self, nearest neighbor, second nearest neighbor, third nearest neighbor, and fourth nearest neighbor, respectively. (Only the peripheral gain elements have neighbors as distant as fourth nearest.) This partly demonstrates the relative insensitivity of the spatial filter to detuning, as dictated by the posited mechanism. There may be other mechanisms augmenting the wavelength selectivity of the spatial filter, but these are not addressed. However, especially in light of the present insensitivity, such mechanisms must be sought. Note that the self-coupling term k_{ii} is always unity, meaning that the contribution of the ith element to itself always returns colinear. (This is analogous to grating diffraction: Irrespective of the wavelength, the zero order is always directed along the specular angle.) In the limits of severe detuning, but ignoring such possibilities as an offset d_{ij} being of magnitude D which would cause a retuning beam to skip over to the next gain element, the coupling efficiency approaches a Kronecker delta function. The effective matrix $\bar{V}^T\bar{V}$ becomes diagonal and the round-trip field transmission of the spatial filter becomes $(\bar{V}^T\bar{V})_{ii}$ for the ith element. In the absence of numerical aperturing the diagonal elements would all be equal. With aperturing they are not. For example, for a 50 percent duty cycle filter with no offset, the effective round trip field transmissions for the spatial filter are 45,46, and 36 percent for the on-axis, adjacent, and peripheral array elements. For a spatial filter

offset of 25 percent, the round-trip transmissions become 5,4, and 14 percent. With no numerical aperturing the transmission would be zero for all diodes in this case, as discussed earlier.

Of course, with the entire array operating coherently at a wavelength not too different from the design wavelength, the feedback into each element can be much greater than what would be consistent with the transmissions discussed in the previous paragraph. But even detuned, that is to say uncoupled, the transmissions for well adjusted spatial filters are not necessarily so low as to prevent lasing. It has been observed that when the #3 (on-axis) or #4 (right-adjacent) gain element is operated by itself in the external cavity, with a 50 percent duty cycle spatial filter and a 90 percent reflectivity end mirror, lasing is obtained with a threshold current of approximately 113mA in either case. Currents for the other gain elements, when powered, were kept below 110mA and no individual threshold was determined. This result seems quite natural in light of the optical analysis of the passive part of the laser but is disconcerting to the point of view that holds that, separately, there can be no lasing, but together, coherently, there can be. There is a range of currents where this is the case, but due to the coupling induced by the spatial filter, it is possible to operate above this range and still have coherent action.

The premise of this section has been to explore the wavelength selectivity of the spatial filter. The first keystone is that detuning produces a shear in the contribution from one gain element to the returning field directed at another gain element. The second keystone is that such a shear translates to a decrease in coupling efficiency between the gain elements in question. Such analysis is incapable of predicting what the operating wavelength <u>should</u> be. However given an operating wavelength, the

analysis does allow one to write the appropriate self consistency equation (Eq. 6.16, with $\bar{V}^T\bar{V}$ modified by the k_{ij}) and predict the concommitant power. It would then be left to an anthropomorphic maximum-emission principle or a multimode rate equation model to conclude what the steady state wavelengths are.

Summarizing Chapter 6, a comprehensive model of the external cavity laser has been presented. The model has been restricted to monochromatic usage which is at the same time an end product and a large step toward developing a multimode theory. The passive part of the laser was analyzed first, showing how the spatial filter couples the fields from the discrete gain elements together before feeding the field back. The amplification mechanism was developed from simple rate and propogation equations. Much attention was focussed on how realistic values for theoretical parameters could be (and were) obtained from isolated measurements on the original diode lasers and the antireflection coated gain elements. These values are used in the simulation studies of Chapter 7. Finally, issues relating to a wavelength detuned system were explored.

Chapter 7. Computer Simulation

The Fortran implementation of the theory presented in the previous chapter undoubtedly ranks as one of the major accomplishments represented by this thesis, along with the theory itself and the first successful operation of the external cavity laser. The implementation of the theory into software should not be viewed as merely an attempt to substantiate past experimental results. Indeed, the limitations on what the theory was intended to encompass were admitted up front; the theory was not intended to explain all features of the data. Rather the computer programs that have been developed must be viewed as a tool to guide and be used for further research efforts. The programs also represent a starting point or framework on which future simulations may be based. As an indication of the complexity of even these fundamental programs, almost 400 executable statements have been used in each. And this figure excludes comment lines, blank lines, and continuation lines. Every attempt has been made to make the programs self-explanatory. Nevertheless, a brief overview might be appreciated in order to point out certain subtleties that can be perplexing otherwise.

There are two programs that have been used for the results of this section: MODEL3 and MODEL4. MODEL3 has been included in its entirety in Appendix B. Those parts of MODEL4 not in common with MODEL3 are listed in Appendix C. The numerical suffixes belie a succession of programs. Generally, there is little difference between the various programs. Certainly the theory is the same. The differences amount to for example, one program calculating the laser behavior of gain element currents that are fixed relative to each other while the average current is scanned, while another program may have a fixed average current while the relative

currents change. One program (MODEL0), does not scan at all, and is meant for quick point checks. Another program selectively nulls certain variables in order to simulate a laser with four of five gain elements blocked (MODEL7). The structure of the programs are identical and many of the subroutines are identical and may be shared. There is one main program and seven subroutines. Two of the subroutines, MATMAT and MATVEC, perform matrix-vector multiplication. This is consistent with the matrix formulation of the operation of the spatial filter and the passive part of the external cavity.

Two subroutines, LISTMAT and LISTVEC, are used for the display of matrices and vectors. The former is used only for debugging purposes and calls to it must be inserted into the program as needed. The latter is often used to display the individual powers and/or fields exiting the gain element array or end mirror. Since power is used to determine the action of the gain elements and since diffraction, the basis of the interaction process in the laser, is linear in field and hence independent of scale, a convenient normalization is chosen whereby the returning power is the modulus-squared of the returning complex "field". This normalization is evident in LISTVEC.

The subroutine PARAM requests measured or assumed values used in the calculation of various parameters needed in the program. Except towards the end of this subroutine, it is identical for all incarnations of the overall program. The matrix $\bar{\bar{V}}^T\bar{\bar{V}}$, representative of the interaction supplied by the spatial filter, is calculated in the main program. Because of the gain dependent phase shifts possible in the gain elements it is necessary to keep track of real and imaginary parts of the field; it is

incorrect to assume that the fields are real. Thus the matrices are 10 x 10 real and the vectors are 10 x 1 real.

The program works by starting with an initial estimate of the array output based on negligible interaction (free-running). This estimate is propagated around the laser until either a convergence or non-convergence criterion is satisfied. The initial estimate is supplied by the subroutine ISOLATED, and is based upon Eq. 6.54. Each iteration is calculated by the subroutine SUCCSUB. SUCCSUB has three distinct parts. The first is the implementation of Eq. 6.14, the calculation of fields returned to the array from fields output from the array. The interaction of the fields is contained in this step. The second part is an individual calculation of the magnitude and phase of each gain element based on the power incident on the antireflection-coated facet. Equation 6.22a is iteratively used in this step. It sometimes happens, usually when the gain is high, that this iteration does not converge. This does not mean that there is no solution, just that it cannot be found based on the structure of the equations and the method of solution. In the program this is referred to as a "type 1" nonconvergence. After a fixed number of iterations, if convergence has not been obtained in the calculation for the particular gain element, SUCCSUB returns to the main program (without bothering with any further calculations) with a flag set to indicate the problem. The third part of SUCCSUB is an ad hoc rotation of phase of the entire output of the array. The necessity for this is the absence of a mechanism by which the operating wavelength can change. In a realistic laser the operating wavelength is determined by the phase condition derived from the self-consistency equation. In the steady state, the phase shift through any part of the circuit travelled by the light about the resonator, is fixed. In the

present model the wavelength is specified and cannot change. In the absence of any compensatory measures, phase would accrue with each iteration and no steady state would be recognized. As such, the phase of each field is rotated through an angle that would make the strongest field to emerge from the array pure real.

Even though it may be possible on an iteration-by-iteration basis to calculate the new fields exiting the array from the old fields exiting the array, convergence may not always ensue. In the program this is referred to as a "type 2" nonconvergence. Detection of this condition is done at the main program level. In case of either a type 1 or type 2 nonconvergence, a warning message is output instead of the usual data.

The structure of the main program is basically a set on nested DO loops, iterating such parameters as current, duty cycle, detuning, etcetera. The calculation of the matrix $\bar{V}^T\bar{V}$, which incorporates duty cycle, offset, and detuning, has already been mentioned. The proportionality between gain-dependent phase shift and logarithmic field gain $\underline{\Delta}n'/\underline{\Delta}n$" is also a scanned variable. In order to "test" the laser's ability to self-compensate for defects in the various path lengths to and from each gain element, a gain independent phase facility was included and is the subject of another DO loop.

The least obvious feature of the main program is a desymmetrization performed on initial estimates for the array output. In systems of equations such as in the present case, multiple solutions generally exist, with differing degrees of stability. The problem is to avoid unstable solutions. In one example of a system with symmetric diode currents and a symmetric starting estimate, but an offset spatial filter, the array output

evolved to a symmetric steady state. This is reasonable, since T(x,y)T(-x,-y) is symmetric and therefore the entire system was symmetric. However, if this solution is slightly desymmetrized and in turn used as an initial estimate, the new solution evolves to one of two mirror-image solutions, neither of which are symmetric. In addition, the sum power emitted by the array, or exiting the end mirror, increases. What has happened is that the phases of the fields output from the array evolve to a non-symmetric configuration. This phase taper steers the maxima of the interference pattern within the focal spot at the spatial filter. The bright fringes thus remain partially aligned with the filter slits. A fringe that is transmitted by a slit, is inverted by the secondary lens and end mirror and impinges on the rear surface of the spatial filter on the opposite side of the optical axis. There, the fringe partially aligns with another slit and is transmitted back to the array. Because of the symmetry between the two non-symmetric solutions there is no greater tendency for a symmetric initial estimate to evolve to one rather than the other solution. Instead, it evolves to neither. To avoid obtaining these unstable spurious solutions the main program desymmetrizes starting estimates of the array output. It can still happen that the eventual solution will be symmetric, as in the case of a non-offset filter with symmetric diode currents, but the system will have arrived at that most stable solution by relaxing from a non-symmetric start.

There are many parameters in even the relatively simple monochromatic model, and it is beyond the scope of this thesis to explore all the possible interrelations between their values and the performance of the laser. A few topics will be addressed that clarify the nature of the external cavity laser operation. A partial list of values for various

parameters appears in Table 7.1. For specific cases discussed below the values of remaining parameters will be given. It should not be expected that the model will be accurate or even realistic at low currents. For one, the laser gain and spontaneous emission both go to zero for i=59 mA and are unrealistic below this. For another thing below threshold in a realistic laser there are many modes, on the order of several tens of comparable intensity [34]. Thus the total power, summed over wavelength, is many times the monochromatic result below threshold. Above threshold, however, the simulation should be a fair representation of a single-mode laser.

(1) The first simulation illustrates the coherent action of the laser by determining the threshold current versus the non-detuned spatial filter duty cycle. It is assumed that the gain elements are run at identical currents. The fields are all real and no gain-dependent or gain-independent phase shifts are assumed. Figure 7.1 shows the calculated results. For reference, three additional curves are included on the plot for diodes being run individually. The curves correspond to the diode position in the array being on-axis, adjacent, or peripheral. The very fact that, for all diodes being powered, the simulation arrives at a steady state different from zero represents a corroboration of the observed coherent operation of the external cavity laser, even though there may not be agreement in the spectrum or in the distribution of optical power among array elements.

(2) The second simulation reveals an interesting interplay between cross-coupling and output power. Again gain-dependent and gain-independent phases are absent. The lasers are being run at individual currents of 88,

PARAMETER	SYMBOL	VALUE
Original diode laser threshold current	i_{th}^{o}	86 mA
Slope of power versus current curve above threshold for original diode laser	dP/di	0.13 mW/mA
Normalization current from analysis of superluminescent diode spectra	i_n	24 mA
Spontaneous carrier lifetime	$(S)^{-1}$	$3x10^{-9}$ sec
Spontaneous emission factor	C_s	$0.5x10^{-5}$
End mirror reflectivity	R_x	0.90
Power coupling between end mirror and gain element, each way	$k=k^{+}=k^{-}$	0.60
Gain element array filling factor (ratio of element width to array spacing)	$2w_x/D$	0.125

Table 7.1. Partial list of parameter values used for simulation studies.

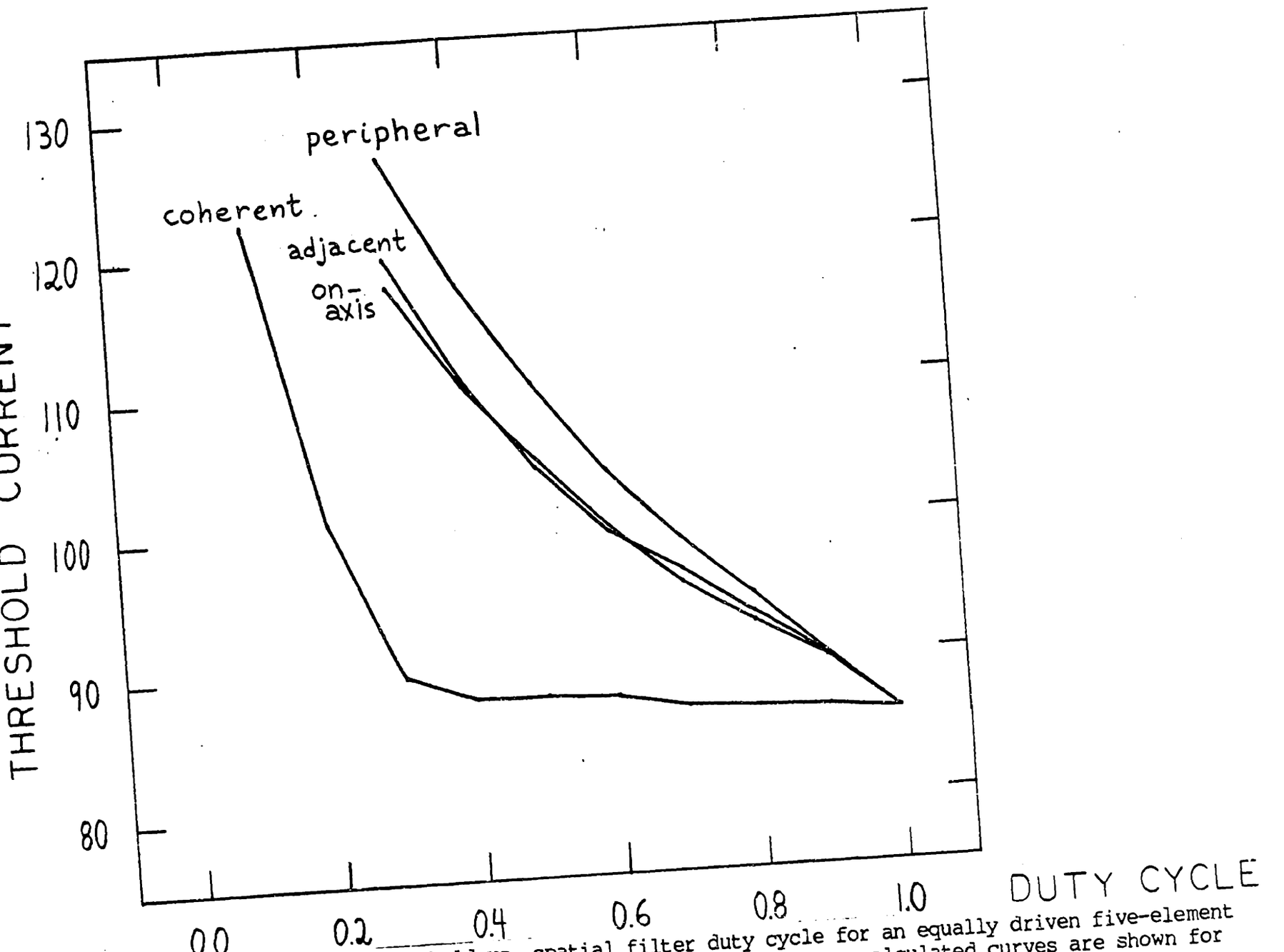

Figure 7.1. Plot of coherent threshold vs. spatial filter duty cycle for an equally driven five-element array and for the parameter values listed in Table 7.1. For reference, calculated curves are shown for solitary operation of the on-axis, adjacent, and peripheral gain elements.

113, 148, 113, and 88 mA. In the absence of a spatial filter, the field strengths at the output of the array take on binomial weightings. The interference pattern arising from a binomial array, as compared to that from a uniformly excited array of the same total power, has principal maxima that are broader and have lower peak value, but is entirely missing any secondary maxima between the principal maxima. Such an interference pattern should fit cleanly through the spatial filter, with no power lost on the opaque areas between slits. Figure 7.2 is a plot of laser output power versus detuning parameter $(D/2w_x)(1-\lambda/\lambda_d)$ with filter duty cycle as a parameter for each curve.

Two things are interesting to note from Figure 7.2. First, for zero detuning but duty cycle decreasing from unity, the laser output power rises from 1.385 mW (100 percent duty cycle) to 1.430 mW (50 percent duty cycle) before dropping to .549 mW (20 percent duty cycle) and beyond, to below threshold. The reason for the rise is that the diffraction due to the spatial filter has allowed the peripheral elements of the array to couple into the large gain present in the central elements of the array. The smaller the duty cycle, the more the coupling to the large gain, and the greater the output. Another explanation is that diffracted light from the central elements is injected into the peripheral elements, equivalently increasing the reflectivity perceived at the antireflection-coated facets. However, past a point the diffraction becomes too great, and power is lost beyond the numerical aperture of the system. Thus the output declines.

The second point to note is the effect of detuning. For all spatial filter duty cycles, the effect of detuning is gradual even though each percent of detuning parameter represents a wavelength excursion of over 1 nm. This shows that the spatial filter is not very selective and so

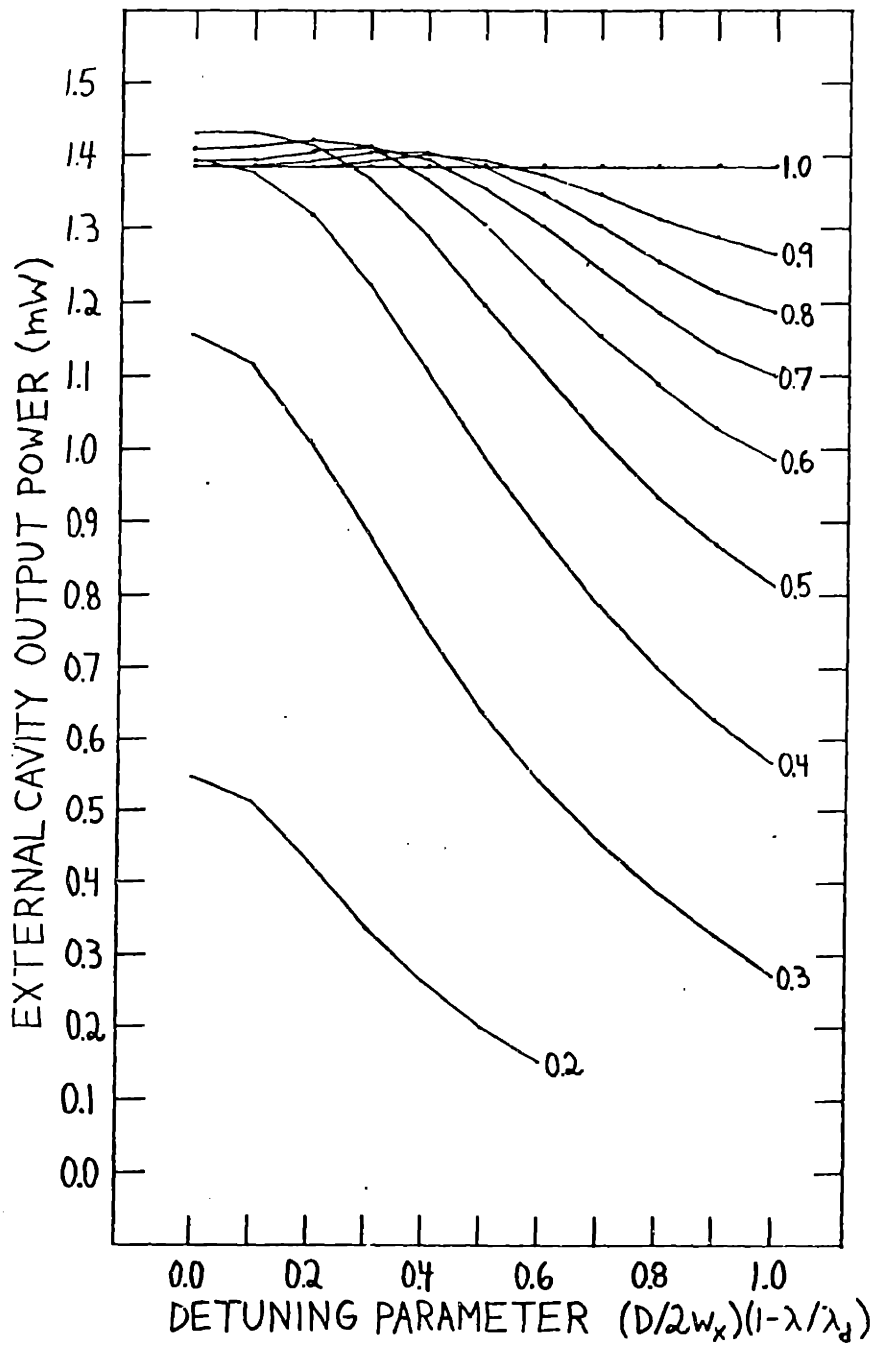

Figure 7.2. Plot of external cavity laser output power vs. detuning for fixed gain element currents and spatial filter duty cycle as a parameter. For duty cycles less than 50 percent, the output power is monotonically decreasing with detuning increasing from zero, while for duty cycles between 50 and 100 percent, there is a slight increase in output power for small detuning but a decrease for large detuning.

should not excercize a major tuning influence on operating wavelength. (Equivalently, for a detuned wavelength, the interference pattern in the Fourier plane scales in size. But until the detuning becomes very large, a significant number of bright fringes in the interference pattern persist in lining up with slits in the spatial filter.) For spatial filter duty cycles larger than 50 percent, there is a noticeable increase in laser output power with small detuning. For these filters with larger detuning, and for less than 50 percent duty cycle filters with any detuning, the power drops. A possible mechanism for this behavior suggests an analogy with the evanescently-coupled diode laser arrays [9-23]. The laser arrays have been analyzed in terms of supermodes, wherein the powers traveling in the different active regions are in fixed ratios to each other. In the typical case, the central elements are more heavily weighted while the power in the peripheral elements is held down through conformation to the supermode. For equal currents through the separate elements, the central elements saturate sooner due to the larger stimulated emission, while the peripheral elements have unused gain left over. The photon densities cannot grow in those elements because they are linked via the supermode to the central, saturated, elements.

The key to comprehending the behavior of the detuned external cavity laser begins by approximating the coupling between elements by coefficients in the Fourier series expansion of $T(x,y)T(-x,-y)$. To understand the trend of the calculated results it is only necessary to consider the second-nearest neighbor coupling. For binary filters with no offset $T(x,y)T(-x,-y)$ is identical to $T(x,y)$, whose expansion coefficients are given by Eq. 6.4b. In particular, for duty cycles greater than 50 percent, the $\pm$2nd

coefficient is negative. Thus, for the phaseless system postulated, the emission of the central element of the array detracts from the return to the peripheral elements, and vice versa. (And similarly for the adjacent elements on either side of the on-axis element, since they are second-nearest neighbors to each other.) This effectively suppresses the amount of power supplied by the peripheral elements. For small detunings, this suppression is partly abated and the power in the affected elements grows. For larger detunings, the powers in the elements tend to the low values consistent with solitary operation of the diodes with a spatial filter. For duty cycles less than 50 percent, the $\pm$ 2nd coefficient is positive and so only harm can come from detuning. This also explains in a different way why the power increases, at zero detuning, for duty cycles decreasing from unity towards 50 percent: the value of the $\pm$2nd coefficient, negative for larger duty cycles, increases toward zero as the duty cycle approaches 50 percent. This removes the suppression between second nearest neighbor and entails an increase in power. For further decreases in duty cycle the behavior of the laser is governed by the general decrease in magnitude of the coefficients connecting the gain elements, that is, diffraction losses in the laser grow, and the output power drops.

(3) The last simulation introduces gain-dependent phase to the external cavity laser. The object is to define ranges of values for the proportionality between gain-dependent phase and logarithmic field gain (i.e., between the real and imaginary parts of the gain-induced index of refraction) for which a stable solution for the cavity output is obtained. These stability ranges are functions of duty cycle and diode current. All the gain elements are being run identically.

Figure 7.3 shows the stability ranges versus duty cycle for the gain

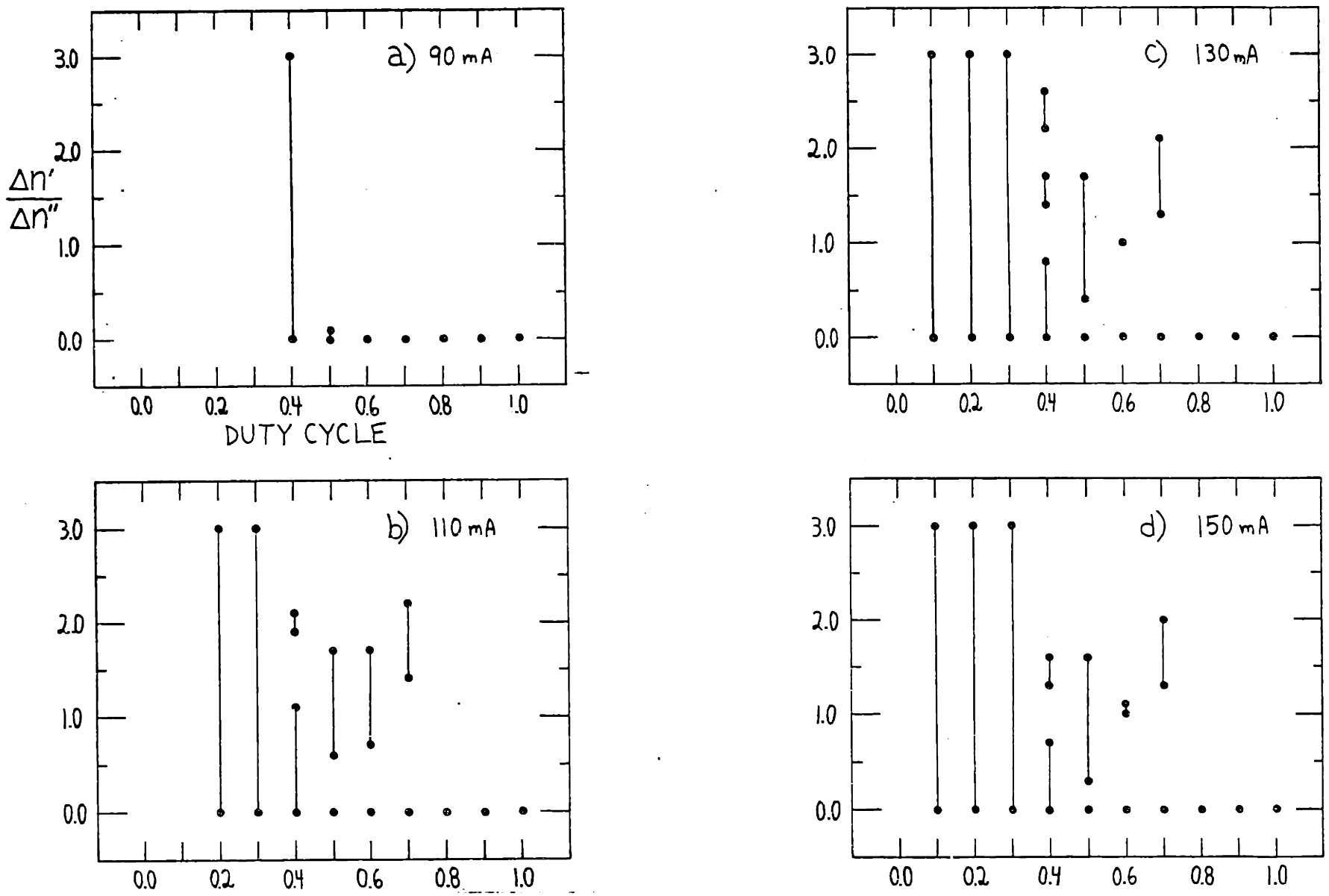

Figure 7.3. Plots of the ranges of $\Delta n'/\Delta n''$ between 0 and 3 vs. spatial filter duty cycle for which the computer simulation of the external cavity laser converges to a solution. Four cases are considered where the gain elements are equally driven at: a) 90 mA; b) 110 mA; c) 130 mA; and d) 150 mA. This important result indicates that, for sufficient current, operation with large duty cycle spatial filters is more likely to result in instability than with small duty cycle spatial filters.

element array being run at 90, 110, 130, and 150 mA. The ratio of real to imaginary parts of the gain-induced index of refraction $\Delta n'/\Delta n''$ ranges from 0 to 3. Only stable solution ranges above threshold (obvious from the level of power) are shown. The extremely important result here indicates that operation with large duty cycle spatial filters is more likely to result in instability. That is, the ranges of the ratio $\Delta n'/\Delta n''$ is more restricted in order for the calculations of the array output to converge. This corresponds closely with experimental observations.

There are several possible causes for apparent instability. The most trivial relates to the structure of the equation to the extent under human control. For example, Eq. 6.22a could be written in two ways. Negligible spontaneous emission is assumed for simplicity:

$$V = \exp\{gNL/S - (V-1)\phi_0^- (1+R_b V)\} \tag{7.1a}$$

$$2R_b V = \sqrt{4R_b[1+(gNL/S - \ln V)/\phi_0^-] + (1-R_b)^2} - (1-R_b) \tag{7.1b}$$

Either form of the equation may be used for a successive substitution iteration [39], but generally only one form will converge, that one for which the magnitude of the derivative with respect to V of the right-hand side is less than 1. This often depends on what the root of the equation is. Eq. 7.1a may work for one range of roots while Eq. 7.1b may work for another. Similarly, not only the individual element gains, but for the entire array output, the solution is found by successive substitution. More sophisticated methods can be used to accelerate convergence (assuming a good estimate to the "root") such as multi-dimensional generalizations of the Newton-Raphson method or the secant method [39]. Nevertheless, since the system equations as implemented yield convergence in so many instances,

it is not likely that instabilities would be due to poor judgement exercized in manipulating the equations.

A second reason for instability is related to first, in that the structure of an equation and the value of its parameters govern the convergence of iterative methods of solution. If the sought after root is near a division of character of the system, iterative methods may not apply. This has been observed, for example, when investigating the dependence of laser output power on spatial filter offset. Up to a certain offset the laser runs above threshold. Past a certain offset the laser runs below threshold. In either case convergence to a solution is rapid. However, over a small range of offsets that mark the transition from above threshold to below, the system is non-convergent. The salient fact is that although a significant change in the character of the system (above versus below threshold) has occurred, on either side of the transition the system behavior is well understood. The instability is only mirroring the transition process. However this too is unlikely to be the case for the observed simulation, since above threshold operation can sometimes be observed on <u>both</u> sides of the instability region.

A third cause of instability is the most profound of all. The iterative process of propagating the fields of the array output around the laser many times is identical to a system of first order difference equations which can be written simply as

$$X_{n+1}=F(X_n) \tag{7.2}$$

where X_n represents the array output on the nth loop around the laser, and F is an extremely complicated nonlinear function which produces the array output on the next loop. Equation 7.2 is another form of the self-consistency condition Eq. 6.16. Solution for the array output is

equivalent to finding a fixed "point" of the difference equation, Eq. 7.2. Equation 7.2 is also a model for a dynamic process, viz., the evolution in discrete time of the array output. Determining a solution is accomplished by using a sufficiently good starting estimate such that it lies on a trajectory that asymptoticly approaches a constant value. It is not necessarily the case, however, that a nonlinear equation of the form Eq. 7.2, will have trajectories that stably lead toward the fixed point. Unless the solution is stable it is not of much use. But rather than attempt to discuss range of system behavior possible in a ten-variable model, it is better to concentrate an single variable nonlinear first-order difference equations. The range of behavior is slightly less rich, but is sufficient for qualitative comparison.

The following single-variable single-parameter difference equation has been extensively reviewed [47]:

$$X_{n+1}=aX_n(1-X_n)$$

It has been shown that for $1<a<4$, Eq. 7.3 has a non-trivial solution on the interval $0<X_n<1$. Only for $1<a<3$ is this solution stable. That is, if the fixed point X^* is perturbed and used to initiate a dynamic sequence determined by Eq. 7.3, the trajectory will asymptoticly lead back to X^*.

For $3<a<4$, very different behavior ensues. First the basic fixed point becomes unstable. The solution bifurcates, yielding two points between which Eq. 7.3 stably alternates. This is the period 2 cycle. After further increases in the parameter, this period becomes unstable, bifurcates, and a period 4 cycle exists, a set of four points among which Eq. 7.3 hops, always in the same order. Further increases produce cycles of periods 8, 16, 32, etcetera. In each case the range over which the

cycle is stable gets smaller and smaller, at the end of which the cycle goes unstable and bifurcates. The process is convergent, and by the point at which a=3.5700... all possible period 2^k cycles will have been produced. This is the point of accumulation. Past this point the chaotic region starts and extends to a=4. In the chaotic region, among other things, there are an infinite number cycles with different periodicities, as well as totally aperiodic trajectories. At a=3.6786..., the first cycle with an odd number of points in a closed trajectory arises, but the odd number is very large. Finally, at a=3.8284..., a period 3 cycle appears, and past this point are cycles with every integer period.

For systems of equations, refinements on the above picture are possible, such as a stable fixed point and a stable period 3 cycle occurring together for the same parameter value. The basic phenomena - fixed points, cycles, bifurcation, accumulation, chaos - remain substantially the same.

As relates to the computer simulation of the external cavity laser, it is suggested that the observed nonconvergence regions are reflections of stable cycles or chaos, i.e., that simple fixed point solutions are not stable with the pertinent values for the parameters. Further, although the model is necessarily monochromatic, it is plausible that the instability is a message that multi-wavelength operation is the preferred mode. Consider a period 2 cycle, with the cavity output flip-flopping between two states with every iteration. In a sense, the laser is "trying" to be in two states at the same time (actually, at two times separated by the round-trip time of the laser). If there were two wavelengths coexisting in the laser, each of the two points of the period 2 cycle could be a different wavelength. Thus the laser would be in both states at the same time, in

effect. There could be stable two-wavelength operation as opposed to unstable single-wavelength operation.

In this chapter a computer implementation of a theoretical model of the external cavity laser has been introduced. An overview of the program structure has been given and some of the more subtle points in the program addressed, such as desymmetrization, field normalization (root-watts), and different kinds of non-convergence. The results of three simulation studies have been reported, in increasing order of heuristic content. The first illustrates the possibility of coherent action and contrasts collective with individual lasing threshold. The second case clarifies the nature of the power emitted by the array, as dependent on element coupling which can sometimes take on negative values; and a dependence on detuning which for some values mitigates the deleterious effect of negative coupling, and for other values weakens the overall coupling, positive or negative. The final topic is an exposition on instability in the monochromatic model, and the conjecture of a connection between instability and multimode operation.

Chapter 8. Summary and Comments

This thesis has been a study of a particular method for obtaining coherent output from an ensemble of diode lasers. Historically, communications has been a prime motivation for obtaining higher and higher electromagnetic power, rendering long distance communication feasible. Such was the case in the radio frequency and the microwave regimes. The attraction of broad bandwidth made it only natural to look then at lasers as possible communication sources. Of course, if one can wait for the state of the art to move forward, it might be possible to obtain the requisite powers with an individual device. However, by coherently coupling an ensemble of state-of-the-art devices, it is possible to produce total power outputs forever beyond the reach of a realistic individual device. Background on this problem has been presented from the last forty years of the electrical engineering field.

The particular scheme for obtaining coherent power from an ensemble of diode lasers has been discussed. A conceptual design of an external cavity laser has been given, followed by intuitive explanations of why coherent action should be expected. The design is distinct from a major competing effort, the evanescently-coupled monolithic diode array. Central to the present design is the multiple-slit spatial filter responsible for the interaction between the diode gain elements and therefore for the coherent operation of the overall laser. The coupling can be thought of as localized to the Fourier plane as opposed to the distributed coupling that takes place in the monolithic array. Also, the diode lasers used in the present design are discrete. The ability to easily exchange spatial filters, and the degrees of freedom inherent in a non-monolithic diode array, couple to make the external cavity laser an ideal vehicle to study

coherent operation.

Details of the realization of the conceptual design of the external cavity laser have been given. A great deal of unreported effort was expended in assisting with the engineering design and debugging the finished product. With the essential cooperation of numerous individuals, the external cavity laser was manufactured without intermediate breadboarding. Although a calculated risk, this resulted in considerable saving of time and money. Many degrees of freedom were built into the design and are discussed in the text. Included are mechanical adjustments done by micromanipulators, sometimes augmented by piezoelectric transducers, and individual gain element current and temperature control. Besides the positioners, salient features in the design of the optical elements have been discussed, namely, the gain elements, the spatial filter, the etalons (when used), the lenses, and the end mirror.

It should be stressed that the laboratory model has been used as a proof-of-principle for the coherent action expected to be caused by placing a multiple-slit spatial filter in the Fourier plane. High output power efficiency and reliability, all necessary qualities in a field-deployed device, were not at issue, since increasing the number of gain elements and re-engineering can be done at a later time. The spectral quality, however, was addressed, because if coherent action could not be shown on a laboratory scale a device based on the concept would not be feasible.

The experimental studies aimed at documenting coherent operation of the external cavity laser. Without doubt coherent action was observed, although preconceptions regarding the underlying mechanisms had to be modified. Most obvious was the fact that multiple wavelength operation was

possible and was often the case. One very telling series of filters showed that multimode operation is more probable with large duty cycle spatial filters. Also, although the use of a multiple-slit spatial filter had been anticipated to have a tuning effect on laser operating wavelength through variation of the filter period, no conclusive tunability was observed. The question then naturally arose as to other potential mechanisms that could have wavelength selectivity. Notable in the proposed answers were the role of non-ideal antireflection coatings producing resonant reflectors superimposed on the gain elements, and the role of gain-dependent phases that make the resonant reflectors nonlinear.

A theoretical model of the external cavity laser was developed. The laser was split into two parts: the passive part with the spatial filter, primary and secondary lenses and the end mirror; and the active part with the array of gain elements and respective collimating lenses. A matrix formulation for the passive part was derived based on Fourier optics and the assumption of a non-detuned spatial filter (i.e., the period of the filter equals the period of the interference pattern produced in the focal plane of the primary lens from the collimated outputs of the array of gain elements). Later modifications to the formulation incorporated detuned filters. A monochromatic model of the amplification mechanism in the gain elements was developed, assuming a two level system with negligible population in the lower level. Parameters of the theory were related to easily obtained measurements so that realistic values could be used in computer simulation studies.

A Fortran implementation of the theory was presented. This was intended as much to be a tool for further phases of research as it was to supply corroboration and confidence in the observed results. The

applicability of the software, of course, is only as good as the mathematical equations it implements, so that the computer simulation cannot directly comment on the multimode character of the observed experimental spectra. The simulation studies have been used to show that: coherent action can occur; the spatial filter is not very wavelength selective, that is, mild detuning does not precipitate a drastic loss in power, in some cases even increasing output; and instability or nonconvergence in the monochromatic model with gain-dependent phase can in some cases be interpreted as foresight of multimode operation.

It is both easy and difficult to comment on the future directions this research might take. On the one hand, this thesis is an outgrowth of a multi-year research program to develop a high-power laser source for communications. Already under way is research on the feasibility of pulsing the gain elements in order to extract high (peak) power within the constraints of coherent operation. Further into the future, it will be topical to investigate techniques of converting the multi-beam output of the external cavity laser into a more usable single beam. Also, in the interests of blue-green wavelength communication, frequency doubling is planned. In order for the doubled wavelength to be green enough, it would be necessary to use lasers with fundamental wavelengths longer than those currently in use. When the research contract was originally proposed, the state-of-the-art power available from diode lasers dictated that very large ensembles of diodes would be needed in order to produce kilowatt level power. To prevent the heat dissipation problems that would result within the confines of a compact diode laser array, it was proposed to spread the diodes out and use individual optical fibers as conduits to channel the

optical power to and from the diodes. The free ends of the fibers would be gathered to form a cold light bundle. Although the heat dissipation problem abates as state-of-the -art diode laser powers increase, thus decreasing the number of diodes needed for a given ensemble power, the idea is still interesting. It can also effectively produce an array with a fill factor impossible to achieve with discrete diodes in juxtaposition.

On the other hand, apart from topics foreseen at the contract proposal stage, the following two topics are suggested by the work presented in this thesis. It would be interesting to have an active spatial filter in the form of an acousto-optic crystal. A standing wave phase grating could easily be produced. The diffraction from the phase grating would couple the gain elements. A useful feature for this kind of filter would be that the period of the grating could be continuously changed in real time simply by varying an external oscillator frequency. The intensity of the grating could be adjusted as well, thereby controlling the diffraction efficiency. It would then be possible to determine if the spatial filter can tune for small changes in period, as opposed to the gross steps of existing filter series. With regard to theory and computer simulation, the software should be rewritten to accommodate complex numbers. The translation from mathematical equation to Fortran statements would then be more transparent. It would also result in halving the amount of array storage needed. For the present versions with real and imaginary parts of the fields regarded separately, 10x10 real arrays are needed (100 elements each). In a complex formulation of the fields, 5x5x2 arrays would be used (50 elements each). More importantly, the program should be modified to implement a two wavelength theory. The extensions necessary to the current theory are significant but straightforward. It would be especially interesting to see

if a situation exists analogous to transverse spatial hole burning: One wavelength could be more prevalent in the central gain elements, corresponding to a fundamental supermode, leaving unused gain in the peripheral gain elements. A second wavelength, in a form of higher-order supermode, may be able to feed on the gain in those elements. More generally it would be instructive to find conditions that lead to stable (or unstable) operation of the laser when the photons are distributed over two or more wavelengths.

Appendix A.

Reprint of "Operation of individual diode lasers as a coherent ensemble controlled by a spatial filter within an external cavity" [30].

cm^2. The standard deviation of threshold current density over 8 cm^2 becomes less than 5%. Table II presents the threshold current density of diodes over 8 cm^2 using two different technologies.

We report also the first reliability study of these index-guided 1.3-μm InP-GaInAsP lasers grown by two-step LP MOCVD growth technique. The diodes were randomly selected for life test. Figure 6 shows the typical operating current as a function of time to maintain 5 mW cw output from LP MOCVD lasers at 70 °C. There is no significant degradation after 1000 h.

In conclusion, 1.3-μm wavelength region InP-GaInAsP buried ridge structure (BRS) lasers were fabricated with two-step LP MOCVD growth technique. Excellent reproducibility and homogeneity with high processing yield rate have been obtained. The threshold current of 11 mA under cw operation has been achieved. The external quantum efficiency as high as 60% has been measured. The optical power emission up to 15 mW has been obtained. Some lasers were randomly selected and aged at 70 °C at a constant optical power emission of 5 mW per facet; no significant change of the threshold current has been observed after 1000 h.

The authors would like to thank D. Leguen, M. Goix, L. Noël, and J. Ricciardi for technical assistance, MM. B. de Cremoux, P. Hirtz, J. C. Boulay, and B. Lent for useful discussions.

[1] M. Razeghi, B. de Cremoux, and J. P. Duchemin, in *Proceedings of* 1.2–1.6 μm GaInAsP-InP *DH Lasers Grown by LP MOCVD*, the Second International Conference MOCVD, Shieffield, U.K. 10–12 April, 1984, edited by B. Mullin in J. Cryst. Growth.
[2] M. Razeghi, "Light Wave Technology for Communication" in MOCVD Growth of GaInAsP Alloys, edited by W. T. Tsang and A. C. Beer (Academic, NY, 1984).
[3] M. Razeghi, R. Blondeau, K. Kazmierski, B. de Cremoux, J. P. Duchemin, and J. C. Bouley, Appl. Phys. Lett. 45, 784 (1984).
[4] M. Razeghi, J. C. Bouley, K. Kazmierski, M. Papuchon, B. de Cremoux, and J. P. Duchemin, Proceeding of the Ninth IEEE International Semiconductor Laser Conference August 7–10, 1984, Rio de Janeiro, Brazil.
[5] W. T. Tsang, R. A. Logan, and M. Ilegems, Appl. Phys. Lett. 32, 311 (1978).
[6] J. C. Bouley, G. Cheminant, J. Charil, P. Devoldere, and M. Gilleron, J. Appl. Phys. Lett. 38, 845 (1981).

Operation of individual diode lasers as a coherent ensemble controlled by a spatial filter within an external cavity

R. H. Rediker and R. P. Schloss
Department of Electrical Engineering and Computer Science and Research Laboratory of Electronics, Massachusetts Institute of Technology, Cambridge, Massachusetts 02139

L. J. Van Ruyven
Development Lab. H.O.C., Nederlandse Philips Bedrijven, 5600 MD Eindhoven, The Netherlands

(Received 13 September 1984; accepted for publication 23 October 1984)

Five diode gain elements (diode lasers with one facet antireflection coated) have been controlled to operate coherently with each other by a spatial filter placed between the antireflection coated facet and the mirror of an external cavity which provides the feedback for laser operation. The locking of the lasers is relatively insensitive to phase adjustment in each laser path. Locking has occurred with lasers whose output wavelength when operating individually differed by 60 Å. It is expected that the maximum tolerance to wavelength difference is much larger because lasers used were selected so simple individual temperature control could bring them into wavelength coincidence. These results point to the feasibility of placing well over a thousand diode lasers in an external cavity with coherent output.

A spatial filter and an external cavity have been used to control the outputs from three diode gain elements (diode lasers with one facet antireflection coated) on one chip of GaAs so these outputs are coherent with each other.[1,2] These results, reported nine years ago, however were very limited. While the optical peak power was measured to be three times the peak power of a single laser no quantitative results were obtained either on the tolerance to initial variations in wavelength and phase between the individual elements, or on any of the practical aspects of stability.

The present work is aimed towards the demonstration of the feasibility of coupling a multiplicity of individual diode gain elements or individual arrays of diode gain elements so their outputs are coherent with each other. As the output power is increased (above about 1–5 W cw) with the concurrent increase in the density of power dissipated, it has been proposed to physically separate the diode gain elements in groups and couple each element into the cavity in series with an optical fiber.[3] The external cavity control of the operation of the series combination of a semiconductor diode gain ele-

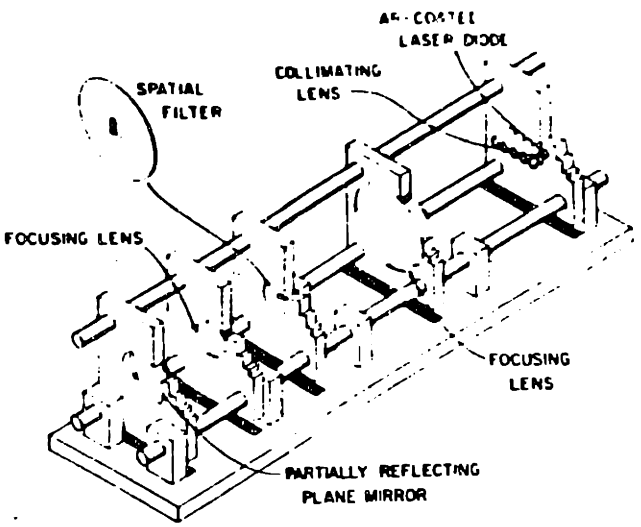

FIG. 1. Artist's conception of five-gain-element external cavity showing the components inside the super-invar four-bar structure.

ment and an optical fiber has been demonstrated.[4]

The practicality of coherently coupling a multiplicity of individual gain elements depends on the difference in wavelengths and phases of the gain elements when operating individually as lasers over which the outputs of the elements can be pulled and locked into one wavelength and phase. The cost to fabricate many semiconductor lasers or many arrays will depend very strongly on the acceptable wavelength spread over which the laser must be specified. Results over the years for the microwave case indicate that a relatively large wavelength and phase spread may be possible.[5–7] In the work to be reported here it is shown that five lasers with wavelength spread of >60 Å at 8350 Å can be pulled and locked. The maximum wavelength spread has not been determined because of the selection in these experiments of lasers whose wavelength variation could be minimized by simple individual temperature tuning.

The five diode gain elements have been placed at one end of an external cavity and have been controlled to operate coherently with each other by a spatial filter placed between the antireflection coated facet and the mirror at the other end which provides the feedback for laser operation. Figure 1 is an artist's conception of the five-gain-element external cavity showing the components inside the cavity. The super-invar four-bar structure supports the separate components. The micromanipulators and piezoelectric transducers used to align the components are not shown. Starting from the right in Fig. 1 are the five semiconductor gain elements. The semiconductor gain elements are originally channeled-substrate-planar (CSP) lasers[8] with undoped active layers. Because of the CSP structure the lasers have negligible astigmatism and because of the undoped active layers they have a gain curve which is mainly determined by the density of states functions of the unperturbed bands and therefore has a relatively broad maximum as a function of wavelength. While special slices were grown for this experiment, the lasers are *not* necessarily neighbors from the slice. The lasers were made from a channeled n^+ substrate with a channel width between 5 and 7 μm (top of channel) and 4 μm (bottom of channel) and a channel depth of about 1.3 μm. The n-type AlGaAs cladding layer with 33% Al has a thickness of 1.62 ± 0.04 μm inside the channel, and $0.2 \pm$ [illegible] μm outside the channel. The flat active layer has a thickness of 0.10 ± 0.02 μm. The p-type AlGaAs cladding layer has a thickness of 3.13 ± 0.68 μm and a p-type GaAs top layer of 0.5 μm provides good ohmic contact. The finished diode lasers have a cavity length of 250 μm and their facets are coated with $\lambda/2$ of Al_2O_3. The lasers were tested for lasing wavelength and for lasing threshold current. The lasers are then antireflection coated on their facet shown facing into the cavity in Fig. 1 with $\lambda/4$ of HfO_2. After the antireflection coating (performed by Design Optics, Sunnyvale, California) the new gain elements were tested in a single-gain-element external cavity again for wavelength and for lasing threshold current. The gain elements were also tested with the external cavity feedback mirror removed. For the five elements used in the experiments described below, the value of threshold currents was typically about 90 mA before antireflection coating, increased by typically about 10 mA in the external cavity after antireflection coating, and was yet at least another 40 mA higher with the feedback mirror removed (we did not test any of the elements at currents above 140 mA).

Continuing to the left of the semiconductor gain element in Fig. 1, the radiation from each of the elements is collimated and then focused by a 25-cm focal length $f/2.5$ antireflection coated lens. At the focal plane is the spatial filter. The theoretically desired spatial filter would have slits to pass the Fraunhofer diffraction pattern (magnitude-squared Fourier transform) of the five light source geometry if the sources are coherent with each other. The light emitted

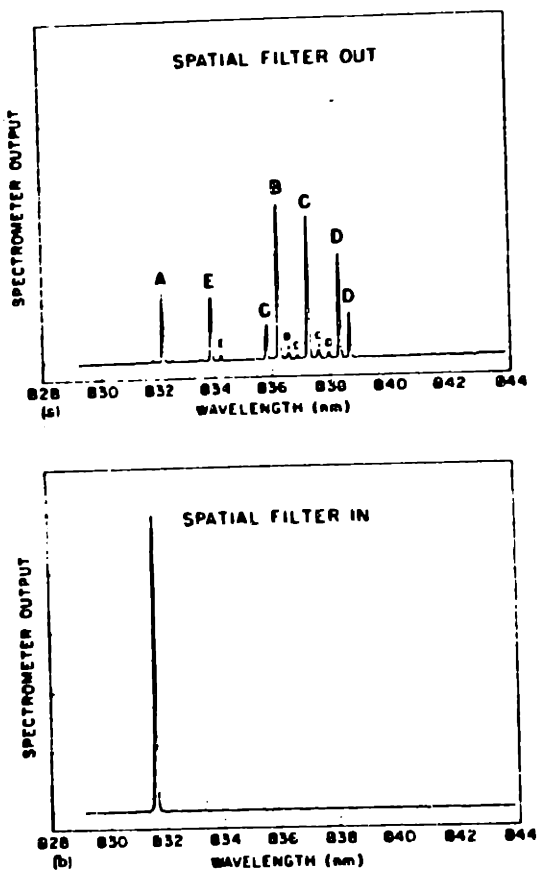

FIG. 2. Spectrum of output from external cavity containing five gain elements: (a) Spatial filter removed from cavity. Letters over peaks indicate gain element from which emission is occurring. (b) All experimental conditions are kept identical but spatial filter is in place in cavity. The scale for the ordinate is the same in (a) and (b).

through the spatial filter is recollimated by a 8.75-cm focal length $f/2.5$ lens and reflected by the partially reflecting mirror at the other end of the cavity. The optical elements are all spaced by the appropriate focal lengths of the lenses. Thus the radiation pattern would undergo a Fourier transform four times as it makes the round trip through the cavity, for the ideal spatial filter. In fact the spatial fiter for the experimental results reported below consisted of eleven 3.8-μm slits on a center-to-center spacing of 10.47 μm.

In Fig. 2(a) is shown the spectrum of the output from the external cavity with the five gain elements lasing individually and the spatial filter removed from the cavity. The gain elements are operating at temperatures about 2 °C above room temperature. The width of the spectral lines is that of the model 12G Perkin–Elmer spectrometer used in the experiments. No gain element by itself lased with the spatial filter in the cavity. (The currents were not increased above 140 mA.) The loss due to the filter was too large. Only when the gain elements lased together coherently was the interference pattern produced, which bunched the radiation so it efficiently passed through the slits of the spatial filter. It should be pointed out that no attempt was made in obtaining Fig. 2(a) for which there are five independent *external cavity* lasers to optimize the current through the gain elements for single mode operation if there is such a regime for any of the lasers.

Figure 2(b) shows the spectrum of the external cavity output with all the experimental conditions unchanged from those used to obtain the spectrum of Fig. 2(a) except the spatial filter was inserted in place. Note the single resolution-limited line and that the individual lasers had been pulled by up to above 6 nm. For the wavelength 831.8 nm the slit center-to-center spacing of 10.47 μm corresponds to Fourier transform spacing of gain elements of 1.986 cm. The spacing in the cavity design is 1.98 cm. The center-to-center spacing of the gain elements although controlled with micrometers to a precision of 0.002 cm is not known to better than $\pm$ 0.01 cm in absolute value. While the results of Fig. 2 are for one set of diode gain element currents and powers, they are typical for other currents and powers. Orignially there was a set of five etalons, one for each gain element on a plate to the left of the elements in Fig. 2. Originally, the temperature of each diode element was controlled to 0.5×10^{-3} °C. Originally all the five external cavity lasers were brought individually to have their major spectral modes coincident to within the resolution of the spectrometer. The spatial filter pulled the ensemble to the output wavelength dictated by its slit spacing. Both the étalons and the temperature control then were eliminated.

The 60-Å pulling that is measured is limited in value because individual lasers were selected in a narrow wavelength range so the temperature control could be used to make all the lasing wavelengths identical. The results are extremely encouraging and point to the feasibility of placing of the order of thousands of diode lasers (possibly with fiber coupling as described earlier[4]) in an external cavity with coherent output. It should be pointed out that the individual diode gain elements were displaced along the axis of the cavity on the order of $\pm \lambda$ (830 nm) and sensitivity to phase variation was also shown to be small.

In the experiments above the power output from the coherent ensemble is approximately 0.4 times the sum of the individual powers of the lasers when the spatial filter is out. A major part of the loss in power can be explained both theoretically and experimentally by the fact the slits in the spatial filter are overfilled and there is significant diffraction loss from the use of the spatial filter. Extensive investigations are under way on optimization of spatial filter design and experimental conditions to bring the power efficiency to near unity as originally reported by Rutz.[1]

The authors wish to thank W. Lenth and D. G. Kocher for extensive discussions and advice during the course of the cavity design and the experimental program. They thank J. W. Caunt for the actual design of the cavity, and D. J. Silversmith and R. W. Mountain for the spatial filter. It is also a pleasure to thank B. Bollen for providing the diode lasers and H. van Bakel for growing the speical slices for this experiment. The work was supported by the Office of Naval Research.

[1] E. M. Phillip-Rutz, Appl. Phys. Lett. 26, 475 (1975).
[2] E. M. Phillip-Rutz, U. S. Patent No. 4 246 548 (20 January 1981).
[3] R. H. Rediker, U.S. Patent No. 4 479 224 (23 October 1984).
[4] R. H. Rediker, R. P. Schloss, D. Welford, and A. Mooradian, IEEE J. Quantum Electron. 19, 433 (1983).
[5] R. Adler, Proc. IRE 34, 351 (1946).
[6] K. Kurokawa, IEEE Trans. Micr. Theor. Tech. 19, 793 (1971).
[7] K. Kurokawa, Proc. IEEE 61, 1386 (1973).
[8] K. Aiki, M. Nakamura, T. Kuroda, J. Umeda, R. Ito, N. Chinone, and M. Maeda, IEEE J. Quantum Electron. 14, 89 (1978).

Appendix B

Fortran simulation of external cavity laser - MODEL3.

```
C     EXTERNAL CAVITY LASER, MODEL 3:
C              OPERATION vs. Iscan, EPS, OFFSET, DETUNING, BETAc, PHASE TAPER
C-----------------------------------------------------------------------
C     MAIN PROGRAM
      real i0,in,ith,iop(5),kappa,netvec(10),iscan,iscanmax,istep,
     &     lastconvec(10)
      dimension gammat(10,10),transp(10,10),psivec(10),gnl(5),tempmat(10,10),
     &          taperminvec(10),bakvec(5)
      common /block 1/ gamgam(10,10),fldgn(10,10),phase(5)
     &       /block 2/ rbrb,rb,cflux,sigma,gnl,energy,rxrx,rx,tx
     &       /block 3/ ith,slope,eps,kappa,in,scarrier,cfactor,i0,iop
     &       /block 4/ betacmin,betacmax,bstep,iscanmax,istep,idisp,
     &                 detuning,epsmin,epsmax,alphamax,tapermax
      data pi,linecnt/3.1415927,1/

100   call param
105   format(f3.1,x,f5.2,x,f5.2,3x,f4.1,4x,f6.3,2x,f6.4,
     &                                          x,e10.4,x,e10.4,x,e10.4)
      linecnt=linecnt+39

C     INCREMENT GAIN-ELEMENT OPERATING CURRENTS
      do 195 iscan=0.,iscanmax,istep
      do 110 i=1,5
      current=iop(i)+iscan/1.e3
      gnl(i)=scarrier*(current-i0)/in
110   continue

C     OBTAIN STARTING ESTIMATE FOR SUPERMODE
      call isolated(taperminvec,abort)
      if (abort.eq.(1.)) goto 199

      if (idisp.eq.0) print ,"EPS ALPHA DETUN ISCAN,mA PH.TAPER
     &  BETAc  A.OUT,mW   B.OUT,mW   C.OUT,mW"
      if (idisp.eq.0) print ,"--- ----- ----- -------- --------
     & ------ ---------- ---------- ----------"
      if (idisp.eq.0) linecnt=linecnt+2
      print ,(iop(j),j=1,5)

C     INCREMENT SPATIAL FILTER DUTY CYCLE
      do 190 eps=epsmax,epsmin,-.1

C     INCREMENT SPATIAL FILTER OFFSET
      astep=.1
      if (alphamax.ne.(0.)) astep=.1*abs(alphamax)/alphamax
      do 185 alpha=0.,alphamax,astep

C     EVALUATE MATRIX OF FOURIER COEFFICIENTS OF SPATIAL FILTER TRANSMISSION
C     AND THE TRANSPOSE OF THIS MATRIX (i.e., 10x10 real representations of
C     corresponding 5x5 complex matrices).
      do 125 m=0,4
      do 120 k=1,5-m
      if (m.eq.0) goto 115

      rm=m
      greal=cos(2.*pi*alpha*rm)*eps*sin(pi*eps*rm)/(pi*eps*rm)
      gammat(k,k+m)=greal
```

```
      gammat(k+5,k+m+5)=greal
      gammat(k+m+5,k+5)=greal
      gammat(k+m,k)=greal
      transp(k,k+m)=greal
      transp(k+5,k+m+5)=greal
      transp(k+m+5,k+5)=greal
      transp(k+m,k)=greal

      gimag=sin(2.*pi*alpha*rm)*eps*sin(pi*eps*rm)/(pi*eps*rm)
      gammat(k,k+m+5)=gimag
      gammat(k+5,k+m)=-gimag
      gammat(k+m,k+5)=-gimag
      gammat(k+m+5,k)=gimag
      transp(k,k+m+5)=-gimag
      transp(k+5,k+m)=gimag
      transp(k+m,k+5)=gimag
      transp(k+m+5,k)=-gimag

      goto 120

115   gammat(k,k)=eps
      gammat(k+5,k+5)=eps
      gammat(k,k+5)=0.
      gammat(k+5,k)=0.
      transp(k,k)=eps
      transp(k+5,k+5)=eps
      transp(k,k+5)=0.
      transp(k+5,k)=0.

120   continue
125   continue

C     CALCULATE TWO-PASS MATRIX FOR SPATIAL FILTER (tuning-independant part)
      call matmat(tempmat,transp,gammat)

C     INCREMENT FILTER DETUNING
      dstep=1.
      if (detuning.ne.(0.)) dstep=detuning/10.
      do 180 detun=0,detuning,dstep

C     COMPLETE CALCULATION OF TWO-PASS MATRIX FOR SPATIAL FILTER
C     BY CONSIDERING FILTER DETUNING
      do 135 i=1,5
      do 130 j=1,5
      ri=i
      rj=j
      coupling=exp(-2.*(ri-rj)*(ri-rj)*detun*detun)
      gamgam(i,j)=tempmat(i,j)*coupling
      gamgam(i,j+5)=tempmat(i,j+5)*coupling
      gamgam(i+5,j)=tempmat(i+5,j)*coupling
      gamgam(i+5,j+5)=tempmat(i+5,j+5)*coupling
130   continue
135   continue

C     DETERMINE INSTABILITY LIMIT w.r.t. BETAC, IF ONE EXISTS
      if (bstep.eq.(0.)) bstep=1.
```

```
      do 175 betac=betacmin,betacmax,bstep
      if (eps.eq.(1.)) betac=0.
      beta=betac
      if (linecnt.gt.275) print ,"APPEND CAPTURE BUFFER (IF DOWNLOADING).
     &  RESET LINECOUNT TO 0."
      if (linecnt.gt.275) input ,linecnt
      if ((linecnt+idisp).eq.0) print ,"EPS ALPHA DETUN ISCAN,mA PH.TAPER
     &  BETAc  A.OUT,mW   B.OUT,mW   C.OUT,mW"
      if ((linecnt+idisp).eq.0) print ,"--- ----- ----- -------- --------
     & ------ ---------- ---------- ----------"

C     INCREMENT GAIN-INDEPENDANT PHASE TAPER
      step=1.
      if (tapermax.ne.(0.)) step=tapermax*pi/10.
      if (betac.eq.(0.)) twitch=0.
      if (betac.ne.(0.)) twitch=1.
C     BEFORE BEGINNING TAPER-ITERATION, USE THE PREVIOUS MINIMUM TAPER RESULT
C     AS THE MOST RECENT CONVERGENT VALUE OF PSIVEC.
      do 137 j=1,10
      lastconvec(j)=taperminvec(j)
137   continue

C     IF BOTH THE RESONATOR AND THE STARTING ESTIMATE ARE SYMMETRIC, SPURIOUS
C     SOLUTIONS CAN ARISE.  MAKE SURE TO DESYMMETRIZE STARTING ESTIMATE.  IT
C     IS ASSUMED THAT THE DESYMMETRIZATION WILL NOT PREVENT EVOLUTION OF THE
C     SYSTEM TO THE "PROPER" SOLUTION, (i.e., when that solution is unique).
C     THE FOLLOWING PERTURBATION SHOULD BE SUFFICIENT IN MOST CASES.
      lastconvec(4)=1.1*lastconvec(4)

      tapermin=1.
      do 170 taper=0.,(tapermax*pi*twitch),step
      phase(1)=-2.*taper
      phase(2)=-taper
      phase(3)=0.
      phase(4)=taper
      phase(5)=2.*taper

C     CONVERGE TO SOLUTION SUPERMODE BY SUCCESSIVE-SUBSTITUTION ITERATION
C     USE THE MOST RECENT CONVERGENT VALUE OF PSIVEC AS A STARTING ESTIMATE
      do 138 j=1,10
      psivec(j)=lastconvec(j)
138   continue
      noconv=0
      do 150 itnum=1,100
      call succsub(psivec,netvec,bakvec,betac,noconv)
      if (noconv.eq.1) print ,"non-convergence (type 1)"
      if (noconv.eq.1) goto 170

      fnorma=0.
      err=0.
      do 140 j=1,10
      fnorma=fnorma+abs(psivec(j))
      err=err+abs(netvec(j))
140   continue
      err=err/fnorma
```

```
      if (abs(err).lt.(1.e-7)) goto 160
      do 145 j=1,10
      psivec(j)=psivec(j)+netvec(j)
145   continue
150   continue

C     IF THE DO-150-LOOP FALLS THROUGH, A STABLE SOLUTION IS NOT POSSIBLE
      print ,"non-convergence (type 2) for taper = ",taper
      linecnt=linecnt+1
C     SYSTEM IS NOT NECESSARILY UNSTABLE FOR GREATER VALUES OF PHASE TAPER,
C     DUE TO "2 PI" AMBIGUITY EFFECT.  TO BE SURE, USE "goto 170" HERE;
C     OTHERWISE, USE "goto 175".
      goto 170

160   call matvec(netvec,gammat,psivec)
      fnorma=0.
      fnormb=0.
      fnormc=0.
      do 165 j=1,10
C     SAVE CONVERGENT SUPERMODE FOR NEXT DO-170 ITERATION
      lastconvec(j)=psivec(j)
C     SAVE CONVERGENT SUPERMODE OF LEAST TAPER FOR NEXT DO-175 ITERATION
      if (tapermin.eq.(1.)) taperminvec(j)=psivec(j)
      netvec(j)=netvec(j)*tx
      fnorma=fnorma+psivec(j)*psivec(j)
      if (j.le.5) fnormb=fnormb+bakvec(j)
      fnormc=fnormc+netvec(j)*netvec(j)
165   continue
      tapermin=0.
      fnorma=1000.*fnorma
      fnormb=1000.*fnormb
      fnormc=1000.*fnormc
      if (idisp.ne.0) print ," "
      if (idisp.ne.0) print ,"EPS ALPHA DETUN ISCAN,mA PH.TAPER
     & BETAc  A.OUT,mW   B.OUT,mW   C.OUT,mW"
      if (idisp.ne.0) print ,"--- ----- ----- -------- --------
     & ------ ---------- ---------- ----------"
      if (idisp.ne.0) linecnt=linecnt+3
      print 105,eps,alpha,detun,iscan,taper,beta,fnorma,fnormb,fnormc
      linecnt=linecnt+1
      if (idisp.ne.0) call listvec(psivec,idisp)
      if (idisp.ne.0) call listvec(netvec,idisp)
      if (idisp.eq.1) linecnt=linecnt+2
      if (idisp.eq.2) linecnt=linecnt+20
C     NEXT TAPER
170   continue
C     NEXT BETAc
175   continue
C     NEXT DETUNING
180   continue
C     NEXT SPATIAL FILTER OFFSET, ALPHA
185   continue
C     NEXT SPATIAL FILTER DUTY CYCLE, EPS
190   continue
C     NEXT INCREMENT IN GAIN ELEMENT OPERATING CURRENTS, Iscan
195   continue
```

```
199   continue
      end
C-----------------------------------------------------------------------
      block data
      common /block 1/ gamgam(10,10),fldgn(10,10),phase(5)
      data fldgn/100*0./
      end
C-----------------------------------------------------------------------
C     ASSOCIATED SUBROUTINES:  MATMAT
C                              MATVEC
C                              PARAM
C                              ISOLATED
C                              LISTMAT (for debugging only)
C                              LISTVEC
C                              SUCCSUB
C-----------------------------------------------------------------------
C     THIS SUBROUTINE CALCULATES THE PRODUCT OF TWO MATRICES
      subroutine matmat(amat,bmat,cmat)
      dimension amat(10,10),bmat(10,10),cmat(10,10)

      do 220 i=1,10
      do 210 j=1,10
      amat(i,j)=0.
210   continue
220   continue

      do 250 i=1,10
      do 240 j=1,10
      do 230 k=1,10
      amat(i,j)=amat(i,j)+bmat(i,k)*cmat(k,j)
230   continue
240   continue
250   continue

      return
      end
C-----------------------------------------------------------------------
C     THIS SUBROUTINE CALCULATES THE PRODUCT OF A MATRIX AND A COLUMN VECTOR
      subroutine matvec(avec,bmat,cvec)
      dimension avec(10),bmat(10,10),cvec(10)

      do 310 i=1,10
      avec(i)=0.
310   continue

      do 330 i=1,10
      do 320 j=1,10
      avec(i)=avec(i)+bmat(i,j)*cvec(j)
320   continue
330   continue

      return
      end
C-----------------------------------------------------------------------
C     THIS SUBROUTINE REQUESTS PARAMETERS FOR: THE IDENTICAL GAIN ELEMENTS
```

```
C     (threshold current, slope of P-I curve above threshold for original
C     laser diodes); THE SPATIAL FILTER DUTY CYCLE, OFFSET, AND DETUNING;
C     THE ARRAY FILLING FACTOR; THE EFFECTIVE EXTERNAL MIRROR REFLECTIVITY;
C     THE NORMALIZATION CURRENT FROM THE ANALYSIS OF THE SUPERLUMINESCENT
C     DIODE SPECTRA; THE CARRIER RECOMBINATION LIFETIME; THE SPONTANEOUS
C     EMISSION FACTOR; THE DERIVATIVE OF THE REAL w.r.t. THE IMAGINARY PART
C     OF THE CARRIER INDUCED REFRACTIVE INDEX, GAIN-INDEPENDANT PHASE SHIFTS
C     AND THE GAIN-ELEMENT CURRENTS.

      subroutine param
      real i0,in,ith,isame,iop(5),kappa,iscanmax,istep
      dimension gnl(5)
      common /block 2/ rbrb,rb,cflux,sigma,gnl,energy,rxrx,rx,tx
     &       /block 3/ ith,slope,eps,kappa,in,scarrier,cfactor,i0,iop
     &       /block 4/ betacmin,betacmax,bstep,iscanmax,istep,idisp,
     &                 detuning,epsmin,epsmax,alphamax,tapermax
      data hc,evolt/12400.,1.6e-19/
      lambda=8300.
      rlrl=.32
      rbrb=.32
      rb=.32^.5
      energy=hc/lambda*evolt
      print ,"ENTER THRESHOLD CURRENT (in mA) FOR ORIGINAL LASER DIODE:"
      input ,ith
      ith=ith/1.e3
      print ,"ENTER SLOPE OF P-I CURVE ABOVE THRESHOLD (in mW/mA) FOR SAME:"
      input ,slope
      print ,"ENTER RANGE (max,min) OF SPATIAL FILTER DUTY CYCLE:"
      input ,epsmax,epsmin
      print ,"ENTER MAXIMUM OFFSET OF SPATIAL FILTER FROM OPTICAL AXIS:"
      input ,alphamax
      print ,"ENTER MAXIMUM DETUNING OF SPATIAL FILTER (in %):"
      input ,detuning
      if (detuning.eq.(0.)) goto 420
      print ,"ENTER ARRAY FILLING FACTOR (in %):"
      input ,fillfac
      detuning=detuning/fillfac
420   print ,"ENTER POWER REFLECTIVITY OF EXTERNAL MIRROR:"
      input ,rxrx
      print ,"ENTER POWER COUPLING BETWEEN GAIN ELEMENT AND EXTERNAL MIRROR:"
      input ,kappa
      tx=(kappa*(1.-rxrx))^.5
      rx=kappa*(rxrx)^.5
      rxrx=rx*rx
      print ,"ENTER NORMALIZATION CURRENT (in mA) FROM"
      print ,"ANALYSIS OF SUPERLUMINESCENT DIODE SPECTRA:"
      input ,in
      in=in/1.e3
      print ,"ENTER SPONTANEOUS CARRIER LIFETIME (in ns):"
      input ,tcarrier
      tcarrier=tcarrier/1.e9
      scarrier=1./tcarrier
      print ,"ENTER SPONTANEOUS EMISSION FACTOR (in units of 1.e-5):"
      input ,cfactor
      cfactor=cfactor/1.e5
      sigma=energy*scarrier/(2*in*slope)
```

```
      cflux=cfactor*in*slope/energy
      i0=ith+in*log(rlrl)
      if ((epsmin.ne.(1.)).or.(epsmax.ne.(1.))) goto 440
      betacmin=0.
      betacmax=0.
      tapermax=0.
      goto 450
 440  print ,"ENTER THE RANGE OF dn'/dn'' (min,max,step), WHERE (n'+in'') IS"
      print ,"THE CONTRIBUTION TO THE REFRACTIVE INDEX BY THE FREE CARRIERS:"
      print ,"(n.b.:  insightful choice of range conserves computation)"
      input ,betacmin,betacmax,bstep

      print ,"ENTER THE MAXIMUM VALUE OF GAIN-INDEPENDANT PHASE TAPER"
      print ,"(in units of pi):"
      input ,tapermax

 450  ith=(ith-in*log(rx/rb))*1000.
      print ,"NEW FREE-RUNNING (eps=1) THRESHOLD IS ",ith," mA"
      ith=ith/1000.
      slope=slope*2.*tx*tx/((1.-rxrx)+(1.-rbrb)*rx/rb)
      print ,"NEW FREE-RUNNING SLOPE IS ",slope," mW/mA"
      current=1000.*i0
      print 455,current
 455  format ("OPERATING CURRENTS MUST EXCEED ",f4.0," mA FOR THIS MODEL")
      print ,"ARE ALL INITIAL OPERATING CURRENTS THE SAME? (1=yes, 0=no)"
      input ,ident
      if (ident.ne.1) goto 465
      print ,"ENTER THE COMMON INITIAL OPERATING CURRENT (in mA):"
      input ,isame
      do 460 i=1,5
      iop(i)=isame
 460  continue
      goto 470
 465  print ,"ENTER THE INDIVIDUAL INITIAL OPERATING CURRENTS (in mA):"
      input ,(iop(i),i=1,5)

 470  do 475 i=1,5
      iop(i)=iop(i)/1.e3
 475  continue

      print ,"ENTER THE SCAN RANGE (max,step) OF OPERATING CURRENT (in mA):"
      input ,iscanmax,istep
      print ,"ENTER TYPE OF SUPERMODE DISPLAY (0=none, 1=pwrs, 2=pwrs & flds):"
      input ,idisp

      return
      end
C-----------------------------------------------------------------------
C     THIS SUBROUTINE CALCULATES AN INITIAL GUESS FOR THE SUPERMODE PSI.
C     IT IS ASSUMED THAT THE LOCKED POWERS ARE OF THE SAME ORDER OF
C     MAGNITUDE AS THE POWERS PRESENT IN THE ABSENCE OF THE SPATIAL FILTER.
      subroutine isolated(taperminvec,abort)
      real gnl(5),iop(5)
      dimension taperminvec(10)
      common /block 2/ rbrb,rb,cflux,sigma,gnl,energy,rxrx,rx,tx
     &       /block 3/ ith,slope,eps,kappa,in,scarrier,cfactor,i0,iop
```

```
      offset=scarrier*log(rx*rb)
      denom=sigma*(1-rbrb+(1-rxrx)*rx/rb)

      do 530 i=1,5
      detop=gnl(i)+offset
      if (detop.lt.(0.)) goto 510
      taperminvec(i)=(detop/denom*energy)^.5
      goto 525

510   if (gnl(i).lt.(0.)) goto 520
      G=exp(gnl(i)/scarrier)
      taperminvec(i)=(cflux*(G-1.)/(1.-rx*rb*G)^2.*energy)^.5
      goto 525

520   print ,"FATAL ERROR.  GAIN IS NEGATIVE FOR ELEMENT NO.",i
      abort=1.
      goto 540

525   taperminvec(i+5)=0.
530   continue
      abort=0.

540   return
      end
C-----------------------------------------------------------------------
C     THIS SUBROUTINE DISPLAYS A 10x10 MATRIX
      subroutine listmat(amat)
      dimension amat(10,10)

      print ,"  ------------------------------------------------------"
      do 710 i=1,10
      print 720,(amat(i,j),j=1,10)
710   continue

720   format (10f7.3)
      print ,"  ------------------------------------------------------"

      return
      end
C     -----------------------------------------------------------------
C     THIS SUBROUTINE DISPLAYS THE FIELD AND POWER STATE VECTORS
      subroutine listvec(avec,idisp)
      dimension avec(10),bvec(5)
      sqthou=(10.)^1.5
      if (idisp.eq.1) goto 835
      print ,"-------------------------------------------------------------
     &-------"

      print ,"      rl(fld-2)     rl(fld-1)
     &     rl(fld 0)     rl(fld+1)     rl(fld+2)"
      do 820 i=1,5
      bvec(i)=avec(i)*sqthou
820   continue
      print 850,(bvec(i),i=1,5)
```

```
      print ," "
      print ,"      im(fld-2)     im(fld-1)
     &     im(fld 0)     im(fld+1)     im(fld+2)"
      do 830 i=1,5
      bvec(i)=avec(i+5)*sqthou
830   continue
      print 850,(bvec(i),i=1,5)
      print ," "

      print ,"   power(mW)-2   power(mW)-1
     &   power(mW) 0   power(mW)+1   power(mW)+2"
835   do 840 i=1,5
      bvec(i)=(avec(i)^2.+avec(i+5)^2.)*1.e3
840   continue
      print 850,(bvec(i),i=1,5)
      if (idisp.eq.1) goto 855

850   format (5e14.4)
      print ,"-------------------------------------------------------------
     &-------"

855   continue
      return
      end
C     ---------------------------------------------------------------------
C     THIS SUBROUTINE CALCULATES THE NET EFFECT OF ONE ROUND TRIP AROUND THE
C     EXTERNAL CAVITY LASER.  THE NET EFFECT IS ZERO FOR THE SELF-CONSISTENT
C     SOLUTION SUPERMODE PSI.
      subroutine succsub(psivec,netvec,bakvec,betac,noconv)
      real netvec(10),iop(5),newreal,newimag
      dimension psivec(10),gnl(5),tmpvec(10),bakvec(5)
      common /block 1/ gamgam(10,10),fldgn(10,10),phase(5)
     &       /block 2/ rbrb,rb,cflux,sigma,gnl,energy,rxrx,rx,tx
     &       /block 3/ ith,slope,eps,kappa,in,scarrier,cfactor,i0,iop

C     DETERMINE FIELDS ARRIVING BACK AT GAIN ELEMENTS
      call matvec(tmpvec,gamgam,psivec)

      do 905 i=1,10
      tmpvec(i)=tmpvec(i)*rx
905   continue

C     DETERMINE NEW POWER EXITING THE GAIN ELEMENT
      pmax=0.
      do 930 i=1,5
      pright=(tmpvec(i)*tmpvec(i)+tmpvec(i+5)*tmpvec(i+5))/energy
      spar=scarrier-2.*sigma*cflux
      cpar=sigma*cflux/spar
      xright=sigma*pright/spar+cpar
      v=1.

C     INTEGRATION OF PROPOGATION EQUATION YIELDS A TRANSCENDENTAL RELATION
C     FOR V=Yright/Xright.  A NEWTON-RAPHSON ITERATION IS USED TO SOLVE IT.
      iter=0
910   z=exp(gnl(i)/spar-(v-1.)*(xright*(rbrb*v+1.)+(1.-rbrb)*cpar))
      corr=(z-v)/(1+z*(2.*xright*rbrb*v+(xright+cpar)*(1.-rbrb)))
```

```
      if (abs(corr).lt.(1.e-7)) goto 920
      v=v+corr
      iter=iter+1
      if (iter.gt.20) noconv=1
      if (iter.gt.20) goto 999
      goto 910

920   yright=v*xright
C     CALCULATE ADJUSTED PHOTON FLUX REFLECTED FROM REAR FACET OF GAIN ELEMENT
      yleft=rbrb*yright+(1.-rbrb)*cpar
C     CALCULATE ACTUAL PHOTON FLUX EXITING FRONT FACET OF GAIN ELEMENT
      const=yright*yleft
      xleft=const/xright
      pleft=(xleft-cpar)*spar/sigma
C     CALCULATE AND SAVE POWER EXITING REAR FACET OF GAIN ELEMENT
      bakvec(i)=(yright-cpar)*spar/sigma*(1.-rbrb)*energy
C     SAVE INDEX OF ELEMENT WITH GREATEST OUTPUT
      if (pmax.gt.pleft) goto 925
      pmax=pleft
      imax=i

C     CALCULATE EFFECTIVE LOG POWER GAIN FOR THE GAIN ELEMENT
925   GG=log(pleft/pright/rbrb)
C     CALCULATE FIELD PHASE SHIFT FOR THE GAIN ELEMENT
      phi=-betac*GG/2.+phase(i)
C     EVALUATE FIELD GAIN MATRIX ELEMENTS
      fgain=(pleft/pright)^.5
      fldgn(i,i)=fgain*cos(phi)
      fldgn(i+5,i+5)=fldgn(i,i)
      fldgn(i,i+5)=-fgain*sin(phi)
      fldgn(i+5,i)=-fldgn(i,i+5)
930   continue

C     PROPAGATE FIELDS THROUGH THE GAIN ELEMENTS
      call matvec(netvec,fldgn,tmpvec)

C     ROTATE SUPERMODE TO MAKE STRONGEST FIELD PURE REAL
      denom=(netvec(imax)*netvec(imax)+netvec(imax+5)*netvec(imax+5))^.5
      cosphix=netvec(imax)/denom
      sinphix=netvec(imax+5)/denom
      do 945 i=1,5
      newreal=cosphix*netvec(i)+sinphix*netvec(i+5)
      newimag=cosphix*netvec(i+5)-sinphix*netvec(i)
      netvec(i)=newreal
      netvec(i+5)=newimag
945   continue

C     CALCULATE CHANGE IN FIELDS FROM THE ACTION OF ONE ROUND TRIP
      do 990 i=1,10
      netvec(i)=netvec(i)-psivec(i)
990   continue

999   continue
      return
      end
C-----------------------------------------------------------------------
```

Appendix C

Fortran simulation of external cavity laser - MODEL4. Only the main program and the PARAM subroutine are included, since the MATMAT, MATVEC, ISOLATED, LISTMAT, LISTVEC, and SUCCSUB subroutines are identical to the subroutines of the same name in MODEL3, listed in Appendix B.

```
C     EXTERNAL CAVITY LASER, MODEL 4: OPERATION vs. EPS, OFFSET, DETUNING,
C                      Iscan, CURRENT SHAPE FACTOR, PHASE TAPER, AND BETAc
C
C     THIS IS A VARIATION ON MODEL3, WITH A SPECIFIED FREE-RUNNING POWER
C     DISTRIBUTION (ranging from uniform to squared-binomial).  DISTRIBUTION
C     "FACTOR" DOES NOT CHANGE AS AVERAGE CURRENT IS SCANNED.
C-------------------------------------------------------------------------
C     MAIN PROGRAM
      real i0,in,ith,iop(5),kappa,netvec(10),iscan,iscanmax,istep,
     &     lastconvec(10),isame
      dimension gammat(10,10),transp(10,10),psivec(10),gnl(5),tempmat(10,10),
     &          taperminvec(10),bakvec(5)
      common /block 1/ gamgam(10,10),fldgn(10,10),phase(5)
     &       /block 2/ rbrb,rb,cflux,sigma,gnl,energy,rxrx,rx,tx
     &       /block 3/ ith,slope,eps,kappa,in,scarrier,cfactor,i0,iop
     &       /block 4/ betacmin,betacmax,bstep,iscanmax,istep,idisp,
     &                 detuning,epsmin,epsmax,alphamax,tapermax,binomial,isame
      data pi,linecnt/3.1415927,1/

100   call param
105   format(f3.1,x,f5.2,x,f5.2,3x,f4.1,4x,f6.3,2x,f6.4,
     &                                          x,e10.4,x,e10.4,x,e10.4)
      linecnt=linecnt+39

C     INCREMENT GAIN-ELEMENT OPERATING CURRENTS
      do 195 iscan=0.,iscanmax,istep
      avgpwr=(isame+iscan/1000.-ith)*slope

C     MODIFY GAIN-ELEMENT OPERATING CURRENTS DISTRIBUTION
C     (when binomial=0., distribution is uniform; when binomial=1.,
C     free-running powers are proportional to 1*1,4*4,6*6,4*4,1*1.)
      iop(1)=ith+(1.-(13./14.)*binomial)*avgpwr/slope
      iop(2)=ith+(1.+(2./14.)*binomial)*avgpwr/slope
      iop(3)=ith+(1.+(22./14.)*binomial)*avgpwr/slope
      iop(4)=iop(2)
      iop(5)=iop(1)
      do 110 i=1,5
      gnl(i)=scarrier*(iop(i)-i0)/in
110   continue

C     OBTAIN STARTING ESTIMATE FOR SUPERMODE
      call isolated(taperminvec,abort)
      if (abort.eq.(1.)) goto 199

      if (idisp.eq.0) print ,"EPS ALPHA DETUN ISCAN,mA PH.TAPER
     &  BETAC  A.OUT,mW   B.OUT,mW   C.OUT,mW"
      if (idisp.eq.0) print ,"--- ----- ----- -------- --------
     & ------ ---------- ---------- ----------"
      if (idisp.eq.0) linecnt=linecnt+2
      print ,(iop(j),j=1,5)

C     INCREMENT SPATIAL FILTER DUTY CYCLE
      do 190 eps=epsmax,epsmin,-.1

C     INCREMENT SPATIAL FILTER OFFSET
      astep=.1
```

```
      if (alphamax.ne.(0.)) astep=.1*abs(alphamax)/alphamax
      do 185 alpha=0.,alphamax,astep

C     EVALUATE MATRIX OF FOURIER COEFFICIENTS OF SPATIAL FILTER TRANSMISSION
C     AND THE TRANSPOSE OF THIS MATRIX (i.e., 10x10 real representations of
C     corresponding 5x5 complex matrices).
      do 125 m=0,4
      do 120 k=1,5-m
      if (m.eq.0) goto 115

      rm=m
      greal=cos(2.*pi*alpha*rm)*eps*sin(pi*eps*rm)/(pi*eps*rm)
      gammat(k,k+m)=greal
      gammat(k+5,k+m+5)=greal
      gammat(k+m+5,k+5)=greal
      gammat(k+m,k)=greal
      transp(k,k+m)=greal
      transp(k+5,k+m+5)=greal
      transp(k+m+5,k+5)=greal
      transp(k+m,k)=greal

      gimag=sin(2.*pi*alpha*rm)*eps*sin(pi*eps*rm)/(pi*eps*rm)
      gammat(k,k+m+5)=gimag
      gammat(k+5,k+m)=-gimag
      gammat(k+m,k+5)=-gimag
      gammat(k+m+5,k)=gimag
      transp(k,k+m+5)=-gimag
      transp(k+5,k+m)=gimag
      transp(k+m,k+5)=gimag
      transp(k+m+5,k)=-gimag

      goto 120

115   gammat(k,k)=eps
      gammat(k+5,k+5)=eps
      gammat(k,k+5)=0.
      gammat(k+5,k)=0.
      transp(k,k)=eps
      transp(k+5,k+5)=eps
      transp(k,k+5)=0.
      transp(k+5,k)=0.

120   continue
125   continue

C     CALCULATE TWO-PASS MATRIX FOR SPATIAL FILTER (tuning-independant part)
      call matmat(tempmat,transp,gammat)

C     INCREMENT FILTER DETUNING
      dstep=1.
      if (detuning.ne.(0.)) dstep=detuning/10.
      do 180 detun=0,detuning,dstep

C     COMPLETE CALCULATION OF TWO-PASS MATRIX FOR SPATIAL FILTER
C     BY CONSIDERING FILTER DETUNING
      do 135 i=1,5
```

```
      do 130 j=1,5
      ri=i
      rj=j
      coupling=exp(-2.*(ri-rj)*(ri-rj)*detun*detun)
      gamgam(i,j)=tempmat(i,j)*coupling
      gamgam(i,j+5)=tempmat(i,j+5)*coupling
      gamgam(i+5,j)=tempmat(i+5,j)*coupling
      gamgam(i+5,j+5)=tempmat(i+5,j+5)*coupling
130   continue
135   continue

C     DETERMINE INSTABILITY LIMIT w.r.t. BETAC, IF ONE EXISTS
      if (bstep.eq.(0.)) bstep=1.
      do 175 betac=betacmin,betacmax,bstep
      if (eps.eq.(1.)) betac=0.
      beta=betac
      if (linecnt.gt.275) print ,"APPEND CAPTURE BUFFER (IF DOWNLOADING).
     &  RESET LINECOUNT TO 0."
      if (linecnt.gt.275) input ,linecnt
      if ((linecnt+idisp).eq.0) print ,"EPS ALPHA DETUN ISCAN,mA PH.TAPER
     &  BETAc  A.OUT,mW   B.OUT,mW   C.OUT,mW"
      if ((linecnt+idisp).eq.0) print ,"--- ----- ----- -------- --------
     & ------ ---------- ---------- ----------"

C     INCREMENT GAIN-INDEPENDANT PHASE TAPER
      step=1.
      if (tapermax.ne.(0.)) step=tapermax*pi/10.
      if (betac.eq.(0.)) twitch=0.
      if (betac.ne.(0.)) twitch=1.
C     BEFORE BEGINNING TAPER-ITERATION, USE THE PREVIOUS MINIMUM TAPER RESULT
C     AS THE MOST RECENT CONVERGENT VALUE OF PSIVEC.
      do 137 j=1,10
      lastconvec(j)=taperminvec(j)
137   continue

C     IF BOTH THE RESONATOR AND THE STARTING ESTIMATE ARE SYMMETRIC, SPURIOUS
C     SOLUTIONS CAN ARISE.  MAKE SURE TO DESYMMETRIZE STARTING ESTIMATE.  IT
C     IS ASSUMED THAT THE DESYMMETRIZATION WILL NOT PREVENT EVOLUTION OF THE
C     SYSTEM TO THE "PROPER" SOLUTION, (i.e., when that solution is unique).
C     THE FOLLOWING PERTURBATION SHOULD BE SUFFICIENT IN MOST CASES.
      lastconvec(4)=1.1*lastconvec(4)

      tapermin=1.
      do 170 taper=0.,(tapermax*pi*twitch),step
      phase(1)=-2.*taper
      phase(2)=-taper
      phase(3)=0.
      phase(4)=taper
      phase(5)=2.*taper

C     CONVERGE TO SOLUTION SUPERMODE BY SUCCESSIVE-SUBSTITUTION ITERATION
C     USE THE MOST RECENT CONVERGENT VALUE OF PSIVEC AS A STARTING ESTIMATE
      do 138 j=1,10
      psivec(j)=lastconvec(j)
138   continue
      noconv=0
```

```
      do 150 itnum=1,100
      call succsub(psivec,netvec,bakvec,betac,noconv)
      if (noconv.eq.1) print ,"non-convergence (type 1)"
      if (noconv.eq.1) goto 170

      fnorma=0.
      err=0.
      do 140 j=1,10
      fnorma=fnorma+abs(psivec(j))
      err=err+abs(netvec(j))
140   continue
      err=err/fnorma

      if (abs(err).lt.(1.e-7)) goto 160
      do 145 j=1,10
      psivec(j)=psivec(j)+netvec(j)
145   continue
150   continue

C     IF THE DO-150-LOOP FALLS THROUGH, A STABLE SOLUTION IS NOT POSSIBLE
      print ,"non-convergence (type 2)"
      linecnt=linecnt+1
C     SYSTEM IS NOT NECESSARILY UNSTABLE FOR GREATER VALUES OF PHASE TAPER,
C     DUE TO "2 PI" AMBIGUITY EFFECT.  TO BE SURE, USE "goto 170" HERE;
C     OTHERWISE, USE "goto 175".
      goto 170

160   call matvec(netvec,gammat,psivec)
      fnorma=0.
      fnormb=0.
      fnormc=0.
      do 165 j=1,10
C     SAVE CONVERGENT SUPERMODE FOR NEXT DO-170 ITERATION
      lastconvec(j)=psivec(j)
C     SAVE CONVERGENT SUPERMODE OF LEAST TAPER FOR NEXT DO-175 ITERATION
      if (tapermin.eq.(1.)) taperminvec(j)=psivec(j)
      netvec(j)=netvec(j)*tx
      fnorma=fnorma+psivec(j)*psivec(j)
      if (j.le.5) fnormb=fnormb+bakvec(j)
      fnormc=fnormc+netvec(j)*netvec(j)
165   continue
      tapermin=0.
      fnorma=1000.*fnorma
      fnormb=1000.*fnormb
      fnormc=1000.*fnormc
      if (idisp.ne.0) print ," "
      if (idisp.ne.0) print ,"EPS ALPHA DETUN ISCAN,mA PH.TAPER
     &  BETAc  A.OUT,mW   B.OUT,mW   C.OUT,mW"
      if (idisp.ne.0) print ,"--- ----- ----- -------- --------
     & ------ ---------- ---------- ----------"
      if (idisp.ne.0) linecnt=linecnt+3
      print 105,eps,alpha,detun,iscan,taper,beta,fnorma,fnormb,fnormc
      linecnt=linecnt+1
      if (idisp.ne.0) call listvec(psivec,idisp)
      if (idisp.ne.0) call listvec(netvec,idisp)
      if (idisp.eq.1) linecnt=linecnt+2
```

```
      if (idisp.eq.2) linecnt=linecnt+20
C     NEXT TAPER
170   continue
C     NEXT BETAc
175   continue
C     NEXT DETUNING
180   continue
C     NEXT SPATIAL FILTER OFFSET, ALPHA
185   continue
C     NEXT SPATIAL FILTER DUTY CYCLE, EPS
190   continue
C     NEXT INCREMENT IN GAIN ELEMENT OPERATING CURRENTS, Iscan
195   continue

199   continue
      end
C-----------------------------------------------------------------------
C     THIS SUBROUTINE REQUESTS PARAMETERS FOR: THE IDENTICAL GAIN ELEMENTS
C     (threshold current, slope of P-I curve above threshold for original
C     laser diodes); THE SPATIAL FILTER DUTY CYCLE, OFFSET, AND DETUNING;
C     THE ARRAY FILLING FACTOR; THE EFFECTIVE EXTERNAL MIRROR REFLECTIVITY;
C     THE NORMALIZATION CURRENT FROM THE ANALYSIS OF THE SUPERLUMINESCENT
C     DIODE SPECTRA; THE CARRIER RECOMBINATION LIFETIME; THE SPONTANEOUS
C     EMISSION FACTOR; THE DERIVATIVE OF THE REAL w.r.t. THE IMAGINARY PART
C     OF THE CARRIER INDUCED REFRACTIVE INDEX, GAIN-INDEPENDANT PHASE SHIFTS
C     AND THE GAIN-ELEMENT CURRENTS.

      subroutine param
      real i0,in,ith,isame,iop(5),kappa,iscanmax,istep
      dimension gnl(5)
      common /block 2/ rbrb,rb,cflux,sigma,gnl,energy,rxrx,rx,tx
     &       /block 3/ ith,slope,eps,kappa,in,scarrier,cfactor,i0,iop
     &       /block 4/ betacmin,betacmax,bstep,iscanmax,istep,idisp,
     &                 detuning,epsmin,epsmax,alphamax,tapermax,binomial,isame
      data hc,evolt/12400.,1.6e-19/
      lambda=8300.
      rlrl=.32
      rbrb=.32
      rb=.32^.5
      energy=hc/lambda*evolt
      print ,"ENTER THRESHOLD CURRENT (in mA) FOR ORIGINAL LASER DIODE:"
      input ,ith
      ith=ith/1.e3
      print ,"ENTER SLOPE OF P-I CURVE ABOVE THRESHOLD (in mW/mA) FOR SAME:"
      input ,slope
      print ,"ENTER RANGE (max,min) OF SPATIAL FILTER DUTY CYCLE:"
      input ,epsmax,epsmin
      print ,"ENTER MAXIMUM OFFSET OF SPATIAL FILTER FROM OPTICAL AXIS:"
      input ,alphamax
      print ,"ENTER MAXIMUM DETUNING OF SPATIAL FILTER (in %):"
      input ,detuning
      if (detuning.eq.(0.)) goto 420
      print ,"ENTER ARRAY FILLING FACTOR (in %):"
      input ,fillfac
      detuning=detuning/fillfac
420   print ,"ENTER POWER REFLECTIVITY OF EXTERNAL MIRROR:"
```

```
      input ,rxrx
      print ,"ENTER POWER COUPLING BETWEEN GAIN ELEMENT AND EXTERNAL MIRROR:"
      input ,kappa
      tx=(kappa*(1.-rxrx))^.5
      rx=kappa*(rxrx)^.5
      rxrx=rx*rx
      print ,"ENTER NORMALIZATION CURRENT (in mA) FROM"
      print ,"ANALYSIS OF SUPERLUMINESCENT DIODE SPECTRA:"
      input ,in
      in=in/1.e3
      print ,"ENTER SPONTANEOUS CARRIER LIFETIME (in ns):"
      input ,tcarrier
      tcarrier=tcarrier/1.e9
      scarrier=1./tcarrier
      print ,"ENTER SPONTANEOUS EMISSION FACTOR (in units of 1.e-5):"
      input ,cfactor
      cfactor=cfactor/1.e5
      sigma=energy*scarrier/(2*in*slope)
      cflux=cfactor*in*slope/energy
      i0=ith+in*log(r1r1)
      if ((epsmin.ne.(1.)).or.(epsmax.ne.(1.))) goto 440
      betacmin=0.
      betacmax=0.
      tapermax=0.
      goto 450
440   print ,"ENTER THE RANGE OF dn'/dn'' (min,max,step), WHERE (n'+in'') IS"
      print ,"THE CONTRIBUTION TO THE REFRACTIVE INDEX BY THE FREE CARRIERS:"
      print ,"(n.b.:  insightful choice of range conserves computation)"
      input ,betacmin,betacmax,bstep

      print ,"ENTER THE MAXIMUM VALUE OF GAIN-INDEPENDANT PHASE TAPER"
      print ,"(in units of pi):"
      input ,tapermax

450   ith=(ith-in*log(rx/rb))*1000.
      print ,"NEW FREE-RUNNING (eps=1) THRESHOLD IS ",ith," mA"
      ith=ith/1000.
      slope=slope*2.*tx*tx/((1.-rxrx)+(1.-rbrb)*rx/rb)
      print ,"NEW FREE-RUNNING SLOPE IS ",slope," mW/mA"
      current=1000.*i0
      print 455,current
455   format ("OPERATING CURRENTS MUST EXCEED ",f4.0," mA FOR THIS MODEL")
      print ,"ENTER THE AVERAGE INITIAL OPERATING CURRENT (in mA):"
      input ,isame
      isame=isame/1000.
      print ,"ENTER CURRENT DISTRIBUTION FACTOR (0.0=flat, 1.0=binomial):"
      input ,binomial
      print ,"ENTER THE SCAN RANGE (max,step) OF OPERATING CURRENT (in mA):"
      input ,iscanmax,istep

      print ,"ENTER TYPE OF SUPERMODE DISPLAY (0=none, 1=pwrs, 2=pwrs & flds):"
      input ,idisp

      return
      end
C-----------------------------------------------------------------------
```

REFERENCES

1. Robert Adler, "A Study of Locking Phenomena in Oscillators," Proc. I.R.E. 34, 351 (1946).

2. Kaneyuki Kurokawa, "Injection Locking of Microwave Solid-State Oscillators," Proc. IEEE 61, 1386 (1973)

3. I. Tatsuguchi, "A frequency-modulated Phase-locked IMPATT power combiner," ISSCC Dig. Tech. Papers, p.18 (1970).

4. S.E. Schwarz and P.L. Gordon, "Hamilton's Principle and the Maximum-Emission Coincidence," Appl. Phys. 40, 4441 (1969).

5. J.F. Reintjes and G.T. Coate, Principle of Radar, New York, McGraw-Hill, p. 712 (1952).

6. A.A. Dvornikov, "Stabilizing the Frequency of an Ensemble of Self-Excited Oscillators by Means of an External Resonator, " Radiophysics and Quant. Electronics 18, 1214.

7. V.V. Grigorash, "Control of the Frequency of an Ensemble of Independent Oscillatros by an External Resonator, " Telecomm. and Radio Eng. 34/35, 85 (1980)

8. Kaneyuki Kurokawa, "The Single-Cavity Multiple Device Oscillator," IEEE Trans. Micr. Theor. and Tech. 19, 793 (1971).

9. J. Ripper and T.L. Paoli, "Optical Coupling of Adjacent Stripe-Geometry Junction Lasers, " Appl. Phys. Lett. 17, 371 (1970).

10. D.R. Scifres, W. Streifer and R.D. Burnham, "High-Power Coupled-Multiple-Stripe Phase-Locked Injection Laser," Appl. Phys. Lett. 34, 259 (1979); ibid "Experimental and Analytical Study of Coupled Multiple Stripe Diode Lasers, "IEEE J. of Quant. Electron. 15,917 (1979).

11. Donald E. Ackley "High-Power Multiple-Stripe Injection Lasers with Channel Guides," IEEE J. of Quant. Electron. 18, 1818 (1982).

12. B.F. Levine, R.A. Logan , W.T. Tsang, G.C. Bethea and F.R. Merritt, "Optically Integrated Coherently Coupled $Al_xGa_{1-x}As$ Lasers," Appl. Phys. Lett. 42, 339 (1983)

13. D.R. Scifres, R.D. Burnham and W. Streifer, "Continuous Wave, High-Power, High Temperature Semiconductor Laser Phase-Locked Arrays," Appl. Phys. Lett. 41, 1030 (1982).

14. D.R. Scifres, R.A. Sprague, W. Streifer and R.D. Burnham, "Focusing of a 7700-A High Power Phased Array Semiconductor Laser, "Appl. Phys.

Lett. 41, 1121 (1982).

15. D.R.Scifres, W. Streifer, R.K. Burnham, T.L. Paoli and C. Lindstrom, "Near and Far Field Patterns of Phase-Locked Semiconductor Laser Arrays," Appl. Phys. Lett. 42, 645 (1983).

16. D.R. Scifres, R.D.. Burnham, C. Lindstrom, W. Streifer and T.L. Paoli,, "Phase-Locked (GaAl)As Laser Emitting 1.5W CW per Mirror," Appl. Phys. Lett. 42, 645 (1983)

17. J. Katz, E. Kapon, C Lindsey, S. Margalit, U. Shreter and A. Yariv, "Phase-Locked Semiconductor Laser Array with Separate Contacts," Appl. Phys. Lett. 43, 521 (1983).

18. D. Botez and J.C. Connolly, "High-Power Phase-Locked Arrays of Index-Guided Diode Lasers," Appl. Phys. Lett. 43, 1096 (1983).

19. E. Kapon, C. Lindsey, J. Katz, S. Margalit and A. Yariv, "Coupling Mechanism of Gain-Guided Integrated Semiconductor Laser Arrays," Appl. Phys. Lett. 44, 389 (1984).

20. W. Streifer, R.D. Burnham, T.L. Paoli and D.R. Scifres, "Phased Array Diode Lasers, " Laser Focus/Elecro-Optics, June 1984.

21. E. Kapon, C. Lindsey, J. Katz, S. Margalit, and A Yariv, "Chirped Arrays of Diode Lasers for Supermode Control, ´ Appl. Phys. Lett. 45, 200 (1984).

22. J.K. Butler, D.E. Ackley and D. Botez, "Coupled-Mode Analysis of Phase-Locked Injection Laser Arrays," Appl. Phys. Lett. 44, 293 (1984)

23. E. Kapon, J. Katz and A. Yariv, "Supermode Analysis of Phase-Locked Arrays of Semiconductor Lasers, " Optics Lett. 9, 125 (1984).

24. E.M. Philipp-Rutz, "Spatialy Coherent Radiation from an Array of GaAs Lasrs, " Appl. Phys. Lett. 26, 475 (1975).

25. H.A. Haus, "A Theory of Forced Mode Locking," IEEE J. of Quant. Electron. 11, 323 (1975).

26. K. Aiki, M. Nakamura, T. Kuroda, J. Umeda, R. Ito, N. Chinone, and M. Maeda, "Transverse Mode Stabilized $Al_xGa_{1-x}As$ Injection Lasers with Channeled-Substrate-Planar Structure," IEEE J. of Quant. Electron. 14, 89 (1978).

27. I.P. Kaminow, G. Eisenstein, and L.W. Stulz, " Measurement of the Modal Reflectivity of an Antireflection Coating on a Superluminescent Diode," IEEE J. of Quantum Elect. QE-19, 493 (1983).

28. W. Lenth, personal communication.

29. Hitachi Laser Diode HLP1000, HLP2000 & HLP3000 Series Application Manual.

30. R.H. Rediker , R.P. Schloss, and L.J. Van Ruyven, "Operation of Individual Diode Lasers as a Coherent Ensemble Controlled by a Spatial Filter within an External Cavity," Appl. Phys. Lett. 46, 133 (1985).

31. W. Streifer, D.R. Scifres and R.D. Burnham, "Analysis of Diode Laser Properties," IEEE J. of Quant. Electron. 18, 1918 (1982).

32. K.J. Eberling, L.A. Coldren, B.J. Miller and J.A. Rentschler, "Single-mode Operation of Coupled-Cavity GaInAsP/InP Semiconductor Lasers," Appl. Phys. Lett. 42, 6 (1983).

33. A. Yariv, Introduction to Optical Electronics, New York, Holt, Rinehart and Winston (1971).

34. Y. Suematsu, S. Akiba and T. Hong, "Measurement of Spontaneous-Emission Factor of AlGaAs Double-heterostructure Semiconductor Lasers," IEEE J. of Quantum Elect. ,QE-13,596 (1977).

35. J.W. Goodman, Introduction to Fourier Optics, McGraw-Hill, New York, (1968).

36. D.T. Cassidy, "Analytic Description of a Homogeneously Broadened Injection Laser," IEEE J. of Quantum Elect. QE-20, 913 (1984).

37. D.T. Cassidy, "Comparison of Rate-equation and Fabry-Perot Approaches to Modeling a Diode Laser," Applied Optics, 22,3321 (1983).

38. D.T. Cassidy, "Consequences of a Lower Levell Population on the Modelling of a Homogeneously Broadened Injection Laser," Appl. Phys. Lett. 44, 489 (1984).

39. F.B. Hildebrand, Introduction to Numerical Analysis, New York, McGraw-Hill (1974)

40. C.H. Henry, R.A. Logan, and K.A. Bertness, "Spectral Dependence of the Change in Refractive Index due to Carrier Injection in GaAs Lasers," J. Appl, Phys. 52, 4457 (1981).

41. J. Katz, E. Kapon, S. Margalit, and A. Y. Yariv, "Rate Equations Analysis of Phase-Locked Semiconductor Laser Arrays under Steady State Conditions," IEEE J. of Quantum Elect., QE-20, 875 (1984).

42. C.H. Lee, T.H. Yoon, and S.Y. Shin, "Period Doubling and chaos in a Directly Modulated Laser Diode," Appl. Phys. Lett. 46, 95 (1985).

43. T.P. Lee, C.A. Burrus, J.A. Copeland, A.G. Dentai, and D. Marcuse, "Short-cavity InGaAsP Injection Lasers: Dependence of Mode Spectra on Single-longitudinal-mode power on Cavity Length,"IEEE J. of Quantum Elect. QE-18, 1101 (1982).

44. D. Marcuse, "Classical Derivation of the Laser Rate Equation," IEEE J. of Quantum Elect., QE-19,1228 (1983).

45. H. Kogelnik, "Coupling and Conversion Coefficients for Optical Modes," Pres. at the Symp. on Quasi-Optics, Polytech. Inst. , Brooklyn, (June, 1964).

46. R.P. Schloss, "Transverse Mode Excitation and Frequency Pulling in Optical Resonators," Master's Thesis, MIT Dept. of Elec. Eng. (1981).

47. R.M. May,"Simple Mathematical Models with very Complicated Dynamics," Nature, 261,459 (1976).